



**Engineering of chimeric antigen receptor T cells with enhanced therapeutic index
in cancer immunotherapy using non-viral gene transfer and genome editing**

**Entwicklung chimärer Antigenrezeptor T-Zellen mit verbessertem
Therapeutischen Index in der Krebsimmuntherapie durch die Verwendung von
nicht-viralen Gentransfer und Genomeditierung**

Thesis for a doctoral degree
at the Graduate School of Life Sciences,
Julius-Maximilians-University Würzburg,
Section Biomedicine

Submitted by
Razieh Monjezi

from
Ahwaz-Iran

Würzburg, 2017

Submitted on:

Office stamp

Members of the *PhD thesis committee*:

Chairperson: Prof. Dr. Caroline Kisker

Primary Supervisor: Dr. Michael Hudecek

Supervisor (Second): Prof. Dr. Hermann Einsele

Supervisor (Third): Prof. Dr. Thomas Hünig

Supervisor (Fourth): Dr. Zoltán Ivics

Date of Public Defense:

Date of Receipt of Certificates:

Affidavit

I hereby confirm that my thesis entitled “Engineering of chimeric antigen receptor T cells with enhanced therapeutic index in cancer immunotherapy using non-viral gene transfer and genome editing” is the result of my own work. I did not receive any help or support from commercial consultants. All sources and/or materials applied are listed and specified in the thesis.

Furthermore, I confirm that this thesis has not been submitted as part of another examination process neither in identical nor in similar form.

Place, date

Signature

Acknowledgements

I would like to express my sincere gratitude and appreciation to my main supervisor, Dr. Michael Hudecek for his guidance, encouragement and constructive criticisms, which brought to the completion of this thesis.

I would also like to sincerely thank my co-supervisors, Dr. Zoltán Ivics Prof. Dr. Hermann Einsele and Prof. Dr. Thomas Hünig for their valuable comments and advices during the entire progress of this project.

Acknowledgments are also extended to Dr. Csaba Miskey who kindly taught me integration site and copy number analyses and helped me with the corresponding experiments.

I owe my deepest gratitude to my labmates: Tea, Estefania, Silvia, Katrin, Sophia and Sabrina for not only their stimulating scientific discussions and helps but also for their love and cares. I would like to show my appreciations to my other labmates: Lars, Hardik, Markus, Julian, Irene, Tanja, Thomas, Julia, Silke, Elke, Fanni and Lyudmila for their kind helps.

I would also like to thank Dr. Gabriele Blum-Oehler and the staff of Graduate School of Life Sciences at University of Würzburg, for their invaluable support all through my PhD study.

I am truly thankful to my dear friends Masoumeh, Karolin, Cuijun, Razieh and Marzieh. I will never forget your cares and love.

Last but not the least, extremely huge thanks to my father, Mohammad Nasir Monjezi, my brothers, Rasoul and Hossein and other loved ones for their endless love, moral support and encouragement, without which I would have never been able to complete this important step of my life.

Dedication

To my adorable mum, Fatemeh Bavarsad (22 Dec.1961- 25 Feb. 2014),

for her unconditional love all through my life

for her patience during the years I was away to do my studies

and for letting me to follow my dreams

I was so blessed to have a mum like you.

Table of contents

Affidavit	3
Acknowledgements	4
Summary	9
Zusammenfassung (summary in German)	11
1 Introduction	14
1.1 Gene-modified T cells for cancer immunotherapy	14
1.2 CAR design and mode of action.....	15
1.3 Gene transfer strategies for CAR delivery into T cells	17
1.4 Discovery and classification of transposable elements.....	19
1.5 SB transposon and its transposition	20
1.6 Use of SB transposition in T-cell engineering.....	22
1.7 SB transposition from minicircle vectors.....	22
1.8 Genome editing to improve the therapeutic index of CAR T cells	23
1.9 Influence of PD-1 on antitumor function of T cells	24
1.10 T-cell genome editing with CRISPR/Cas9.....	26
1.11 Study objectives and specific aims.....	28
2 Materials	31
2.1 Equipment and consumables	31
2.2 Software	33
2.3 Chemicals and reagents	33
2.3.1 Molecular biology	33
2.3.2 Cellular biology and immunology	35
2.4 Kits from commercial vendors	36
2.5 FACS antibodies	37
2.6 Media and buffers	38
2.7 Cell lines	40
2.8 Human subjects	40
3 Methods	41
3.1 Cell culture.....	41
3.1.1 Isolation of human T-cell subsets	41
3.1.2 Preparation of lentiviral vectors	42
3.1.3 Titration of lentivirus	43

3.1.4	Lentiviral transduction of T cells	43
3.1.5	Enrichment of CAR ⁺ T cells prior to functional assays	44
3.1.6	Enrichment of <i>PD-1</i> knockout T cells after genome editing.....	44
3.1.7	Antigen dependent expansion of CD19-CAR T cells	45
3.1.8	Antigen independent expansion of <i>PD-1</i> knockout T cells	45
3.1.9	Preparation of CAR T-cell clones by limiting dilution for transposon copy number analysis	46
3.2	Immunological methods	46
3.2.1	Immunophenotyping.....	46
3.2.2	Cytotoxicity assay.....	47
3.2.3	Cytokine secretion assay and ELISA.....	47
3.2.4	CFSE proliferation assay.....	47
3.3	Preclinical <i>in vivo</i> experiments	48
3.3.1	Adoptive transfer of T cells in NOD/SCID/ γ c ^{-/-} (NSG) mice.....	48
3.3.2	Analysis of antitumor efficacy and persistence of CAR T cells.....	48
3.4	Molecular methods.....	49
3.4.1	Construction of transposon and lentiviral vectors.....	49
3.4.2	Cloning of PD-1 sgRNAs into lentiCIRSPR v2 plasmid.....	49
3.4.3	Nucleofection of T cells with SB vectors	50
3.4.4	Nucleofection of T cells with Cas9 RNP.....	51
3.4.5	Preparation of <i>in vitro</i> -transcribed RNAs.....	51
3.4.6	T7 endonuclease I assay.....	51
3.4.7	Integration site analysis of lentiviral and SB integrants	53
3.4.7.1	Construction of the SB insertion library and sequencing.....	53
3.4.7.2	Bioinformatic analysis.....	56
3.4.8	Copy number determination of SB insertions.....	57
3.4.8.1	Linker-mediated PCR	57
3.4.8.2	Droplet digital PCR.....	59
3.5	Statistical analysis.....	61
4	Results	62
4.1	Generation of CAR T cells through non-viral SB transposition from plasmids	62
4.2	Preparation of minicircle DNA vectors from conventional transposon and transposase plasmids.....	63
4.3	Transposition using minicircle DNA encoding transposase and transposon enables high level stable gene transfer in T cells	65
4.4	Use of minicircle DNA rather than plasmid DNA reduces electroporation-induced toxicity	68
4.5	Transposition from MCs using mRNA-encoded SB-transposase	68

4.6	MC-mediated SB-transposition confers potent antitumor functions to CD19-CAR T cells <i>in vitro</i>	71
4.7	CD19-CAR T cells generated via MC transposition show potent antitumor activity <i>in vivo</i>	74
4.8	Transposon insertion site analysis reveals a close-to-random genomic integration pattern in the genome of CD19-CAR T cells.....	76
4.9	CD19-CAR transposons mobilized from MCs are frequently integrated into genomic safe harbors	81
4.10	CD19-CAR MC transposon copy number analysis in the genome of T cells	82
4.11	CAR transposon copy numbers can be modulated using titrated amounts of MC DNAs.....	85
4.12	Interim conclusion for first aim.....	87
4.13	Editing of human <i>PD-1</i> in Jurkat cells using lentiCRISPR/Cas9	88
4.14	Editing of human <i>PD-1</i> in CD8+ T cells using lentiCRISPR/Cas9.....	91
4.15	Non-viral ablation of <i>PD1</i> in CD8+ T cells via Cas9 RNP	93
4.16	Single-step fully non-viral generation of <i>PD-1</i> KO CD19-CAR+ T cells via MC-based CAR transposition and Cas9 RNP	95
4.17	Interim conclusion	98
5	Discussion	100
5.1	Efficiency of SB transposition from MC DNAs for generating CAR T cells.....	100
5.2	Biosafety aspects of SB transposon insertions mobilized from MCs.....	102
5.3	Compatibility of CAR transposon copy numbers with clinical application.....	104
5.4	Generation of CD19-CAR T cells using MC-mediated transposition for clinical application	106
5.5	Non-viral KO of <i>PD-1</i> using Cas9 RNP to improve the therapeutic index of CAR T cells.....	107
5.6	Conclusion and perspective: roadmap to clinical translation	110
	List of figures.....	112
	List of tables	114
	List of abbreviations	115
	References	118
	Curriculum vitae	131

Summary

The advances in genetic engineering have enabled us to confer T cells new desired functions or delete their specific undesired endogenous properties for improving their antitumor function. Due to their efficient gene delivery, viral vectors have been successfully used in T-cell engineering to provide gene transfer medicinal products for the treatment of human disease. One example is adoptive cell therapy with T cells that were genetically modified with gamma-retroviral and lentiviral (LV) delivery vectors to express a CD19-specific chimeric antigen receptor (CAR) for cancer treatment. This therapeutic approach has shown remarkable results against B-cell malignancies in pilot clinical trials. Consequently, there is a strong desire to make CAR T cell therapy scalable and globally available to patients. However, there are persistent concerns and limitations with the use of viral vectors for CAR T cell generation with regard to safety, cost and scale of vector production. In order to address these concerns, we aimed to improve non-viral gene transfer and genome editing tools as an effective, safe and broadly applicable alternative to viral delivery methods for T-cell engineering.

In the first part of the study, we engineered CAR T cells through non-viral *Sleeping Beauty* (SB) transposition of CAR genes from minimalistic DNA vectors called minicircles rather than conventional SB plasmids. This novel approach dramatically increased stable gene transfer rate and cell viability and resulted in higher yield of CAR⁺ T cells without the need of long *ex vivo* expansion to generate therapeutic doses of CAR⁺ T cells. Importantly, CD19-CAR T cells modified by MC-based SB transposition were equally effective as LV transduced CD19-CAR T cells *in vitro* and in a murine xenograft model (NSG/Raji-ffLuc), where a single

administration of CD8+ and CD4+ CAR T cells led to complete eradication of lymphoma and memory formation of CAR T cells after lymphoma clearance.

To characterize the biosafety profile of the CAR T cell products, we did the most comprehensive genomic insertion site analysis performed so far in T cells modified with SB. The data showed a close-to-random integration profile of the SB transposon with a higher number of insertions in genomic safe harbors compared to LV integrants. We developed a droplet digital PCR assay that enables rapid determination of CAR copy numbers for clinical applications.

In the second part of the study, we ablated expression of PD-1, a checkpoint and negative regulator of T cell function to improve the therapeutic index of CAR T cells. This was accomplished using non-viral CRISPR/Cas9 via pre-assemble Cas9 protein and *in vitro*-transcribed sgRNA (Cas9 RNP). Finally, we combined our developed Cas9 RNP tool with CAR transposition from MC vectors into a single-step protocol and successfully generated *PD-1* knockout CAR+ T cells. Based on the promising results achieved from antibody-mediated PD-1 blockade in the treatment of hematological and solid tumors, we are confident that *PD-1* knockout CAR T cells enhance the potency of CAR T cell therapies for treatment of cancers without the side effects of antibody-based therapies.

In conclusion, we provide a novel platform for virus-free genetic engineering of CAR T cells that can be broadly applied in T-cell cancer therapy. The high level of gene transfer rate and efficient genome editing, superior safety profile as well as ease-of-handling and production of non-viral MC vectors and Cas9 RNP position our developed non-viral strategies to become preferred approaches in advanced cellular and gene-therapy.

Zusammenfassung (summary in German)

Die Fortschritte des genetischen Engineerings erlauben uns, T-Zellen neue, erwünschte Funktionen zu verleihen oder ihnen bestimmte, unerwünschte endogene Eigenschaften zu nehmen, um ihre Antitumorfunktion zu verbessern. Aufgrund ihrer Effizienz im Gentransport, werden virale Vektoren für das T-Zellengineering verwendet, um gentransferierte, medizinische Produkte zur Behandlung humaner Krankheiten herzustellen. Ein Beispiel hierfür ist die adoptive Zelltherapie mit T-Zellen, die mit gamma-retroviralen und lentiviralen (LV) Vektoren genetisch modifiziert wurden, so dass sie einen CD19-spezifischen chimären Antigenrezeptor (CAR) exprimieren. In klinischen Pilotstudien zu B-Zellerkrankungen zeigte dieser therapeutische Ansatz bereits beachtliche Erfolge. Hieraus resultiert das Bestreben, die CAR-T-Zelltherapie für Patienten skalierbar und weltweit zugänglich zu machen. Aufgrund gesundheitlicher Risiken, finanzieller Kosten und dem Umfang der Vektorenproduktion bestehen jedoch anhaltende Bedenken und Grenzen bezüglich der Verwendung viraler Vektoren für die Herstellung von CAR-T-Zellen. Um diese Problematiken zu umgehen, beabsichtigten wir, den nicht-viralen Gentransfer sowie genomverändernde Techniken soweit zu verbessern, dass sie als eine effiziente, sichere und umfassend einsetzbare Alternative zum virusbasierten T-Zellengineering verwendet werden können.

Im ersten Teil dieser Arbeit stellten wir durch die *Sleeping Beauty* (SB) Transposition von CAR-Genen auf minimalistischen DNA Vektoren (sogenannten Minicircles) CAR-T-Zellen her. Die Minicircles wurden anstelle von konventionellen SB Plasmiden verwendet. Mithilfe dieser neuen Vorgehensweise wurden die Rate des stabilen

Gentransfers sowie das Überleben der Zellen drastisch erhöht und führte zu einer gesteigerten Rate an CAR⁺ T-Zellen, ohne dass eine langwierige *ex vivo* Expansion zur Herstellung therapeutisch relevanter CAR-T-Zelldosen nötig wurde. CD19-CAR-T-Zellen, die mit MC-basierter SB-Transposition modifiziert wurden, zeigten *in vitro* und in einem murinen Xenograftmodell (NSG/Raji-ffLuc) eine vergleichbar hohe Effizienz, wie LV-transduzierte CD19-CAR-T-Zellen. Hierbei genügte eine einzige Verabreichung von CD4⁺ und CD8⁺ CAR-T-Zellen für eine komplette Eliminierung des Lymphoms und der anschließenden Gedächtnisbildung von CAR-T-Zellen. Um die Biosicherheit der CAR-T-Zellprodukte zu charakterisieren, führten wir die bislang umfassendste vergleichende Analyse von Genominsertionsstellen nach SB-basierter Modifikation von T-Zellen durch. Im Vergleich zur LV Integration zeigten diese Daten ein beinahe zufälliges Integrationsmuster des SB Transposons mit höheren Integrationsraten in genomisch „sicheren Häfen“. Wir entwickelten eine Analyse basierend auf digitaler Tröpfchen-PCR, um eine rasche Ermittlung der Anzahl an CAR-Genkopien in klinischen Anwendungen zu ermöglichen.

Im zweiten Teil der Arbeit verminderten wir die Expression von PD-1, einer Prüfzelle und negativen Regulator der T-Zellfunktion, um den therapeutischen Index der CAR-T-Zellen zu verbessern. Dies wurde durch die Verwendung eines nicht-viralen CRISPR/Cas9, durch das Zusammensetzen von Cas9 Protein und *in vitro*-transkribierter sgRNA (Cas9 RNP), erzielt. Schließlich verwendeten wir unsere entwickelte Cas9 RNP-Technik in Kombination mit CAR-Transposition von MC-Vektoren, um PD-1-knock out, CAR-positive T-Zellen herzustellen. Da die antikörperbasierte PD-1-Blockade in der Behandlung hämatologischer und solider Tumore vielversprechende Ergebnisse zeigt, sind wir zuversichtlich, dass PD-1-

knock out CAR-T-Zellen die Effizienz von CAR-T-Zelltherapien verschiedener Krebsarten verbessern können und dabei die Nebenwirkungen der antikörperbasierten Therapien umgehen.

Wir zeigen in der vorliegenden Arbeit Möglichkeiten mit virusfreien, gentechnischen Methoden CAR-T-Zellen herzustellen, die in der T-Zellkrebstherapie umfassend Anwendung finden können. Das hohe Level der Gentransferraten und der effizienten Genomeditierung, ein zu bevorzugendes Sicherheitsprofil sowie die einfache Handhabung und Produktion nichtviraler MC-Vektoren und Cas9 RNP machen es möglich, dass unser neuentwickelter, nichtviraler Ansatz zu einer bevorzugten Herangehensweise in der künftigen Zell- und Gentherapie werden kann.

1 Introduction

1.1 Gene-modified T cells for cancer immunotherapy

Cancer is one of the leading causes of morbidity and mortality worldwide. Approximately, 14 million new cases and 8.2 million cancer related deaths were reported in 2012. It is anticipated that annual rate of new cancer cases will reach 22 million within the next 2 decades¹. Conventional therapies including surgery, radio- and chemo-therapy as well as stem cell transplantation continue to be refined and are often effective in eliminating tumors. These treatments may confer long-term disease free survival and even cure in a proportion of patients. However, they are associated with toxic side effects, require extensive care, and extended treatments. Thus, there is a strong desire for more effective and safer treatment options with fewer side effects.

Recently, an improved understanding of cancer pathogenesis and advanced knowledge of immunology have given rise to novel treatments, including targeted therapies and cancer immunotherapy. Targeted approaches aim to inhibit molecular pathways that are crucial for tumor growth and maintenance; whereas, immunotherapy endeavors to stimulate a host immune response against tumor cells². Nowadays, by the aid of genetic engineering via introducing new desired transgenes or knock out of undesired endogenous genes it is possible to generate human T cells that display desired specificities and enhanced functionalities compared with natural immune system³⁻⁶. Cancer immunotherapy with T cells that are genetically modified to express a tumor-specific exogenous T cell receptor (TCR) or a tumor-targeting chimeric antigen receptor (CAR) has shown remarkable responses in patients⁷.

Intriguingly, a patient's own T cells can be used for genetic manipulation; these cells are expanded *ex vivo* and then infused back into the same patient based on the adoptive cell transfer protocols (ACT)^{8, 9} (Figure 1.1a). As T cells are capable of forming long-lasting memory, a single infusion may be sufficient to confer therapeutic antitumor effects and subsequently life-long protection from re-lapse, even in patients who show poor responses or are not responding to conventional treatments¹⁰. Consequently, cancer immunotherapy with TCR and CAR T cells is intensively investigated as a novel treatment modality in patients with hematologic malignancies and solid tumors^{7, 10-12}. T cells are conventionally engineered via viral vectors, which are associated with biosafety concerns, high production cost and regulatory demands. In this study, we aimed to enhance non-viral gene delivery and genome editing tools to improve engineering of T cells for broad clinical implementation and increase the therapeutic index of CAR T cells in cancer immunotherapy.

1.2 CAR design and mode of action

Chimeric antigen receptors (CAR) are synthetic receptors that link the antigen specificity of a monoclonal antibody (mAb) to the killing and proliferation capabilities of T cells. CARs are comprised of an extracellular domain derived from single-chain variable fragment (scFv) of a mAb, which serves as the antigen binding moiety. The extracellular spacer domain provides flexibility and reach for antigen binding. A transmembrane (TM) domain links the extracellular domain to an intracellular signaling/activation module, most commonly composed of a T cell receptor (TCR)-derived CD3 ζ chain and one or more co-stimulatory domains such as CD28 or 4-1BB (Figure 1.1b). Compared with endogenous TCRs, the mAb-derived targeting domain

of CARs provides them distinct attributes in antigen binding and tumor recognition¹³. In addition, CARs recognize intact cell surface proteins in a major histocompatibility complex (MHC)-independent manner. Therefore, most of the CAR-based approaches are insensitive to tumor escape mechanisms related to MHC loss variants¹⁴. However, in contrast to natural TCRs, CARs detection is limited to antigens that are expressed on the tumor cell surface.

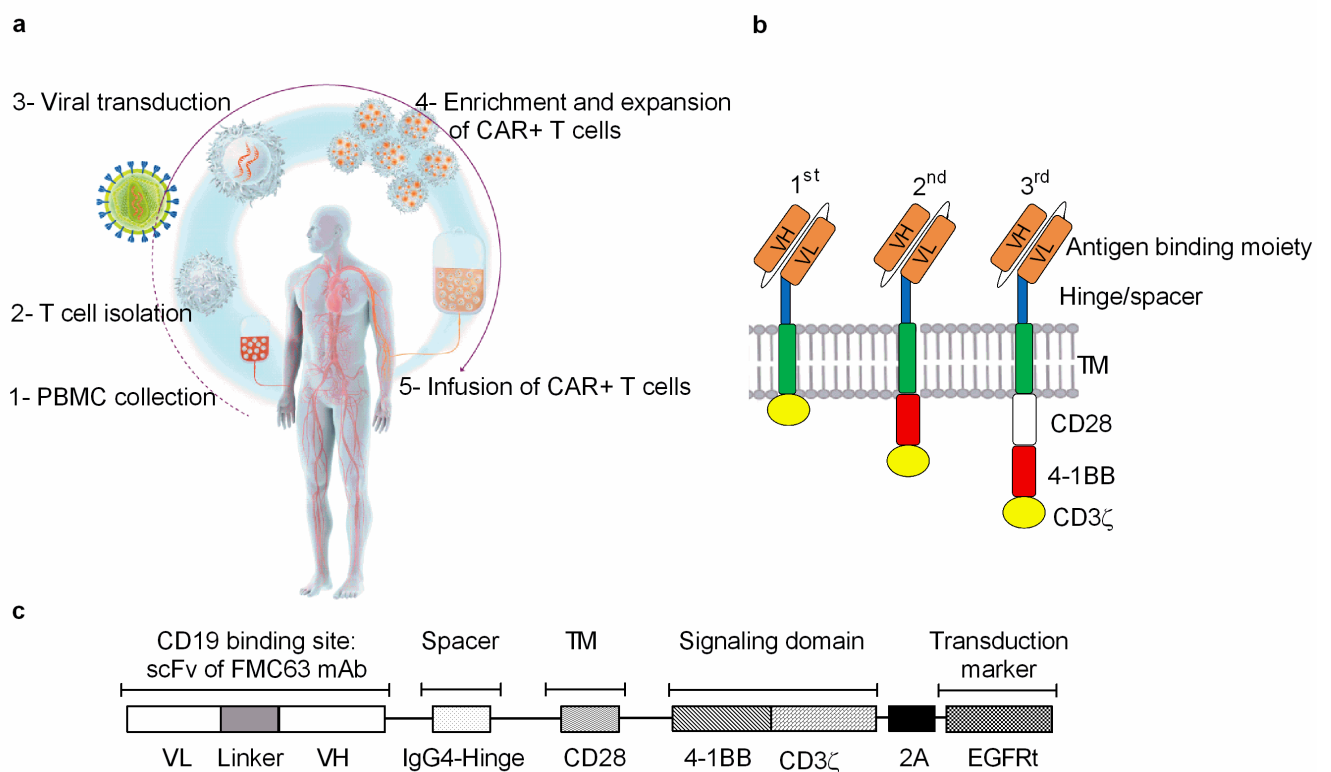


Figure 1.1. Immunotherapy with chimeric antigen receptor T cells.

(a) Clinical principle of chimeric antigen receptor (CAR) T-cell therapy. Desired T-cell subsets are isolated from a patient's own PBMC and transduced with viral vector encoding CAR construct. Afterwards, CAR+ T cells are enriched, expanded *ex vivo* and infused back into the patient. **(b)** General structure of first, second and third generation CARs. While 1st generation CARs only possess a CD3 ζ activation domain, 2nd and 3rd generation CARs are additionally equipped with one and two co-stimulatory domains, respectively. The extracellular domain of CAR consists of antibody-derived antigen binding scFv with the variable fragment of heavy chain, VH, and the variable fragment of light chain VL, which are connected with a linker. The hinge region connects scFv with the transmembrane domain (TM). The intracellular domain consists of the co-stimulatory domains (CD28 or 4-1BB) and the activating domain, CD3 ζ . **(c)** Structure of the second generation CD19 CAR construct used in this study. scFv is derived from FMC63 monoclonal antibody and fused to intracellular CD3 ζ and 4-1BB signaling domain via the hinge region of IgG4. The transmembrane domain is derived from CD28 and followed by human truncated epidermal growth factor (EGFRt) as transduction and depletion marker.

In this study, we used a second generation CD19 specific CAR that contains a scFv fragment derived from FMC63 mAb linked to the intracellular CD3 ζ and 4-1BB co-stimulatory domain by IgG4-hinge as a spacer domain. This CD19-CAR has been successfully used in clinical trials in acute lymphoblastic leukemia (ALL) and Non-Hodgkin lymphoma (NHL)⁷.

The CAR transgene is expressed from a cassette with EF1/HTLV hybrid promoter and is fused to a truncated form of human epidermal growth factor-receptor (EGFRt) by a T2A ribosomal skip sequence. The EGFRt serves as a transduction marker and a tool for enrichment of CAR expressing T cells (Figure 1.1c). Moreover, it can be used for depleting CAR T cells via EGFR binding antibodies^{15, 16}.

1.3 Gene transfer strategies for CAR delivery into T cells

Transgenes can be transferred into cells through viral and non-viral delivery vehicles. Integrative vectors are used to accomplish stable transgene expression. In contrast, non-integrative vectors result in short term expression of desired transgenes.

To generate CAR T cells with sustained antitumor potency and potential for memory formation, stable CAR expression is preferred. Lentiviral (LV) and γ -retroviral (RV) vectors have been successfully used for stable CAR expression with high CAR transfer rate in T cells¹⁷. However, they have several limitations as gene delivery vectors for gene therapy. First, their integration-site profile is associated with potential safety concerns. It is known that viral vectors have integration-site preferences for distinct regions of genome including active genes and active transcription units^{18, 19}. This integration-site preference can cause insertional mutagenesis. It has been reported that two of ten patients with X-linked severe

combined immunodeficiency that were treated by CD34+ hematopoietic stem cells (HSC) being engineered by RV vector developed T-cell leukemia due to insertional activation of *LMO-2* oncogene^{20, 21}. However, due to terminal differentiation, T cells may have a lower risk to experience insertional mutagenesis compared with HSC. In addition, the need for extensive purification and quality control to prevent replication-competent virus as well as the costs associated with their production and handling hampers their use for treatment of large cohorts of patients^{22, 23}. Further, laboratories involved in CAR/TCR research need to rapidly screen panel of new CAR designs and specifications. In this regard, non-viral vectors are preferred as they have a faster and easier production procedure. Non-viral vectors such as plasmid DNAs are cost effective for industrial and research scale production, stable during storage and have low/moderate immunogenicity and genotoxicity once are transferred into the host cells²⁴. However, there are two major problems regarding non-viral vectors in gene therapy. First, their episomal feature results in transient gene expression and loss of therapeutic efficacy over time. Second, they show inefficient gene delivery into specific cells^{25, 26}. During the past decade, introduction of a non-viral gene delivery system called *Sleeping Beauty* (SB) transposon has addressed the problem of stable transgene expression²⁷. This delivery system combines the advantages of integrating viral vectors (i.e. long-lasting transgene expression) with those of non-viral delivery systems (i.e. lower immunogenicity, enhanced safety profile and reduced cost of manufacturing)²⁸. However, the problem of gene transfer efficiency remains unsolved which we aimed to address in this study.

1.4 Discovery and classification of transposable elements

The cytogeneticist Barbara McClintock discovered transposable elements (TE) that are also known as jumping genes or transposons, in the 1940s in maize^{29, 30}. TEs are defined as discrete segments of DNA that have the distinctive ability to move and replicate within genomes. The idea of mobile DNA was not valued at this time when scientists saw genes as static structures in the nucleus. In the 1970s, other molecular biologists confirmed the molecular mechanism she demonstrated in the genome of maize. Finally, she was awarded the Nobel Prize in physiology and medicine in 1983 for her discovery.

TEs have been identified in all organisms and 45% of the human genome consists of them³¹, which are mostly inactive due to mutations or deletions. TEs can be divided into two major classes according to their mechanism of transposition. The majority of TEs, about 42%, belongs to the class I or retrotransposons. Transposition of retrotransposons is performed by a “copy-and-paste” mechanism, which requires an RNA intermediate. The RNA intermediate is reverse transcribed into a cDNA, which is then integrated at a new donor site as double stranded cDNA. This mechanism leaves the TE at the donor site intact and leads to insertion of an additional copy of the TE at a new target site³². About 3% of the human genome comprises members of the class II that are called DNA transposons. DNA transposons move directly as DNA, by a “cut-and-paste” mechanism of transposition. The element gets excised from the donor locus and is subsequently reinserted elsewhere³².

1.5 SB transposon and its transposition

Sleeping Beauty (SB) transposon belongs to class II of TEs. DNA transposons have been inactive in vertebrate for millions of years. In 1997, an ancient transposon fossils in salmonid fish was reactivated via reverse mutagenesis²⁷. This revived transposon was called *Sleeping Beauty* since it was “kissed” alive after a long inactive “sleep”. The original SB transposon is 1639 bp in length and contains one terminal inverted repeat (IR) of about 230 bp at each end. Each IR contains two direct repeats (DR) of about 32 bp. One DR is found directly on the outer end of the IR and the other 165-166 bp inwards the transposon. Each DR contains a core site for binding of the enzymatic component of the SB transposon system, so called the transposase, resulting in four transposase binding sites per transposon, two within each IR³³. In its natural form, the two IRs flanks transposase. However, the transposase gene can be separated from the IRs and be replaced by other DNA sequences³⁴. This is because transposase can mobilize transposons *in trans*, as long as they retain the IRs (Figure 1.2a). The transposase gene can be located on the same DNA molecule as the transposon³⁵, or supplied on another DNA molecule³⁶, or in the form of mRNA³⁷.

During the last years, SB has gone through a number of modifications in order to enhance the potency of the system for gene engineering³⁸. These includes molecular evolution of a hyperactive transposase called SB100X that yields enhanced stable gene transfer in several human cell types including T cells^{39, 40}. SB transposition process is a cut-and-pasted based event and is executed in four main steps: (1) binding of the transposase to its sites within the transposon IRs; (2) formation of a synaptic complex in which the two ends of the elements are paired and held together by transposase subunits; (3) excision of the transposon from the donor site; and

(4) joining of the transposon to a TA dinucleotide site in the target DNA and host-mediated repair of the double strand break (DSB) at the donor site^{32, 41, 42} (Figure 1.2b).

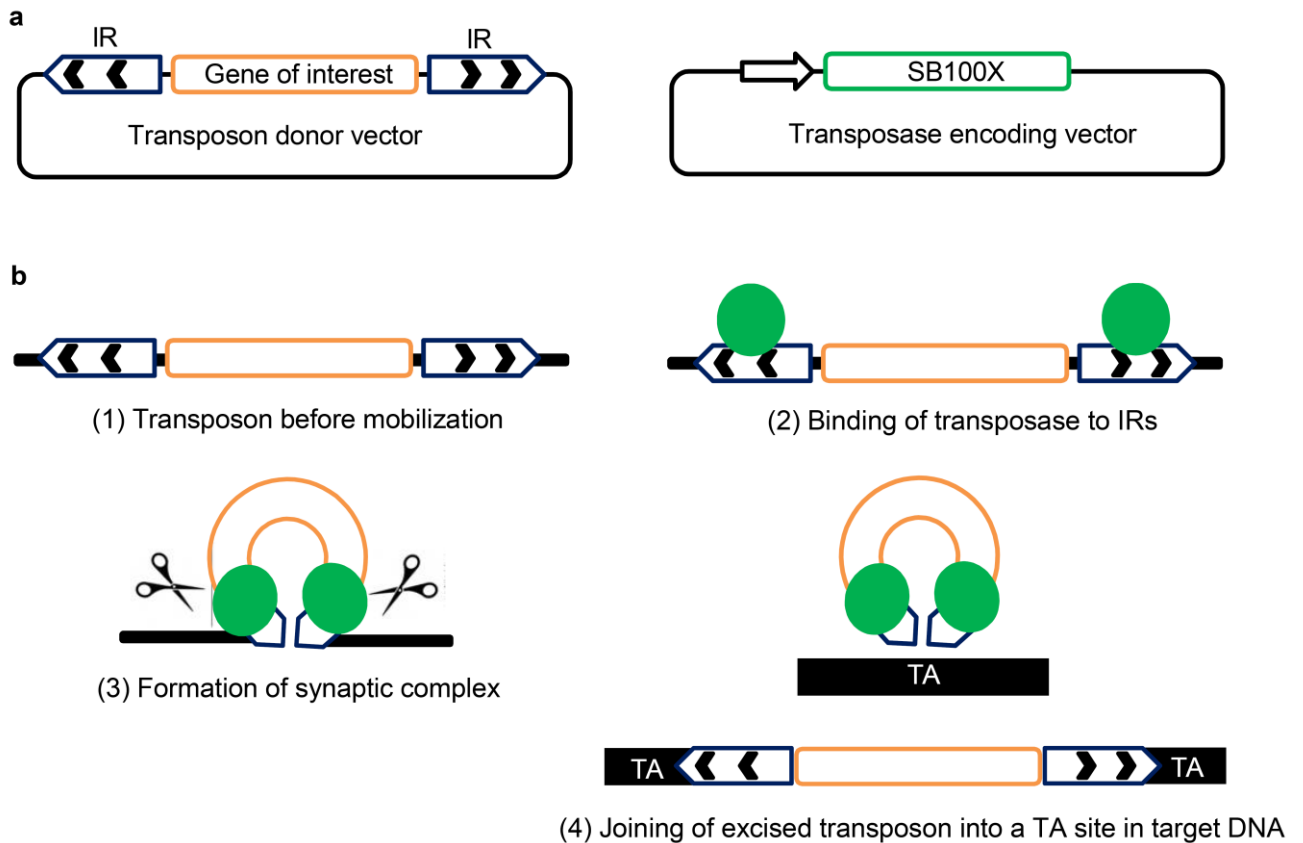


Figure 1.2. *Sleeping Beauty* and its mechanism of transposition.

(a) Components and structure of two-component *Sleeping Beauty* gene transfer system. A gene of interest is cloned between the terminal inverted repeats (IRs, pentagons) that contain binding sites for the transposase (black chevrons inside IRs). The SB100X hyperactive transposase (green box) is expressed from a separate vector. **(b)** The transposase (shown as circles) binds to its sites within the transposon IRs. Excision takes place in a synaptic complex. Excision separates the transposon from the donor DNA. The excised transposon integrates into a TA site in target genome that will be duplicated and will be flanking the newly integrated transposon.

One of the factors that affects the transposition activity is the molecular ratio of transposon to transposase. Within a certain range of concentration, more transposase in the cell results in an increase in transposition. However, when transposase concentration exceeds an optimal concentration in a given cell, one

experiences an inhibitory effect known as overproduction inhibition⁴³. Mechanism of this phenomenon is still unknown. Consequently, the optimal ratio of transposon to transposase needs to be determined in any given cell.

1.6 Use of SB transposition in T-cell engineering

The SB transposons have been used for gene delivery in animals and human cell culture and has shown great promise for use in human gene therapy⁴⁴.

The potential to use SB-mediated transposition to integrate CAR and TCR transgenes in human T cells has been investigated *in vitro*^{28, 45-47}. The first-in-human CAR T cell clinical trial presented a protocol for generating clinical grade CAR T cell via SB transposition in the USA⁴⁸. The trial illustrated some challenges for generating CAR T cells. First, this approach resulted in very low gene transfer rate. Second, it led to severe T-cell toxicity associated with electroporation of large sized plasmids. Third, long *ex vivo* culture time was required to generate therapeutic doses of gene-modified T cells, which led to an increase in the mRNA level of exhaustion markers^{48, 49}. Therefore, most investigators continue to use viral vectors to manufacture CAR-modified and other gene-engineered T cells^{11, 50-52}. To address these problems, we hypothesized that CAR transposition from smaller sized vector called minicircle DNAs rather than conventional SB plasmids that were used in this approach may enhance both transposition rate and cell viability and eventually reduce *ex vivo* culture time.

1.7 SB transposition from minicircle vectors

We have observed a correlation between the amount of electroporated plasmid and T-cell toxicity. On the other hand it is known that SB transposition efficiency is

correlated with the size of transposon donor plasmid^{53, 54}. When the plasmid size is reduced, lower amount of it can be used to achieve same molar amount for transfection. Moreover, a reduction in the size of SB plasmids will bring the left and right IRs closer to each other, which is known to lead in a better SB transposition activity^{38, 53, 54}. In order to enhance SB transposition activity and improve T-cell viability after electroporation, we produced minicircle DNA vectors (MCs) as an alternative to plasmids as sources of SB transposon and transposase. MCs are minimal expression cassettes derived from conventional plasmids via an intramolecular recombination step during propagation in *E. coli*⁵⁵⁻⁵⁷. The recombination step separates unwanted bacterial backbone from the desired transgene and the sequences it requires for expression. It has been shown that MCs are more stable and confer superior levels of transient gene expression compared to conventional plasmids when transfected into mammalian cells^{58, 59}. Further, MCs have been implemented as SB-transposon donors that following transfection, allowed stable genomic modification of HeLa cells⁵³. Transposition-mediated stable gene delivery out of MC vectors in primary human cells has to date not been explored. In order to enhance the efficiency of the SB system for T cell engineering, we set the first aim of this study to investigate the potential of SB mediated transposition from MC vectors for generating CAR-modified T cells.

1.8 Genome editing to improve the therapeutic index of CAR T cells

Introduction of CAR transgenes into T cells has substantially improved their antitumor function in the treatment of hematological malignancies. Moreover, some research groups have incorporated suicide genes like inducible caspase9 into CAR T cells to

enhance their safety feature for clinical application^{60, 61}. Apart from adding new desired features like tumor-specificity via gene transfer strategies, currently targeted nucleases have made it possible to edit the endogenous genes of T cells to improve their antitumor reactivity⁴. These additional genetic manipulations are required for improving the therapeutic index of CAR T cells to overcome the obstacles that have hampered their antitumor efficacy mostly against solid tumors. The resistance of solid tumors to CAR therapies may be due to multiple factors including physical and metabolic barriers, tumor-derived soluble factors and cytokines, immunosuppressive immune cells within tumor microenvironment as well as the intrinsic regulatory mechanism of T cells⁶². Consequently, in the second part of this study, we aimed to knock out programmed cell death 1 (*PD-1*) in CAR+ T cells as an example of immune checkpoint surface receptors that negatively regulates T cell antitumor response. Some solid tumors and hematological malignancies that have been treated by CAR T cells utilize this and other immune checkpoints to attenuate antitumor CAR T-cell responses⁶³⁻⁶⁵.

1.9 Influence of PD-1 on antitumor function of T cells

Programmed cell death protein 1 (PD-1), also known as CD279 is encoded by the *PDCD1* gene. PD-1 is an inhibitory receptor that exhibits minimal expression on resting cells and is broadly induced on activated T cells⁶⁶. It has two distinct ligands PD-1 ligand 1 (PD-L1) and PD-L2. PD-L1 is expressed on both hematopoietic and non-hematopoietic cells. Whereas, the expression of PD-L2 is more restricted to cells of the immune system⁶⁶. Interaction between PD-1 and its ligands recruits inhibitory signals that lead to reduction in T-cell cytokine production, proliferation and survival⁶⁷.

⁶⁸. The upregulation of PD-1 expression by tumor-infiltrating lymphocytes⁶⁹ along with the expression of PD-L1 by numerous tumor types⁷⁰ suggest that this pathway might be one of the limiting factors that induces T-cell anergy⁷¹ and hinders T cells in mediating antitumor reactivity within the tumor microenvironment. In particular, the broad expression pattern of PD-L1 on normal, non-hematopoietic cells is mirrored by PD-L1 expression on carcinomas of lung, breast, colon, kidney, bladder, ovary, and cervix, as well as non-epithelial tumors, including melanoma, glioblastoma, multiple myeloma, T-cell lymphoma, and various leukemias⁷²⁻⁷⁶. Systemic administration of anti-PD-1 antibodies like nivolumab that inhibit PD-1/PD-L1 pathway has resulted in durable objective responses in patients with non-small cell lung cancer, melanoma and renal cell carcinoma and Hodgkin lymphoma^{77, 78 79-84}. Of note, systematic administration of anti-PD-1 antibodies can result in some immune-related adverse events (IRAEs)⁷⁹.

Studies have shown that CAR T cells that lost their tumor reactivity after trafficking to solid tumor microenvironment, could retain their antitumor function when were isolated away from the tumor⁶⁴. This supports the impact of inhibitory signals within the tumor microenvironment in the failure of CAR T-cell therapy of solid tumors. Moreover, it has been demonstrated that blockade of the PD-1 immunosuppressive pathway significantly improves the function of human epidermal growth factor receptor-2 (HER-2)-specific CAR T cells and leads to enhanced tumor eradication in immune competent HER-2 transgenic mice⁸⁵. Recently, studies have shown that introduction of fusion receptors composed of PD-1 extracellular domain linked to the cytoplasmic domain of CD28 can enhance the tumor reactivity of tumor-specific T cells as well as the CAR T cells by reversing inhibitory effect of PD-1 binding^{86, 87}. In addition, mesothelin-specific CAR T cells that were genetically engineered to

obtain a PD-1 dominant negative receptor, could restore their effector function *in vitro* and *in vivo*⁶⁵. As an alternative strategy, *PD-1* can be knocked out specifically in CAR T cells using genome editing tools. Genome editing tools like clustered regularly interspaced short palindromic repeats/CRISPR-associated Cas9 nuclease (CRISPR/Cas9) may facilitate the generation of genome edited CAR T cells. Therefore, we set the second aim of this study to knock out *PD-1* in CAR+ T cells as an example of immune checkpoint receptors.

1.10 T-cell genome editing with CRISPR/Cas9

Over the last decade, targeted nucleases as powerful genome editing tools have revolutionized biological research and translational applications. Compared with protein-guided nucleases like zinc finger nucleases (ZFNs) and transcription activator-like effector nucleases (TALENs) RNA-guided nucleases such as CRISPR/Cas9 are cost-effective, highly efficient and have simple and easy design principles for broad genome editing application⁸⁸. The CRISPR/Cas9 system is originally a microbial adaptive immune system that uses RNA-guided nucleases to cleave foreign genetic elements^{89, 90}. It confers targeted gene editing via a single guide RNA (sgRNA) that guides the Cas9 endonuclease to the desired DNA locus through complimentary base pairing. Cas9 endonuclease creates a site-specific double strand break (DSB) on DNA substrates. This happens exclusively when a short DNA sequence, known as the protospacer adjacent motif (PAM) exists next to the twenty-nucleotide target site. The CRISPR/Cas9 system used in this study is derived from *Streptococcus pyogenes* that requires a 5'-NGG PAM in target site (Figure 1.3)^{88, 91, 92}. DNA cleavage triggers genome editing through two different DNA

repairing mechanisms. First, DSB is repaired by non-homologous end joining (NHEJ), which is an error-prone process that causes small insertions or deletions. Second, in the presence of a homologous recombination (HR) DNA template DSBs are repaired by homology-directed repair (HDR) mechanism. This enables targeted insertion of a desired DNA sequence into the genome⁹³.

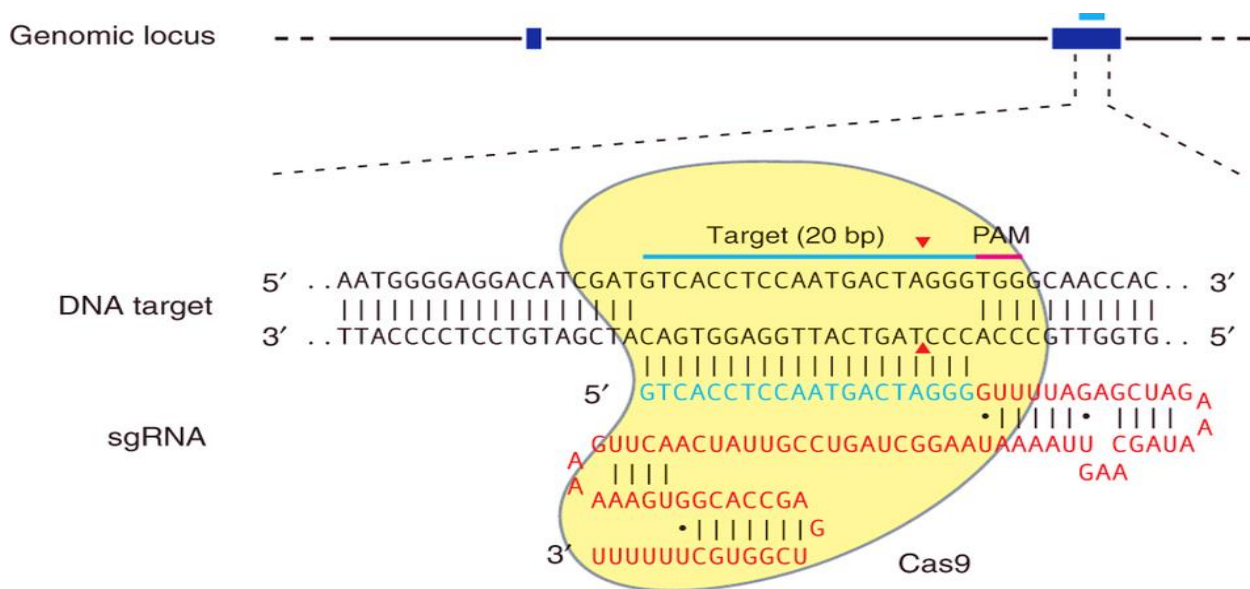


Figure 1.3. Schematic of CRISPR/Cas9 system.

A single guide RNA (sgRNA) is generated from 20 nucleotide guide (in blue) fused to a scaffold (in red). The guide sequence pairs with the target site (blue bar on top strand), which is followed by a requisite 5'-NGG adjacent motif (PAM; pink). Cas9 creates a DSB ~3 bp upstream of the PAM (red triangle)⁸⁸.

A large body of gene editing preclinical works has been performed via CRISPR/Cas9 technology to edit mammalian germ line sequences and cell lines^{94, 95}. Although, most investigators commonly transfer cas9 and sgRNA into cells via plasmid delivery, this method is not similarly efficient in T cells^{4, 96}. Recent reports demonstrate that pre-assembled recombinant Cas9 protein and *in vitro*-transcribed sgRNA (Cas9

ribonucleoprotein complex; Cas9 RNP) can accomplish genome editing in cultured mammalian cell lines with high specificity and precision compared with the plasmid delivery of the Cas9 and sgRNA. Use of short-lived Cas9 RNP reduces the off-target effects in this protocol^{97, 98}. Moreover, it has been shown that Cas9 RNP enables efficient ablation of target loci in human T cell genome^{99, 100}. Eventually, this allows T cells to be edited *ex vivo* and then reintroduced into patients. This strategy underscores the therapeutic potential of a non-viral CRISPR/Cas9-mediated genome editing method for disruption of immune inhibitory checkpoints, and other desired genome sequences that have a significant impact on clinical application of adoptive T-cell therapies of cancer^{4, 99}. Very recently, researchers managed to combine lentiviral delivery of CAR transgene with RNA electroporation of CRISPR/Cas9 to co-introduce the RNAs that encode the Cas9 and sgRNAs targeting endogenous *TCR*, *Beta-2 microglobulin (B2M)* and *PD-1* in T cell genome via a multi-step protocol¹⁰¹. However, so far no complete non-viral strategy for generating genome edited CAR T cells via a single-step protocol is reported.

1.11 Study objectives and specific aims

Immunotherapy with T cells that are modified with viral gene transfer to express a chimeric antigen receptor (CAR) has shown remarkable efficacy against B-cell malignancies in clinical trials⁷. However, the potential for insertional mutagenesis and genotoxicity of viral vectors is a safety concern, and the costs associated with their production, handling and regulatory demand a roadblock for rapid and broad clinical translation. Recently, the first-in-human clinical trial used non-viral *Sleeping Beauty* (SB) transposition for generating CAR T cells⁴⁸. This trial revealed several challenges

for generating CAR T cells via SB transposition. **(1)** This approach resulted in a very low gene transfer rate. **(2)** It caused high T-cell toxicity associated with the nucleofection of large sized plasmid DNAs. **(3)** Due to low gene transfer rate and high T-cell toxicity, long *ex vivo* culturing with extensive expansion cycles (median of 28 days) was required to generate therapeutic doses of gene-modified T cells, which led also to T-cell exhaustion^{48, 49}. To address these problems, we hypothesized that CAR transposition from smaller sized vectors known as minicircles may enhance both transposition rate and cell viability and reduce *ex vivo* culture time (Figure 1.4). This hypothesis led to the first objective of this study, which was:

- 1) to enhance non-viral *Sleeping Beauty* transposition for introduction of chimeric antigen receptors (CARs) into T cells using minicircle vectors.

Although adoptive transfer of CAR T cells has shown significant success in treating B-cell malignancies like B-ALL, its clinical proof of concept has not yet been obtained in solid tumor treatment. The resistance of solid tumors to CAR therapies may be due to multiple factors as mentioned before (section 1.8). There are studies demonstrating that utilization of checkpoint blockade antibodies like the ones that target PD-1/PD-L1 pathway enhances antitumor effects of CAR T cells in the treatment of solid tumors and lymphomas^{65, 85, 102}. However, there are some problems associated with combined CAR and antibody therapies. **(1)** Rapid expansion of PD-1-expressing CAR T cells due to stimulation by tumor antigens may require sequential administration of anti-PD-1 antibody. **(2)** The sequential systematic administration of the blocking antibodies carries the risk of severe IRAEs. **(3)** Long-term antibody treatment is costly. To address these issues we thought to

knock out *PD-1* as an example of immune checkpoint receptors specifically in CAR T cells. We hypothesized that combination of SB-mediated CAR transposition from MC vectors with disruption of *PD-1* via non-viral Cas9 RNP may lead to generation of *PD-1* knockout CAR+ T cells in a single-step (Figure 1.4). Hence, the second objective of this study was:

- 2) to establish a single-step and fully non-viral T-cell engineering strategy for generating *PD-1* knockout CAR T cells through the combination of SB-mediated CAR transposition from MCs and *PD-1* knockout via Cas9 RNP.

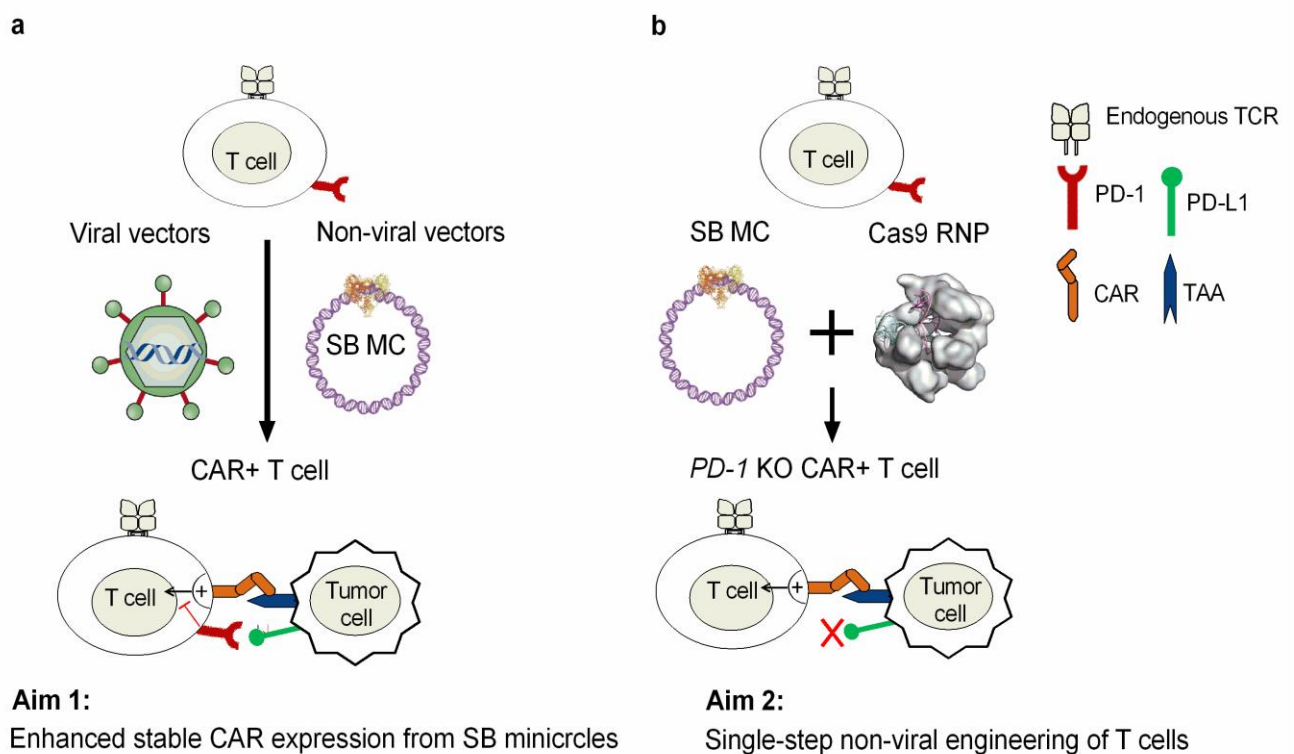


Figure 1.4. Improving non-viral gene delivery and genome editing strategies in T-cell engineering.

(a) The first objective of this study. We aimed to replace the conventional viral delivery for stable CAR expression on T cells with enhanced CAR transposition from SB MCs. **(b)** The second objective of the study. We aimed to generate *PD-1* KO CAR+ T cells via a fully non-viral strategy. In this single-step strategy, Cas9 RNP will edit *PD-1* locus and SB MCs will stably deliver CAR into T cells in a single electroporation reaction. SB MC: *Sleeping Beauty* minicircle DNA vectors, Cas9 RNP: Cas9 ribonucleoprotein, *PD-1* KO CAR+ T cells: *PD-1* knocked out CAR+ T cells, TAA: tumor-associated antigen.

2 Materials

2.1 Equipment and consumables

Equipment, consumable specification	Supplier
25, 75 cm ² surface area cell culture flasks	Corning, Kaiserslautern
96 well half-area plates, Corning® Costar®	Corning, Kaiserslautern
96 well PCR plate	Peqlab, Erlangen
96 well plate ,white, flat bottom, Corning® Costar®	Corning, Kaiserslautern
96, 48, 12, 24 well plates, Corning® Costar® U bottom	Corning, Kaiserslautern
Biocoll separating solution	Merck, Darmstadt
Biological safety cabinets, Herasafe™ KS	Thermo Fisher, Waltham, MA, USA
Centrifuge tubes, 10, 15, 50 mL	Geriener Bio-One, Frickenhausen
Centrifuge, Heraeus Megafuge 40R	Thermo Fisher, Darmstadt,
CO ₂ Incubators, Heracell™ 150i and 240i	Thermo Fisher, Darmstadt,
DG8™ Cartridges and Gaskets	Bio-Rad, Munich
Electrophoresis power supply, Consort E802	Consort, Turnhout, Belgium
Flow cytometer, BD FACSCanto™ II	BD Biosciences, Heidelberg
Flow cytometry tubes, Röhre 5 mL	Sarstedt, Nümbrecht
Gel electrophoresis system, Owl™ Minigel	Thermo Fisher, Darmstadt
Gel imaging system, ChemiDoc™ MP	Bio-Rad, Munich
Heat block, neoBlock1	neoLab, Heidelberg
Ice maker	Scotsman, Vernon Hills, IL, USA
Incubator	Memmert, Schwabach
Leucosep tubes	Geriener Bio-One, Frickenhausen

Equipment, consumable specification	Supplier
M220™ Focused-ultrasonicator™	Covaris, Woburn, MA, USA
MACS separation columns, 25 LS	Miltenyi, Bergisch Gladbach
Microcentrifuge, Fresco 17	Thermo Fisher, Darmstadt
Microscope, Primo Vert	ZEISS; Jena
Multimode multiplate reader ,Infinite 200 PRO	TECAN- Männedorf, Switzerland
NanoDrop 2000	Thermo Fisher, Darmstadt
Nucleofector, 4D-Nucleofector™ X Unit	Lonza, Basel, Switzerland
PCR thermal cycler, Mastercycler, ep Gradient	Eppendorf, Hamburg
PCR thermal cycler, Mastercycler, Personal	Eppendorf, Hamburg
Pierceable Foil Heat Seal	Bio-Rad, Munich
PX1™ PCR Plate Sealer	Bio-Rad, Munich
QX100™ Droplet Generator	Bio-Rad, Munich
QX100™ Droplet Reader	Bio-Rad, Munich
Refrigerator, -4 and -20 °C	Liebherr, Bulle, Switzerland
Rnase free Biosphere plus SafeSeal microtube,1.5 mL	Sarstedt, Nümbrecht
Shaker Incubator	INFORS HT, Basel, Switzerland
Ultracentrifuge, Sorvall WX80	Thermo Fisher, Darmstadt
Ultra-low temperature freezer, -80 °C FORMA 900	Thermo Fisher, Darmstadt
UV transilluminator	neoLab, Heidelberg
Water bath	Memmert, Schwabach

2.2 Software

Software	Application	Company
BEDtools v2.17	Illumina data analysis	
Bowtie	Illumina data analysis	
FlowJo X 10.0.7	FACS analysis	Tree Star Inc. Ashland, OR, USA
Graphpad Prism 6	Statistical analysis	La Jolla, CA, USA
Image Lab™	T7EI analysis	Bio-Rad, Munich
QuantaSoft	ddPCR analysis	Bio-Rad, Munich
SeqLogo tool	Illumina data analysis	
Shortread tool in R	Illumina data analysis	

2.3 Chemicals and reagents

2.3.1 Molecular biology

Name	Manufacturer
0.5-10 Kb RNA Ladder	Invitrogen, Karlsruhe
1 Kb DNA Ladder	NEB, Frankfurt am Main
100 bp DNA Ladder	NEB, Frankfurt am Main
Antarctic Phosphatase	NEB, Frankfurt am Main
Cas9 protein	PNA Bio, Newbury Park, CA, USA
CviQI	NEB, Frankfurt am Main
ddPCR™ Supermix	Bio-Rad, Munich
DEPC	Sigma-Aldrich, Steinheim
dNTP Mix (10 mM)	Invitrogen, Karlsruhe
DpnI	NEB, Frankfurt am Main

Name	Manufacturer
Droplet Generation Oil for Probes	Bio-Rad, Munich
EcoRI	NEB, Frankfurt am Main
Ethanol absolute for molecular biology	AppliChem, Darmstadt
FspBI	Fermentas, St-Leon-Rot
GelRed™ Nucleic Acid Gel Stain	Biotium, Ferment, CA, USA
Isopropyl alcohol	Sigma-Aldrich, Steinheim
LB Agar plates with 100 µg/mL Carbenicillin	TEKnova, Hollister, CA, USA
LB Agar plates with 34 µg/mL Chloramphenicol	TEKnova, Hollister, CA, USA
LB Agar plates with 50 µg/mL Kanamycin	TEKnova, Hollister, CA, USA
LB broth 1x	Thermo Fisher, Darmstadt
NEBNext dA-Tailing Module	NEB, Frankfurt am Main
NEBNext End Repair Module	NEB, Frankfurt am Main
NEBNext High-Fidelity 2x PCR Master Mix	NEB, Frankfurt am Main
NEBuffer 2	NEB, Frankfurt am Main
NEBuffer 3.1	NEB, Frankfurt am Main
NheI	NEB, Frankfurt am Main
PacI	NEB, Frankfurt am Main
Phusion® High-Fidelity DNA polymerase	NEB, Frankfurt am Main
PmeI	NEB, Frankfurt am Main
RNaseZap® RNase	Ambion, Carlsbad, CA, USA
SacI	NEB, Frankfurt am Main
Standard Taq DNA polymerase	NEB, Frankfurt am Main
T4 DNA Ligase	NEB, Frankfurt am Main

Name	Manufacturer
T4 Polynucleotide Kinase (TPK4)	NEB, Frankfurt am Main
T7 Endonuclease I	NEB, Frankfurt am Main
Tris-acetate-EDTA (TAE) 50x	Sigma-Aldrich, Steinheim
Tris-EDTA Buffer Solution (TE, pH 8.0)	Sigma-Aldrich, Steinheim
Water, molecular biology grade	AppliChem, Darmstadt

2.3.2 Cellular biology and immunology

Name	Manufacturer
2-Mercaptoethanol	Life Technologies, Darmstadt
7-AAD	BioLegend, Fell
Anti-biotin MicroBeads	Miltenyi, Bergisch Gladbach
Anti-CD62L MicroBeads	Miltenyi, Bergisch Gladbach
Anti-PE MicroBeads	Miltenyi, Bergisch Gladbach
Cell trace CFSE	Life Technologies, Darmstadt
Dimethyl sulfoxide (DMSO)	Sigma-Aldrich, Steinheim
D-Luciferin firefly, Potassium Salt	Biosynth, Staad, Switzerland
Dulbecco's Modified Eagle Medium (DMEM)	Life Technologies, Darmstadt
Dulbecco's Phosphate-Buffered Saline (DPBS)	Life Technologies, Darmstadt
Dynabeads® Human T-Activator CD3/CD28	Life Technologies, Darmstadt
Ethylenediaminetetraacetic acid (EDTA) 0.5 M	Life Technologies, Darmstadt
Fetal calf serum (FCS)	Life Technologies, Darmstadt
GlutaMax-I 100X	Life Technologies, Darmstadt

Name	Manufacturer
Glutamine 200 mM	Life Technologies, Darmstadt
HEPES 1M	Life Technologies, Darmstadt
Human AB Serum	Bayerisches Rotes Kreuz
Ionomycin	Sigma-Aldrich, Steinheim
PBS, pH 7.4, contains TWEEN® 20 (dry powder)	Sigma-Aldrich, Steinheim
PE Streptavidin 0.2 mg/mL	BioLegend, Fell
Penicillin/Streptomycin 10,000 U/mL	Life Technologies, Darmstadt
Phorbol 12-myristate 13-acetate (PMA)	Sigma-Aldrich, Steinheim
Polybrene (Millipore, 10 mg/mL)	Merck, Darmstadt
Purified Anti-human CD3 (OKT3)	Life Technologies, Darmstadt
Recombinant human IL-2 (PROLEUKIN® S)	Novartis, Basel, Switzerland
RPMI 1640, GlutaMAX™ Supplement, HEPES	Life Technologies, Darmstadt
Trypan blue	Life Technologies, Darmstadt

2.4 Kits from commercial vendors

Kit	Manufacturer
CalPhos Mammalian Transfection Kit	Clontech, Taraka
DNA Clean and Concentrator Kit	Zymo Research
ELISA Max™ Set Deluxe (IL-2 and IFN γ kits)	BioLegend
MEGAclean™ Kit	Ambion
MEGashortscript™ Kit	Ambion
mMESSAGE mMACHINE® T7 Ultra Kit	Ambion
NEBNext dA-Tailing Module	NEB

Kit	Manufacturer
NEBNext End Repair Module	NEB
NucleoBond® Xtra Maxi EF	MACHEREY-NAGEL
Nucleofector™ Kits for Human T Cells	Lonza
PureLink Genomic DNA Mini kit	Invetrogen
PureLink Quick Gel Extraction PCR Purification kit	Invetrogen
PureLink Quick Plasmid Miniprep Kit	Invetrogen
TOPO® TA Cloning® Kit	Invetrogen
Zero Blunt® PCR Cloning Kit	Invetrogen

2.5 FACS antibodies

Ligand	Clone/Poly	Conjugation	Isotype	Manufacturer
CD279 (PD-1)	PD1.3.1.3	PE	Mouse IgG2b	Miltenyi
CD3	BW264/56	APC	Mouse IgG2a, k	Miltenyi
CD4	SK3	PerCP	Mouse IgG1, k	BD Biosciences
CD4	M-T466	VioBlue	Mouse IgG1, k	Miltenyi
CD45	HI30	FITC	Mouse IgG1, k	BD Biosciences
CD45RA	L48	FITC	Mouse IgG1, k	BD Biosciences
CD45RO	UCHL1	PE	Mouse IgG2, k	BD Biosciences
CD62L	DREG-56	PE	Mouse IgG1, k	BioLegend
CD8	BW135/80	VioBlue	Mouse IgG2a, k	Miltenyi
EGFR (Cetuximab)	C225	Biotin	Human IgG1, k	ImClone LLC
EGFR (Cetuximab)	C225	AlexaFluor 647	Human IgG1, k	ImClone LLC

2.6 Media and buffers

T cell medium (TCM)

1640 RPMI, with 25 mM HEPES and Glutamax	500 mL
Human AB Serum (heat inactivated at 56 °C for 30 min)	10%
Penicillin/Streptomycin 10,000 U/mL	100 U/mL
GlutaMax-I 100X	1%
2-Mercaptoethanol 50 mM	0.1%
Mix all components and filter sterilize (0.22 µm PES-membrane)	

Tumor cell lines medium

1640 RPMI, with 25 mM HEPES and Glutamax	500 mL
FCS	10%
Penicillin/Streptomycin 10,000 U/mL	100 U/mL
Glutamine 200 mM (100X)	1%
Mix all components and filter sterilize (0.22 µm PES-membrane)	

Adherent cell lines medium (cDMEM)

DMEM	500 mL
FCS	10%
Penicillin/Streptomycin 10,000 U/mL	100 U/mL
Glutamine 200 mM (100X)	1%
HEPES 1M	2.5%
Mix all components and filter sterilize (0.22 µm PES-membrane)	

T cell freeze-down medium

TCM	80%
Human AB Serum	10%
DMSO	10%

Mix all components and filter sterilize (0.22 µm PES-membrane)

Tumor cell freeze-down medium

Tumor cell lines culture medium	50%
FCS	40%
DMSO	10%

Mix all components and filter sterilize (0.22 µm PES-membrane)

MACS buffer

DPBS	500 mL
EDTA 0.5 M	0.4%
FCS	0.5%

Mix all components and filter sterilize (0.22 µm PES-membrane)

FACS buffer

DPBS	500 mL
EDTA 0.5 M	0.4%
FCS	0.5%
Sodium azide (NaN ₃)	0.1%

PBS/EDTA

DPBS	500 mL
EDTA 0.5 M	0.4%
FCS	0.5%

2.7 Cell lines

Name	Description/modification
JeKo-1 (ATCC: CRL-3006)	Lymphoma
Jurkat (ATCC TIB-152)	Clone E6-1, acute T-cell leukemia
K562 (ATCC: CCL-243)	Chronic myelogenous leukemia, transduced with ffluc
K562/CD19	K562 cell line transduced with ffluc and CD19
Lenti-X (Clontech)	293-T HEK
Raji (ATCC: CCL-86)	Burkitt lymphoma, transduced with ffluc
TM-LCL	Lymphoblastoid cell line, EBV-transformed B cell line, donor initials: TM

2.8 Human subjects

Peripheral blood was obtained from healthy donors after written informed consent to participate in research protocols approved by the Institutional Review Board of the University of Würzburg (UW).

3 Methods

3.1 Cell culture

3.1.1 Isolation of human T-cell subsets

Peripheral blood mononuclear cells (PBMCs) were isolated from healthy donor peripheral blood by density centrifugation over Ficoll-Hypaque. Blood was mixed with room temperature DPBS at maximum final volume of 35 mL and carefully added to a 50 mL Leucosep tube that was previously equilibrated with 15 mL of room temperature Biocoll separating solution. Density centrifugation was performed for 15 min, at 310 x g, at 22 °C, with acceleration and deceleration settings of 9 and 2, respectively. The PBMCs accumulate above of the Leucosep filter. These cells were washed twice with cold (4 °C) PBS/EDTA buffer, and centrifuged for 10 min at 220 x g, at 4 °C. The cells were then directly used for MACS separation. CD8 and CD4 bulk, naïve or memory T cells were purified by negative isolation using Miltenyi MACS MicroBeads and magnetic cell separation protocol according to manufacturer's instruction. Central memory T cells were purified from the memory subsets by positive selection for CD62L. For magnetic separation, LS columns were used for up to 150x10⁶ cells. Isolated cells were cultivated overnight in TCM (T cell culture medium) including 50 U/mL of recombinant human IL-2 (rh IL-2) and were activated with anti-CD3/CD28 Dynabeads at a cell to bead ratio of 1:1 (Life Technologies) for further experimental procedures.

3.1.2 Preparation of lentiviral vectors

Lentiviral vectors were produced in 293T-HEK cells (Lenti-X). To produce CD19-CAR encoding lentiviral vector 15 µg of CD19 CAR-encoding lentiviral plasmid and 10 µg, 1 µg and 2 µg of three helper plasmids, PCHGP-2, PCMV-Rev2 and PCMV-G were used per 10 cm² petri dish, respectively. For lentiviral vectors encoding Cas9 and *PD-1* specific single guide RNAs (sgRNAs), 20 µg of lentiCRISPR v2 plasmids encoding Cas9 and different sgRNAs, 5 µg of pMD2.G and 10 µg of psPAX2 were used per 10 cm² petri dish.

Lenti-X cells were cultured at 80% cell confluency in 10 cm² petri dishes, with three plates being used for one batch of lentivirus and incubated for six hours to allow cells to settle. Transfection with the lentiviral and helper plasmids was performed using a calcium phosphate-based method (Clontech). The plasmids at the appropriate ratios and amounts were diluted in 2 M CaCl₂ solution and the final volume set to 500 µL per petri dish with dH₂O (1500 µL for 3 plates). The plasmid mixture was drop wise added to equal volume of 2x HEPES-buffered saline (HBS). The mixture (3 mL) was incubated for 20 min at room temperature, equal amount of DMEM/10%FCS were added to the mixture and 2 mL of the final DNA suspension was added to each plate in a slow drop-wise manner and the plates were gently twirled to distribute the DNA mixture evenly. Plates were incubated at 37 °C overnight. Viral supernatant from 3 plates was collected into one 50 mL centrifuge tube 72 hours after transfection. It was centrifuged at 2160 x g for 15 min at 8 °C to remove any cell debris, passed through a 0.45 µm vacuum filter unit and was added to one centrifuge tube underlaid with 4 mL of 20% sucrose. The sample was centrifuged at 138510 x g for 2 hours at 4 °C by ultracentrifugation. The viral pellet was covered with 200 µL of PBS and after at

least 3 hours incubation at 4 °C was resuspended and aliquoted in 20 µL fractions. Viral vectors were stored at -80 °C for future use.

3.1.3 Titration of lentivirus

In order to determine the viral titer, Jurkat cells were plated in a 48-well plate at a cell density of 1×10^6 cells/mL in 250 µL of tumor cell lines culture medium with 5 µg/mL polybrene that facilitates viral entry into the cells. Serial dilutions of lentivirus (0.5, 1, 2, 5 or 10 µL) were added to consecutive wells and incubated for 4 hours at 37 °C. Following incubation, the medium was topped up to 1 mL and the cells cultured for another 48 hours. For CD19-CAR expressing vectors, CAR expression was analyzed by flow cytometry using the EGFRt transduction marker encoded within the lentiviral vector¹⁵. For lentiCRISPR v2 construct which carries a puromycin resistant gene, cells were treated with 1 µg/mL of puromycin and number of living cells were determined using trypan blue staining method 3 days after puromycin addition. The lentivirus titer in transforming units (TU)/mL was calculated using the following equation based on the percentage of EGFRt positive cells for CAR constructs or living cells for lentiCRISPR v2 constructs:

$$\text{Virus titer (TU/mL)} = \frac{\text{Cell count at day of transduction} + \frac{\% \text{ EGFRt+ /living cells}}{100}}{\text{Volume of virus added (mL)}}$$

3.1.4 Lentiviral transduction of T cells

Prior to lentiviral (LV) transduction, T cells were cultured at a density of $0.25 - 0.5 \times 10^6$ T cells/mL in a 48-well plate in TCM with 50 U/mL rh IL-2 and were activated with anti-CD3/CD28 Dynabeads (Life Technologies). The following day, 2/3 of medium

was removed; CAR-encoding lentivirus at a multiplicity of infection (MOI) of 5, and polybrene at a final concentration of 5 $\mu\text{g}/\text{mL}$ were added to the T cells, and inoculation performed by centrifugation at 800 $\times g$ for 45 min at 32 °C. For lentiCRISPR v2 viral vectors the MOI of 0.5 was used. Following centrifugation, the T cells were immediately transferred to 37 °C, rested for 4 hours, and then 1 mL of fresh, warm TCM and 50 U/mL rh IL-2 were added to each well. During subsequent days, a half-medium change with pre-warmed TCM was performed and rh IL-2 supplemented to a final concentration of 50 U/mL every second day. The anti-CD3/CD28 Dynabeads were removed using a hand-held magnet on day 6 post-stimulation and the T cells were transferred to larger plates or tissue culture flasks (12-well plate, then T25 flask) as appropriated to propagate.

3.1.5 Enrichment of CAR+ T cells prior to functional assays

Prior to functional testing, EGFRt-positive T cells that were generated whether via lentiviral transduction or nucleofection of SB vectors were enriched using biotin-conjugated anti-EGFR mAb and anti-biotin MicroBeads (Miltenyi), and were expanded in an antigen dependent manner with irradiated TM-LCL feeder cells for 7 days.

3.1.6 Enrichment of *PD-1* knockout T cells after genome editing

Prior to enrichment, T cells modified with CRISPR/Cas9 for *PD-1* knockout were activated with 1 μL of each PMA (1 mg/mL) and Ionomycin (1 mM) per 1×10^6 cell/mL in TCM for 24-36 hours. PMA/Ionomycin (PMA/Iono) stimulation recruits the expression of PD-1 on T-cell surface. In the next step, *PD-1* knocked out T cells were

enriched using anti-PD-1 PE antibody and anti-PE MicroBeads (Miltenyi) via negative selection based on manufacturer's protocol.

3.1.7 Antigen dependent expansion of CD19-CAR T cells

Following enrichment, and before functional assays, EGFRt+ CD8+ and CD4+ T-cell subsets were expanded by irradiated TM-LCL (80 Gy) cells at a T cell to TM-LCL ratio of 1:7. Next day, cultures were supplemented with 50 U/mL of rh IL-2 and cells were fed with fresh TCM and 50 U/mL rh IL-2 every second day. The phenotype of the expanded T cell lines was analyzed on day 7 of expansion.

3.1.8 Antigen independent expansion of *PD-1* knockout T cells

Following the treatment with puromycin, T cells transduced with lentiCRISPR v2 vectors were expanded by stimulation with anti-CD3 mAb (OKT3) and irradiated feeder cells as described¹⁰³. In brief, OKT3 was used at a final concentration of 30 ng/mL, irradiated TM-LCL (80 Gy) were used at a T cell to TM-LCL ratio of 1:100 and irradiated PBMC (30 Gy) were used at a T cell to PBMC ratio of 1:600. The cell cultures were supplemented with 50 U/mL of rh IL-2 on day 1. A complete medium change performed on day 4, and the cell cultures were fed with fresh medium and 50 U/mL rh IL-2 every second day.

3.1.9 Preparation of CAR T-cell clones by limiting dilution for transposon copy number analysis

After EGFRt enrichment, T cells were cultured at concentrations of 0.5 to 2 cells/well. For each setting (i.e. 0.5, 1, 2 cells/well), a master mix in a sterile reservoir that contained T cell culture medium, irradiated TM-LCLs and PBMCs, 50 U/mL rh IL-2 and diluted T cells in a final volume of 200 μ L/well was prepared, mixed well and distributed to 96-well plates using a multichannel pipette. The plates were wrapped in aluminum foil to prevent evaporation of medium and incubated for up to 10-14 days in a CO₂ incubator. The plates were screened on day 10 or 11 for positive wells. Prior to flow cytometry analysis a master-plate with positive clones was created. EGFRt+ clones were further expanded using antigen dependent expansion protocol.

3.2 Immunological methods

3.2.1 Immunophenotyping

T cells were washed by centrifugation at 200 x g for 4 min with FACS buffer and stained with the following conjugated mAbs: CD4, CD8, CD45RA, CD45RO and CD62L, hCD45 and CD279 (for PD-1) in FACS buffer and incubated for 25 min at 4 °C, washed as above; cells were resuspended in FACS buffer before flow cytometry measurement. Viability staining solution 7-AAD was used for exclusion of dead cells. CAR+ (i.e. EGFRt+) T cells were detected by staining with biotin-conjugated anti-EGFR antibody (ImClone Systems Inc.) and PE-streptavidin or by staining with anti-EGFR antibody conjugated to AlexaFluor 647. Flow cytometry measurements were performed on a BD FACSCanto II and data analyzed using FlowJo software (Treestar).

3.2.2 Cytotoxicity assay

Target cells expressing firefly luciferase were incubated in triplicate at 5×10^3 cells/well with effector T cells at various effector to target (E: T) ratios in a white 96-well flat bottom plate at a final volume of 150 μ L. After 4-hour incubation, luciferin substrate was added to the final concentration of 0.3 mg/mL to the co-culture and the luminescence signal in wells that contained target cells and T cells was measured using a luminometer (Tecan) and compared to target cells alone. Specific lysis was calculated using the standard formula¹⁰⁴.

3.2.3 Cytokine secretion assay and ELISA

5×10^4 T cells were plated in triplicates with target cells at a ratio of 2:1 (Raji and Jeko-1), or 4:1 (K562/CD19 and K562). After 24-hour incubation, concentrations of secreted IFN- γ and IL-2 in supernatant of co-culture were measured by ELISA kits (BioLegend) based on manufacturer's protocol.

3.2.4 CFSE proliferation assay

For analysis of proliferation, 5×10^4 T cells were labeled with 0.2 μ M carboxyfluorescein succinimidyl ester (CFSE, Thermo Fisher). After quenching the excess CFSE with FCS, cells were washed and plated in triplicates with target cells at a ratio of 4:1 (K562/CD19 and K562) in medium without exogenous cytokines. After 72-hour incubation, cells were labeled with anti-CD8/CD4 mAb and 7-AAD to exclude dead cells from analysis. Samples were analyzed by flow cytometry and division of living T cells was assessed by CFSE dilution. The proliferation index was calculated using FlowJo software.

3.3 Preclinical *in vivo* experiments

The University of Würzburg Institutional Animal Care and Use Committee approved all mouse experiments. Six- to eight-week old female NSG mice were obtained from Charles River. The NSG/Raji model has been described before¹⁰⁵.

3.3.1 Adoptive transfer of T cells in NOD/SCID/ γ c-/- (NSG) mice

Six- to eight-week old female NSG mice were inoculated with 5×10^5 firefly luciferase expressing Raji tumor cells by tail vein injection on day 0. On day 7, groups of $n=5$ mice received intravenous injections of 5×10^6 CAR-modified or unmodified control (mock) T cells containing equal proportions of CD8+ and CD4+ T-cells.

3.3.2 Analysis of antitumor efficacy and persistence of CAR T cells

Bioluminescence imaging was performed weekly to determine tumor burden and distribution in mice. Blood samples were obtained 3, 7 and 14 days after T cell transfer (i.e. day 10, 14, 21 after tumor inoculation) and frequency of human T cells in the peripheral blood was determined by staining with anti-human CD45, anti-hCD3, anti-hCD4 and anti-hCD8 antibodies by flow cytometry analysis. Bone marrow of mice were harvested upon termination of the experiment on day 35 after tumor inoculation. Persistence of CAR T cells and presence of tumor cells in the bone marrow were tested by flow cytometry. Finally, survival of mice was analyzed by Kaplan-Meier analysis.

3.4 Molecular methods

3.4.1 Construction of transposon and lentiviral vectors

A DNA cassette with EF1/HTLV hybrid promotor, Kozak and eGFP sequence followed by a Stop codon was synthesized (GeneArt, Regensburg, Germany) and subcloned into the pT2/HB transposon donor vector³³ (kind gift from Perry Hackett, Addgene plasmid #26557). Then, the eGFP sequence was replaced with a gene encoding a CD19-CAR (FMC63 targeting domain, IgG4-Fc Hinge spacer, CD3 ζ and 4-1BB co-stimulation) *in cis* with a T2A element and truncated epidermal growth factor receptor (EGFRt), derived from the previously described lentiviral vector epHIV7^{15, 106}. The pCMV(CAT)T7-SB100X vector was a kind gift from Zsuzsanna Izsvak (Addgene plasmid # 34879)³⁹. MCs encoding eGFP and CD19-CAR_EGFRt transposons, and SB100X were generated from parental plasmids by PlasmidFactory (Bielefeld, Germany) via site-specific recombination. Next, MC vectors were purified by affinity chromatography.

3.4.2 Cloning of PD-1 sgRNAs into lentiCRISPR v2 plasmid

lentiCRISPR v2 plasmid was a kind gift from Feng Zhang (Addgene plasmid # 52961). This plasmid contains two expression cassettes, hSpCas9 and the chimeric guide RNA. It also includes a puromycin selection marker. The cloning protocol is previously described¹⁰⁷. Briefly, lentiCRISPR v2 vector (5 μ g) was digested with BsmBI (3 μ L), dephosphorylated using Antarctic Phosphatase (NEB) at 37 °C and gel purified. A pair of complementary oligos based on target site (20 bp each) were designed using CRISPR Design Tool algorithm at "http://crispr.mit.edu/". The oligos were annealed and phosphorylated with

T4 Polynucleotide Kinase (NEB) in T4 ligation buffer (NEB) in a total volume of 10 μL in a thermal cycler using following conditions: 37 °C 30 min, 95 °C 5 min, and ramp down to 25 °C at 5 °C/min. The annealed oligos were diluted at a ratio of 1:200 into sterile water and were cloned into the digested lentiCRISPR v2 plasmid using T4 DNA ligase (NEB). The accuracy of sgRNAs' sequences was confirmed by Sanger sequencing.

3.4.3 Nucleofection of T cells with SB vectors

Desired T-cell subsets were activated with anti-CD3/CD28 Dynabeads at a cell to bead ratio of 1:1. Transfection of transposon and transposase vectors was performed 36 hours after bead activation into 1×10^6 T cells in 20 μL of P3 primary cell 4D-Nucleofector supplemented buffer using 16-well Nucleocuvette strips and FI-115 program on a 4D-Nucleofector according to the manufacturer's instructions (Lonza). 1 μg of each conventional transposon and transposase plasmids was used per 1×10^6 T cells. For MC vectors corresponding equimolar amount of each DNA vector, 0.6 μg of CD19-CAR MC and 0.5 μg of SB100X donor MC were used. When combination of CD19-CAR MC and SB100X mRNA (an optimal ratio of 1:4, 0.6 μg CD19-CAR MC: 2.4 μg SB100X mRNA) was used for transfection, RNase free tubes and pipette tips were used and cells were washed once with room temperature PBS before resuspension in buffer. After nucleofection, T cells were propagated in TCM containing 50 U/mL of rh IL-2. Trypan blue staining was performed to quantify viable T cells. Prior to functional testing, EGFRt-positive T cells were enriched and expanded with irradiated TM-LCL cells for 7 days and functional analysis of CD19-CAR T cells were performed as described earlier.

3.4.4 Nucleofection of T cells with Cas9 RNP

CD8⁺ T cells were activated with anti-CD3/CD28 Dynabeads prior to nucleofection as described before. 15 µg of Cas9 recombinant protein, 0.75 mg/mL, was mixed with 10 µg of *in vitro*-transcribed sgRNA, 0.5 mg/mL, (a Cas9 to sgRNA molar ratio of 1:3) or 20 µg of *in vitro*-transcribed sgRNA, 1 mg/mL, (molar ratio of 1:6) in a RNase free microtube and incubated for 10 min at room temperature to generate the pre-assembled Cas9 ribonucleoprotein complex (Cas9 RNP). Next, the Cas9 RNP complex was added to 1×10^6 T cells in 20 µL of P3 primary cell 4D-Nucleofector supplemented buffer and the cell suspension was nucleofected as explained before.

3.4.5 Preparation of *in vitro*-transcribed RNAs

PolyA-tailed ARCA-capped SB100X mRNA was produced by *in vitro* transcription from the T7 SB100X plasmid and column purified in-house using the mMessage mMachine kit and purified by MEGAclean Kit (Ambion) or purchased at EUFETS (Idar-Oberstein, Germany). For preparation of *in vitro*-transcribed single guide RNA #2 (sgRNA2), first the sgRNA2 with a T7 promoter was cloned into a pCR-Blunt vector using Zero Blunt® PCR cloning kit (Invitrogen). The cloned sgRNA2 and its T7 promoter were separated from the vector by EcoRI digestion and used as a template for *in vitro* transcription using MEGashortscript T7 transcription kit (Ambion). The *in vitro*-transcribed sgRNA was purified by MEGAclean Kit (Ambion).

3.4.6 T7 endonuclease I assay

In order to determine the target editing efficiency of designed *PD-1* sgRNAs, genomic DNA (gDNA) of modified cells was isolated using PureLink Genomic

DNA Kit (Invitrogen). Primers flanking the target site were designed (Table 1) and the target site was amplified using 100 ng of gDNA and Phusion High-Fidelity DNA polymerase (NEB) using following thermocycler setting:

Initial denaturation	98 °C	3 min	
Denaturation	98 °C	10 s	} 35 cycles
Annealing	68°C	25 s	
Extension	72 °C	30 s	
Final extension	72 °C	5 min	

The desired PCR amplicon was purified from agarose gel and DNA concentration was determined by a NanoDrop (Thermo Fisher). For generation of hetero- and homoduplexes about 400 ng of purified PCR amplicon was heated in a thermal cycler in 20 μ L of 1x NEBuffer2 using following condition:

95 °C 10 min, 95 °C - 85 °C, -2 °C/s, 85 °C 1 min, 85 °C - 75 °C, -3 °C/s, 75 °C 1 min, 75 °C - 65 °C, -3 °C/s, 65 °C 1 min, 65 °C - 55 °C, -3 °C/s, 55 °C 1 min, 55 °C - 45 °C, -3 °C/s, 45 °C 1 min, 45 °C - 35 °C, -3 °C/s, 35 °C 1 min, 35 °C - 25 °C, -3 °C/s, 25 °C 1 min, 25°C-4 °C.

1 μ L of T7 endonuclease I (diluted 1:1 with 1x NEBuffer2) was added to 100-200 ng of the heated amplicon (in 11 μ L of 1x NEBuffer2) and the 12 μ L mixture was incubated at 37 °C for not longer than 15-20 min in a water bath. The reaction was stopped with 1.5 μ L of 0.25 M EDTA and whole reaction was checked on a 2.5% agarose gel. T7 Endonuclease I recognizes and cleaves non-perfectly matched DNA hetero-duplexes generated during denaturing and reannealing cycles. The intensity of the bands was measured using Image Lab™ Software (Bio-Rad) and gene

modification efficiency (insertion or deletion %, indel%) for each sgRNA was calculated using following formula:

$$\text{Indel\%} = \left[1 - \sqrt{1 - \left\langle \frac{b+c}{a+b+c} \right\rangle} \right] \times 100$$

Where “b” and “c” are intensity of cleaved heteroduplexes and “a” is the intensity of uncleaved homoduplex amplicon.

Table 3.1. Primers used for T7 endonuclease I assay.

Primer name	Sequence (5'→3')	PCR product	Cleavage product
PD-1-Exon1-Fwd	TCTGTCACTCTCGCCCACGT	609 bp	411+198 bp
PD-1-Exon1-Rev	AGCCTGACCCGTCATTCTAC		
PD-1-Exon2-Fwd	AGGGGGTGAAGGCTCTTAGT	526 bp	369+157 bp
PD-1-Exon2-Rev	ACCACGCTCATGTGGAAGTC		

3.4.7 Integration site analysis of lentiviral and SB integrants

3.4.7.1 Construction of the SB insertion library and sequencing

Genomic DNA (gDNA) of CD8+ EGFRt+ T cells of three donors were isolated at least one month post-transfection. 2 µg DNA was sheared with a Covaris M220 ultra-solicitor device to an average fragment size of 600 bp in Screw-Cap microtubes in 50 µL, using the following settings: peak incident power 50W, duty factor 20%, cycles per burst 200, treatment 28 s. 1.2 µg of the sheared DNA was blunted and

5'-phosphorylated using the NEBNext End Repair Module (NEB), and 3'-A-tailed with NEBNext dA-Tailing Module (NEB) based on manufacturer's protocol. The DNA was purified with the Clean and Concentrator Kit (Zymo) and eluted in 8 μ L 10mM Tris pH8 (EB) for ligation with 50 pmol of T-linker (Table 2) with T4 ligase (NEB) in 20 μ L volume, at 16 °C, overnight. T-linkers were created by annealing the 100-100 pmol of the oligonucleotides Linker_Truseq_T+ and Linker_Truseq_T- in 10 mM Tris-Cl pH8, 50 mM NaCl, 0.5 mM EDTA. After heat-inactivation, ligation products enclosing fragments of non-integrated transposon donor plasmid DNA were digested with DpnI (NEB) in 50 μ L for 3 hours and the DNA was column-purified and eluted in 20 μ L elution buffer. 6 μ L eluate was used for the PCR I with 25 pmol of the primers specific for the linker and for the transposon inverted repeat, Linker and T-Bal-Long primers, respectively (Table 2), with following thermocycler setting:

Initial denaturation	98 °C	30 s	
Denaturation	98 °C	10 s	} 10 cycles
Annealing	72 °C	30 s	
Denaturation	98 °C	10 s	} 15 cycles
Annealing	1 °C/s to 62 °C	30 s	
Extension	72 °C	30 s	
Final extension	72 °C	5 min	

All PCR reactions were performed with NEBNext High-Fidelity 2x PCR Master Mix (for PCR primer sequences see Table 2). The PCR was column purified and eluted in 20 μ L elution buffer and 10 μ L used for PCR II with the Nested and LAM-SB-50 primers, with the following thermocycler setting:

Initial denaturation	98 °C	30 s	
Denaturation	98 °C	10 s] 12 cycles
Annealing	1 °C/s to 65°C	30 s	
Extension	72 °C	30 s	
Final extension	72 °C	5 min	

One third of the column-purified PCR II was used for PCR III with the PE-nest-ind-N and SB-20h-bc-ill-N primers (where N is the number of the Illumina TrueSeq indexes) for barcoding the samples of different T-cell donors, using the following thermocycler setting:

Initial denaturation	98 °C	30 s	
Denaturation	98 °C	10 s] 12 cycles
Annealing	1 °C/s to 64°C	30 s	
Extension	72 °C	30 s	
Final extension	72 °C	5 min	

The final PCR products were separated on a 1% agarose gel and the smears of 200-500 bp were gel-isolated and purified. The libraries were sequenced on an Illumina HiSeq instrument at Beckman Coulter Genomics on a rapid flow-cell using single-end 100 nucleotide sequencing setup.

Table 3.2. Primers and oligos used for integration library preparation.

Primer name	Sequence (5'→3')
Linker_TrueSeq_T+	GTAATACGACTCACTATAGGGCTCCGCTTAAGGGACTCAG ACGTGTGCTCTTCCGATCT
Linker_TrueSeq_T-	GATCGGAAGAGCACACG-Amino
T_Bal_long	CTTGTGTCATGCACAAAGTAGATGTCCTAACTGACT
LAM_SB_50	AGTTTTAATGACTCCAACCTAAGTG
SB20h-bc-ill-N	AATGATACGGCGACCACCGAGATCTACACTCTTTCCCTAC ACGACGCTCTTCCGATCT-TruSeq-Illumina-Index- CTTAAGTGTATGTAACTTCCGACT
PE-nest-ind1-N	CAAGCAGAAGACGGCATACGAGAT-reverse-complement-of- TruSeq-Illumina-Index- GTGACTGGAGTTCAGACGTGTGCTCTTCCGATCT

3.4.7.2 Bioinformatic analysis

Reads were allocated to each donor using barcodes, trimmed using the Shortread tool in R software¹⁰⁸ and the remaining sequences quality-trimmed as soon as 2 of 5 nucleotides had a phred score less than 20. The resulting reads were uniquely mapped to the hg19 human genome assembly with Bowtie¹⁰⁹. Any SB insertion site was considered valid if there were at least 10 independent reads supporting it. Nucleotide compositions of SB insertion sites were calculated and plotted using the SeqLogo tool in R software.

We used BEDtools v2.17.0¹¹⁰ for annotating the insertion sites or a set of computationally generated 10,000 random genomic positions in annotated human genomic features (<http://genome.ucsc.edu>). The set of cancer-related genes was obtained from <http://www.bushmanlab.org/links/genelists>¹¹¹. The category non-genic was created by subtracting the coordinates of all annotated transcripts from the

chromosome lengths of the hg19 genome assembly. For relating insertion site frequencies of SB and HIV to gene expression levels we used published gene expression data of activated human T cells¹¹².

BED files of ChIP-Seq data obtained on activated human T cells were retrieved from <http://dir.nhlbi.nih.gov/papers/lmi/epigenomes/hgtcell.aspx>¹¹³ and the MACS ChIP-Seq peak-calling algorithm¹¹⁴ “macs14 -t *.bed -g hs --nomodel --nolambda --space=30”.

Genomic coordinates of ultraconserved elements were obtained¹¹⁵ and all human microRNA genes downloaded (<http://www.mirbase.org/ftp.shtml>). The ‘genomic safe harbor’ coordinates were obtained by intersecting all coordinates of all safe harbor subcategories for the hg19 human genome assembly.

3.4.8 Copy number determination of SB insertions

3.4.8.1 Linker-mediated PCR

gDNA was isolated from EGFRt+ T-cell clones at least one month post-transfection of SB100X mRNA and MC transposon. 1 µg of DNA per clone was digested with FspBI (Fermentas) and DpnI (NEB). The latter digest was applied to fragment non-integrated MCs, which could otherwise disturb the copy number determination. The digested DNA was column purified, and eluted in 20 µL of elution buffer. 5 µL of eluate was ligated with 50 pmol of FspBI overhang-specific linkers overnight at 16 °C. Linkers were created by annealing the 100-100 pmol of the oligonucleotides L (+) and L(-) FspBI in 10 mM Tris-Cl pH8, 50 mM NaCl, 0.5mM EDTA (Table 3). 1 µL of the ligation reaction was used as the template for the first PCR reaction with the

primers Linker (specific for the ligated linker) and T-Bal-rev (specific for the 5' inverted terminal repeat of the transposons) using the following thermocycler setting:

Initial denaturation	94 °C	3 min	
Denaturation	94 °C	30 s] 10 cycles
Annealing	1 °C/s to 63 °C	30 s	
Extension	72 °C	1 min	
Denaturation	94°C	30 s] 15 cycles
Annealing	1 °C/s to 61 °C	30 s	
Extension	72 °C	1 min	
Final extension	72 °C	10 min	

1 µL of 100-times diluted PCR reaction was used in the nested PCR with the primers Nested and T-Bal using the following thermocycler setting:

Initial denaturation	94 °C	3 min	
Denaturation	94 °C	30 s] 10 cycles
Annealing	1 °C/s to 65 °C	30 s	
Extension	72 °C	1 min	
Denaturation	94°C	30 s] 15 cycles
Annealing	1 °C/s to 63 °C	30 s	
Extension	72 °C	1 min	
Final extension	72 °C	10 min	

5 µL of the nested PCR reaction was loaded on a 1.5% agarose gel to visualize the bands, which correspond to the insertion sites with flanking genomic DNA.

Table 3.3. Primers used for linker mediated copy number analysis.

Primer name	Sequence (5'→3')
L(+)	GTAATACGACTCACTATAGGGCTCCGCTTAAGGGAC
L(-)FspBI	TAGTCCCTTAAGCGGAG-Amino
Nested	AGGGCTCCGCTTAAGGGAC
Linker	GTAATACGACTCACTATAGGGC
T_Bal rev	GAATTGTGATACAGTGAATTATAAGTG
T_Bal	CTTGTGTCATGCACAAAGTAGATGTCC

3.4.8.2 Droplet digital PCR

Prior to droplet digital PCR (ddPCR), 300 ng of each gDNA were digested with 1 μ L of DpnI (20,000 U/mL) in 3 μ L of NEBuffer 3.1 at a final volume of 30 μ L at 37 °C. This restriction enzyme cleaves the vectors that are not integrated. Samples were fragmented with 1 μ L of CviQI (10,000 U/mL) at final volume of 35 μ L for 2 hours at 25 °C. Next, primers (600 nM of each), probes (200 nM) and 17 ng of each digested template were added to the ready-to-used ddPCR Supermix at the final volume of 25 μ L at room temperature for efficient droplet generation. 20 μ L of the PCR mixture was added to a specific well in the DG8 Cartridges and 70 μ L of Droplet Generation Oil was added to all the wells and incubated for 2 min at room temperature. Then, the cartridges were covered by a gasket and were put in a QX100 Droplet Generator. After a couple of minutes, approximately 20,000 droplets are generated per well. 40 μ L of generated droplets were transferred into a 96-well PCR plate and sealed with a single sealing foil in the PX1 PCR Plate Sealer (Bio-Rad). The PCR reaction was performed in a thermal cycler using the following setting:

Initial denaturation	95 °C	10 min	
Denaturation	94 °C	30 s	} 40
Annealing	2 °C/s to 60°C	1 min	
Final extension	98 °C	10 min	

After the PCR reaction, fluorescence measurements for each droplet were performed by a QX100 Droplet Reader. The results were analyzed using QuantaSoft software and ribonuclease P/MRP 30 subunit (*RPP30*) gene was used as the copy number reference (2 copies per genome).

The primers and probes used for amplification of integrated CD19-CAR transgene (CAR-Fwd, probe and Rev), non-integrated CD19-CAR MC vector (MC-Fwd, probe and Rev) and *RPP30* (RPP30-Fwd, probe and Rev) are summarized in Table 3.4.

Table 3.4. Primers and oligos used for ddPCR copy number analysis.

Primer name	Sequence (5'→3')
CAR-Fwd	ATCTGGATGTCGGGGATCAG
CAR-probe	FAM-AGCAGCATGGTGGCGGCGCT-BH1
CAR-Rev	GCTTGCTCAACTCTACGTCT
MC-Fwd	CCGACCTTAATGCGCCTC
MC-probe	FAM-GCGCTGTAGCCTCACGCCACATATGT-BH1
MC-Rev	AGGATTAAATGTCAGGAATTGTGAA
RPP30-Fwd	GGTAACTACAGCTCCCAGC
RPP30-probe	HEX-TGGACCTGCGAGCGGGTTCTGACC-BH1
RPP30-Rev	CTGTCTCCACAAGTCCGC

3.5 Statistical analysis

Data are presented as mean \pm SD. Statistical analyses were performed by Student's t test, one-way ANOVA or Mann-Whitney test with GraphPad Prism Software. Results with $p < 0.05$ were considered significant.

4 Results

The first objective of this study was to improve the non-viral *Sleeping Beauty* (SB) transposition to provide an alternative strategy for viral delivery of CAR transgenes into T cells. To fulfil this aim, in the first step, we established a novel strategy that leveraged the SB transposition of CD19-CAR in T cells. Next, we confirmed the antitumor efficacy of CD19-CAR T cells generated by this strategy. Finally, we carefully assessed the biosafety of our developed non-viral gene transfer strategy.

4.1 Generation of CAR T cells through non-viral SB transposition from plasmids

Ratio of transposase to transposon is one of the factors that may affect efficiency of SB transposition³⁸. Therefore, we first explored the optimal ratio of transposon to transposase by titrating the amounts of GFP transposon donor plasmid to SB100X transposase plasmid (1:1 to 4:1) in T cells. The ratio of 1:1 resulted in the highest GFP expression (Figure 4.1a)⁴⁶. We also tested different ratios of CD19-CAR transposon-to-transposase (1:1, 2:1, and 1:2). Similarly, ratio of 1:1 resulted in the highest CAR expression (Figure 4.1b). Consequently, we transfected T cells with transposon and transposase plasmid vectors (1 µg of each) at an optimal 1:1 ratio. However to increase the gene transfer rate achieved via SB-mediated CAR transposition, we tested transgene transposition via transfection of minicircle vectors encoding transposon and transposase into T cells.

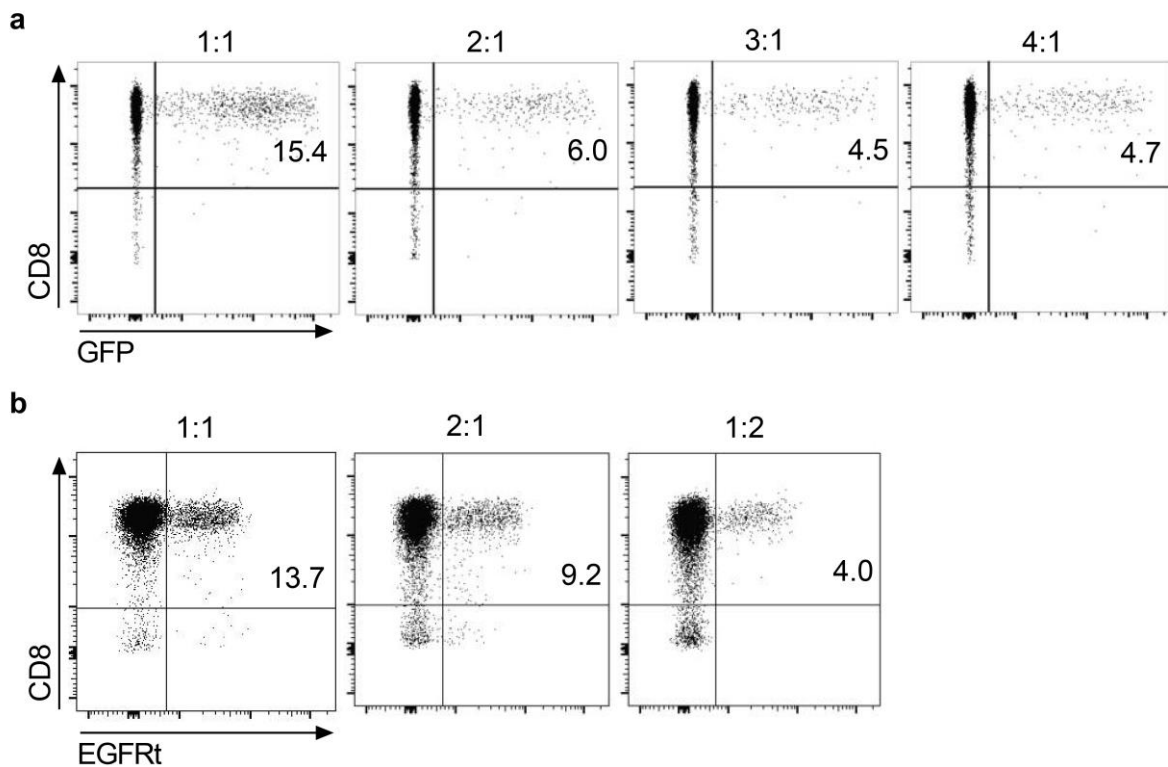


Figure 4.1. Titration of transposon and SB100X transposase DNA plasmids.

(a) CD8+ T cells were transfected with increasing amounts of GFP-encoding transposon donor plasmid and 1 μ g of SB100X transposase-encoding plasmid (ratios of 1:1, 2:1, 3:1 and 4:1). Flow cytometry analysis of GFP expression in CD8+ T cells was performed on day 14 post transfection (gated on living, i.e. 7-AAD negative cells). **(b)** CD8+ T cells were transfected with 1 μ g CAR-encoding transposon donor plasmid and different amount of SB100X transposase-encoding plasmid (ratios of 1:1, 2:1 and 1:2). Flow cytometry analysis of EGFRt expression in CD8+ T cells was performed on day 14 post transfection (gated on living, i.e. 7-AAD negative cells).

4.2 Preparation of minicircle DNA vectors from conventional transposon and transposase plasmids

First, we prepared minicircle DNA vectors (MCs) from a set of parental pT2 transposon donor vectors expressing eGFP or an optimized CD19-CAR *in cis* with an EGFRt transduction marker, and from a plasmid encoding hyperactive SB100X transposase. MCs are generated from minicircle producer parental plasmids via a site-specific intramolecular recombination mediated by a phage integrase between

recombination sites which separate the transgene and its promoter from bacterial backbone sequences of the parental plasmid (Figure 4.2a).

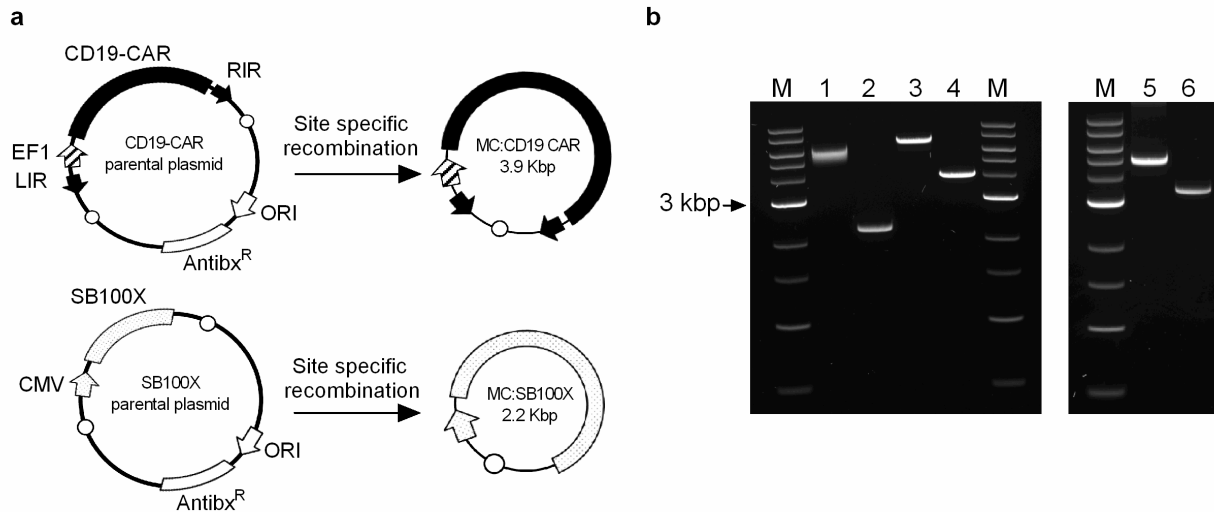


Figure 4.2. Production of minicircle (MC) vectors.

(a) Schematic of MC vectors prepared from minicircle producer parental plasmids through site specific intramolecular recombination. MCs contain exclusively the transgene and its promoter, but no bacterial origin of replication and antibiotic resistance genes. EF1, elongation factor-1 alpha promoter; CMV, cytomegalovirus promoter; ORI, bacterial origin of replication; Antibx^R, antibiotic resistance gene; LIR, left inverted repeat; RIR, right inverted repeat; open circle, recombination site. (b) Restriction digestion analysis of conventional plasmids and purified MCs. Lane 1, SB100X plasmid digested with SacI; lane 2, MC-SB100X digested with PacI; lane 3, pT2/HB:CD19-CAR transposon plasmid digested with NheI; lane 4, CD19-CAR MC digested with PacI, lane 5, pT2/HB:eGFP plasmid digested with NheI; lane 6, eGFP MC digested with PmeI; lane M, 1kb DNA ladder (NEB). The DNAs were analyzed on 0.8% agarose gel.

This recombination process results in a smaller supercoiled MC DNA, which contains exclusively the transgene and its promoter devoid of undesired bacterial plasmid backbone. The size of the pT2 plasmids encoding CD19-CAR and eGFP were reduced to 3.9 kbp and 3.4 kbp from 6.6 kbp and 4.8 kbp, respectively. SB100X plasmid size was reduced from 4.7 to 2.2 kbp (Figure 4.2b).

4.3 Transposition using minicircle DNA encoding transposase and transposon enables high level stable gene transfer in T cells

We then analyzed the transposition rate and stability that could be accomplished when transposon and transposase were encoded by MCs, and compared it to the use of corresponding conventional plasmid DNA vectors. We performed gene transfer into CD3/CD28-activated CD8⁺ and CD4⁺ T cells of healthy donors using equimolar amounts of plasmid DNAs and corresponding MC DNAs. First, we nucleofected T cells using MC vectors encoding eGFP transposon and SB100X transposase as a general model.

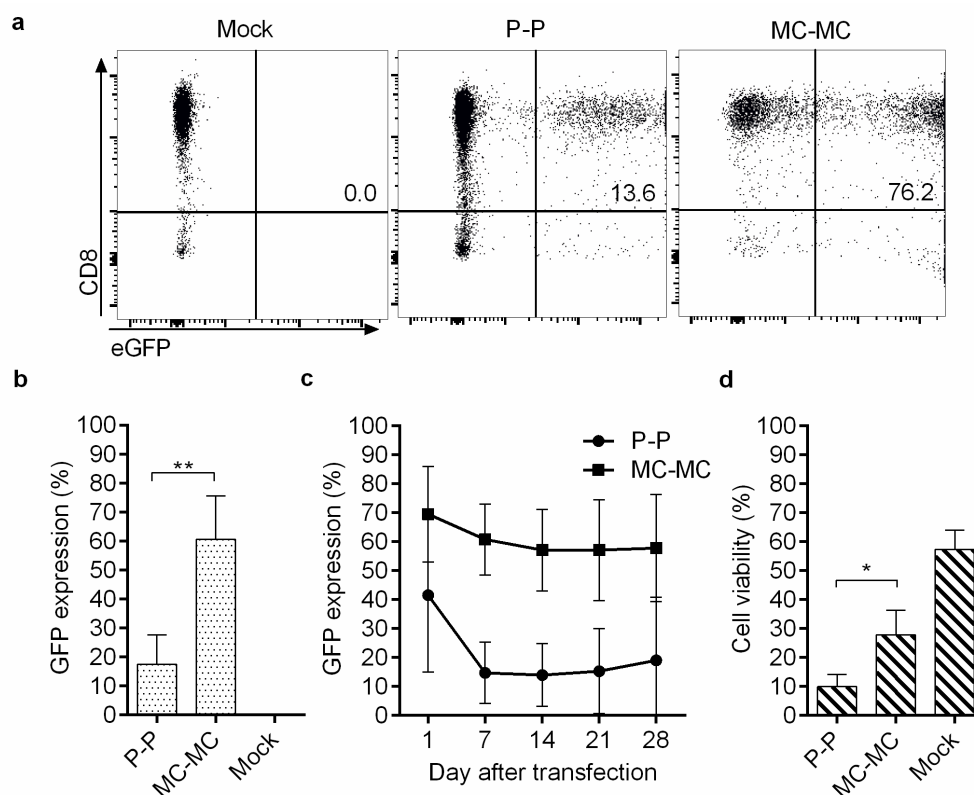


Figure 4.3. SB-transposition of eGFP from MC or plasmid vectors.

(a, b) CD8⁺ T cells were transfected with 1 μ g of each plasmids encoding eGFP and SB100X (P-P) or their corresponding equimolar amounts of MCs (MC-MC). eGFP expression was assessed by flow cytometry on day 14 (gated on living, i.e. 7-AAD negative cells). Data represent mean values \pm SD of three independent experiments, $p < 0.001$. (c) Stability of eGFP expression was assessed by flow cytometry over 28 after transfection (mean values \pm SD of in three independent experiments). (d) Viability of T cells 48 hours post-transfection was assessed by 7-AAD staining and flow cytometry analysis (mean values \pm SD of three independent experiments). Statistical analysis was performed using Student's t test, $p < 0.05$.

eGFP positive T cells were 3.2-fold higher in CD8+ T cells modified with MCs compared to plasmids ($n=3$, $p<0.05$) (Figure 4.3a).

Next, we wanted to know if similar results can be produced when a functional transgene like CD19-CAR is used. Serial analyses of transgene expression were performed between d7 and d28 after gene transfer.

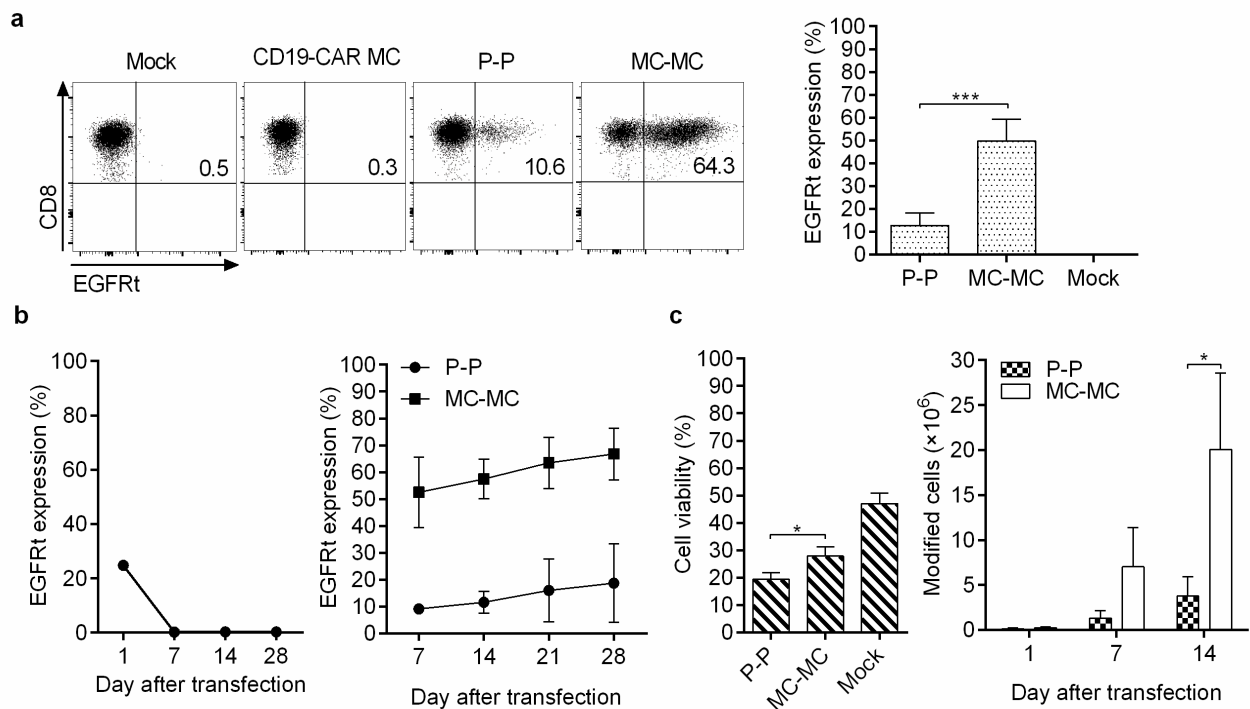


Figure 4.4. CAR transposition using MC and plasmid-encoded SB-transposase and transposon.

(a) Transposition rate after transfection of MC vs. plasmid-encoded SB100X transposase and CD19-CAR transposon. On day 0, CD8+ T cells were transfected with 1 μ g of each plasmid (P-P) or an equimolar amount of MC DNA (MC-MC). Flow cytometry analysis was performed to determine the percentage of T cells that express EGFRt marker encoded *in cis* with the CD19-CAR on day 14 (gated on living, i.e. 7-AAD negative cells). Right diagram shows mean percentage \pm SD of EGFRt+ T cells on day 14 ($n=7$; $p<0.0001$). **(b)** Transposition rate and stability of EGFRt expression was determined by flow cytometry within 4 weeks after transfection. CD8+ T cells were transfected with CD19-CAR MC without SB100X transposase (left diagram). CD8+ T cells were transfected with MC-MC or P-P (right diagram). Mean percentage \pm SD of EGFRt+ T cells from three different experiments is shown. **(c)** mean percentage \pm SD of living T cells 48 hours after transfection assessed by 7-AAD staining (left diagram, $n=3$; $p<0.05$). Yield of CAR-modified T cells that were obtained from 1×10^6 input CD8+ T cells within 14 days of culture following transfection (right diagram). The yield was calculated from absolute number of living T cells, multiplied by the fraction of EGFRt+ cells ($n=4$; $p<0.05$).

The results revealed higher percentages of transgene positive T cells at all analyzed time points after modification with MCs rather than plasmid DNAs. On day 14, the mean percentage of CAR positive (i.e. EGFRt+) T cells was 49.8% with MCs but only 12.8% when plasmids were used. Thus, on average 4.4-fold higher CAR expression was achieved after transfection of MC- rather than plasmid-encoded SB100X transposase and CAR transposon (n=7, p<0.0001) (Figure 4.4a). No stable CAR expression was detected in the absence of SB100X (Figure 4.4b). Furthermore, one-month follow-up of the cells revealed that stable transgene expression is achieved after day 14, confirming the stable gene transfer through MC *Sleeping Beauty* (SB) transposition (Figure 4.4c, Figure 4.3b). Of note, in resting T cell lines modified with CD19-CAR, the percentage of transgene positive T cells even moderately increased over time (Figure 4.4b), potentially due to intrinsic signaling of the receptor¹¹⁶. Moreover, using MCs rather than conventional plasmids resulted in higher CD19-CAR transposition in CD4+ T cells. This confirmed our observation that MCs are superior to conventional plasmids in mediating transposition (Figure 4.5).

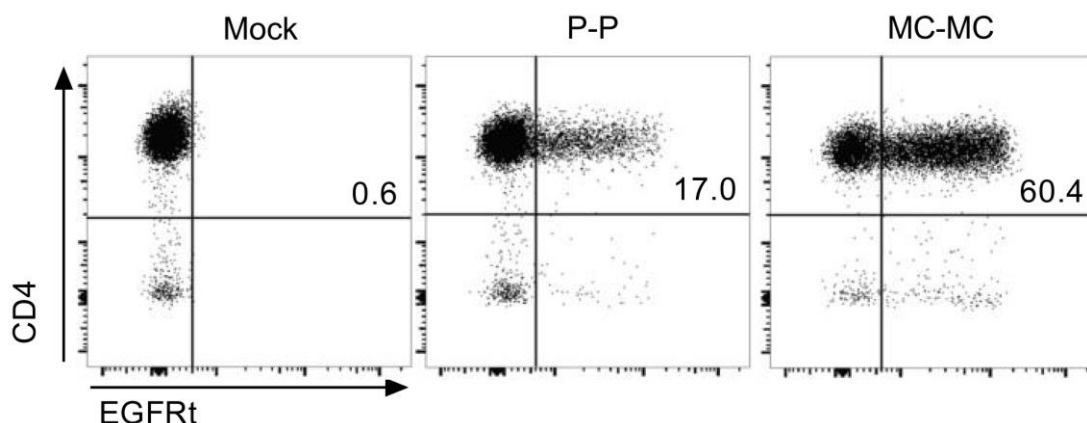


Figure 4.5. SB transposition from MCs in CD4+ T cells.

CD4+ T cells were transfected with 1 μ g of each conventional plasmids encoding a CD19-CAR transposon and SB100X transposase (P-P) or equimolar amounts of corresponding MCs (MC-MC) (n=3). A representative flow cytometry dot plot of EGFRt expression on day 14 is shown (gated on living, i.e. 7-AAD-negative cells).

4.4 Use of minicircle DNA rather than plasmid DNA reduces electroporation-induced toxicity

The introduction of plasmid DNA by electroporation into T cells is associated with severe toxicity to the cells and has thus far limited the ability to rapidly produce therapeutic doses of gene-modified T cells with this approach⁴⁹. We observed that in addition to mediating superior transposition, the use of MCs rather than plasmids is associated with a significantly lower degree of toxicity to T cells. The percentage of living T cells assessed by 7-AAD staining 48 hours after nucleofection was 1.44-fold higher for CAR-modified (n=3) and 2.02-fold higher (n=3) for control eGFP when T cells were modified with MCs rather than plasmids ($p < 0.01$, Figure 4.4c, Figure 4.3c). The higher transposition rate and lower toxicity of MCs translated into approximately 6-fold higher yield of CD19-CAR T cells that could be obtained within 14 days of culture without antigen dependent expansion (n=4, $p < 0.05$, Figure 4.4c). Our data demonstrate that the use of MCs as transposon and transposase donor vectors is feasible, highly efficient and superior to plasmid DNAs in mediating transposition in human T cells.

4.5 Transposition from MCs using mRNA-encoded SB-transposase

Next, we investigated whether providing SB100X as mRNA instead of MC DNA is sufficient for accomplishing transposition from MC transposon donor vectors. We prepared the SB100X mRNA via *in vitro* transcription using pcGlobin2-SB100X plasmid, which contains a T7 promoter. Agarose gel electrophoresis of the poly-A tailed SB100X mRNA shows a size between 1 and 1.5 kbp (Figure 4.6a). Next, we

performed titration experiments to determine the optimal ratio of SB100X mRNA and MC (1:1, 2:1, 4:1, 8:1).

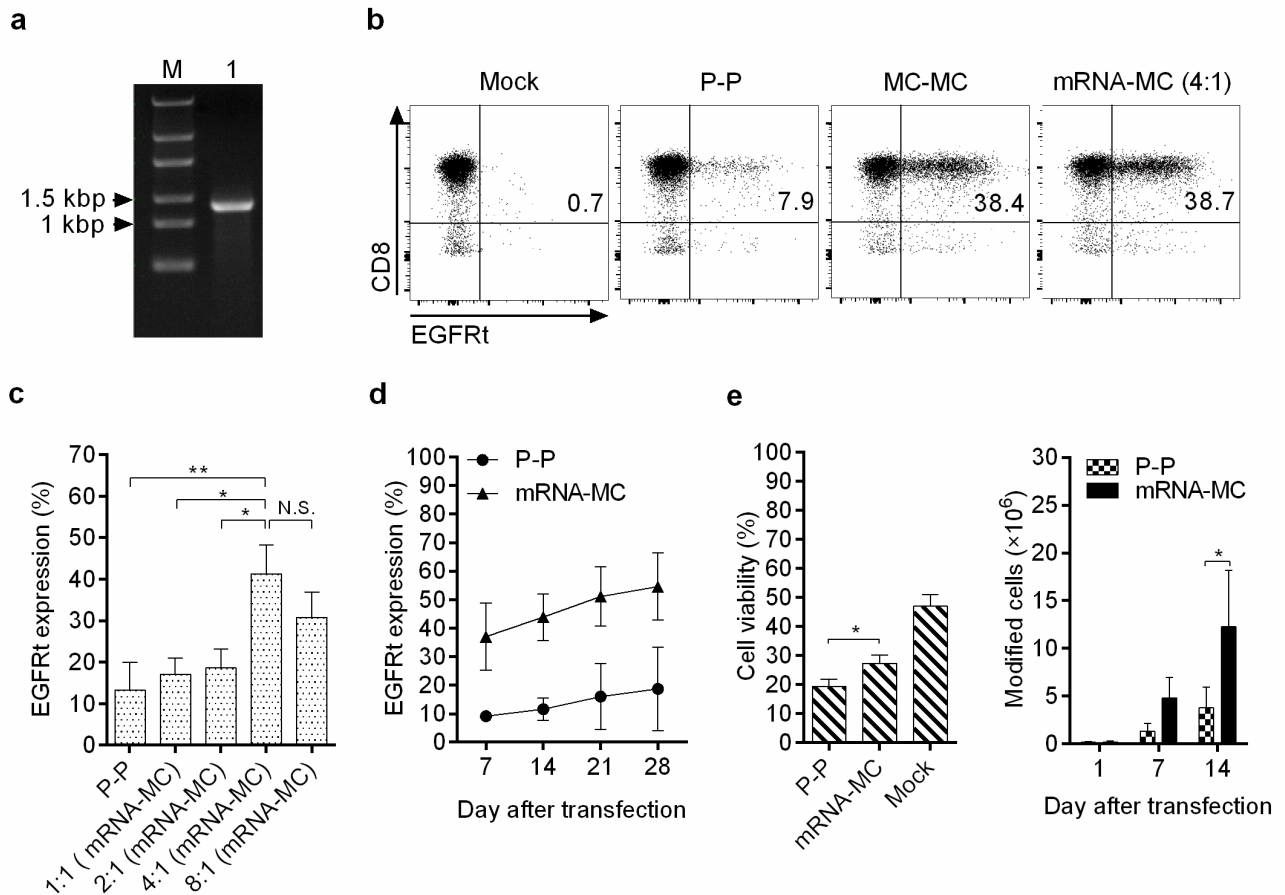


Figure 4.6. mRNA as the transient source of SB100X transposase.

(a) Electrophoresis of *in vitro*-transcribed poly-A tailed ARCA capped SB100X mRNA on 1% agarose gel. Lane M, RNA marker, lane 1, SB100X mRNA. **(b)** Flow cytometry analysis of EGFRt expression on day 14 post-transfection (gated on living, i.e. 7-AAD negative cells). CD8+ T cells were nucleofected with 1 μ g each of transposon and transposase-encoding plasmid (P-P), corresponding equimolar amounts of MC DNA (MC-MC) or SB100X mRNA and CD19-CAR MC (mRNA-MC ratio of 4:1). Mock controls were nucleofected without vector and mRNA. **(c)** Titration of SB100X mRNA. CD8+ T cells were transfected with different ratios of SB100X mRNA and CD19-CAR MC. EGFRt expression was assessed on day 14 after transfection by flow cytometry (mean values \pm SD obtained of three independent experiments). Statistical analysis was performed using Student's t test. * $p < 0.05$ and ** $p < 0.005$ indicate statistically significant differences. **(d)** Comparison of transposition rate and stability after transfection with plasmid-encoded transposase and transposon (P-P), and SB100X mRNA in combination with CD19-CAR MC transposon at optimal ratio of 4:1. The percentage of EGFRt+ T cells was determined by flow cytometry at distinct time points (mean values \pm SD obtained of three independent experiments). **(e)** T cell viability was assessed 48 hours post-transfection by 7-AAD staining (left diagram; $p < 0.05$), and the total yield of gene-modified T cells that was obtained within 14 days of culture after transfection calculated (right diagram; $p < 0.05$) (mean values \pm SD of three independent experiments). Statistical analysis was performed using Student's t test.

EGFRt expression was analyzed by flow cytometry on day 14 post-transfection. We found superior transposition rates with the mRNA-MC combination compared to plasmids at all ratios (Figure 4.6b,c). The highest transposition rate was achieved when SB100X mRNA and CD19-CAR MC were used at a 4:1 ratio, which yielded a 3.7-fold higher gene transfer rate than the plasmid combination (P-P) ($n=5$; $p<0.005$) (Figure 4.6b-d). A further increase in the amount of SB100X mRNA (8:1 ratio) resulted in a decline of transposition efficacy, potentially due to overproduction inhibition effect³⁸. The use of SB100X mRNA in combination with MC transposons was also associated with a significantly higher proportion of living T cells 48 hours post-transfection compared to plasmids (1.4-fold higher; $n=3$; $p<0.05$). This led to a substantially higher yield of gene-modified T cells at the end of a 14-day culture period (mean 3.6-fold higher; $n=4$; $p<0.05$) (Figure 4.6e).

Importantly, the high transposition rate that we accomplished with the optimal SB100X mRNA and CD19-CAR MC combination (4:1 ratio) was reproducible in purified naïve, central memory and effector memory CD8+ T cells (Figure 4.7).

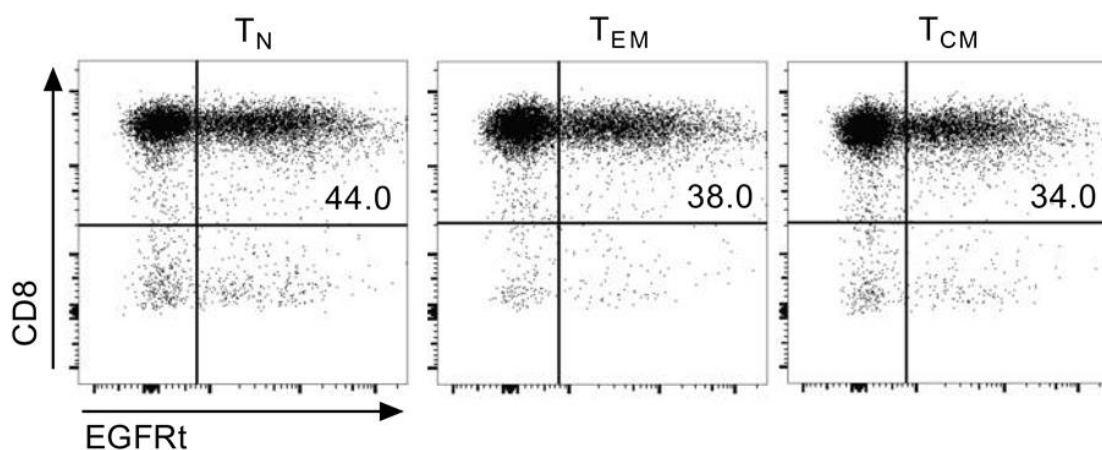


Figure 4.7. SB transposition from MC in CD8+ naïve and memory T-cell subsets.

CD8+ naïve (CD45RA+RO-62L+, T_N), effector memory (CD45RA-RO+62L-, T_{EM}) and central memory (CD45RA-RO+62L+, T_{CM}) T cells were purified and transfected with SB100X mRNA and CD19-CAR MC. Flow cytometry dot plots show EGFRt expression on day 14 after transfection (gating on living, i.e. 7-AAD-negative cells).

This indicates that our gene transfer strategy does not have a bias for introducing CD19-CAR into a phenotypically and functionally distinct subset within a bulk CD8+ T cell population. In summary, our data demonstrate that providing SB100X as relatively short-lived mRNA is sufficient to accomplish transposition from MC transposon donor vectors. This leads also to superior levels of stable gene transfer and enhanced T-cell viability compared to plasmids (Figure 4.6d,e).

4.6 MC-mediated SB-transposition confers potent antitumor functions to CD19-CAR T cells *in vitro*

We next sought to compare the functionality of T cells that were CAR-modified by SB-transposition from MCs and plasmids, to those that were modified with the same CD19-CAR construct via LV transduction.

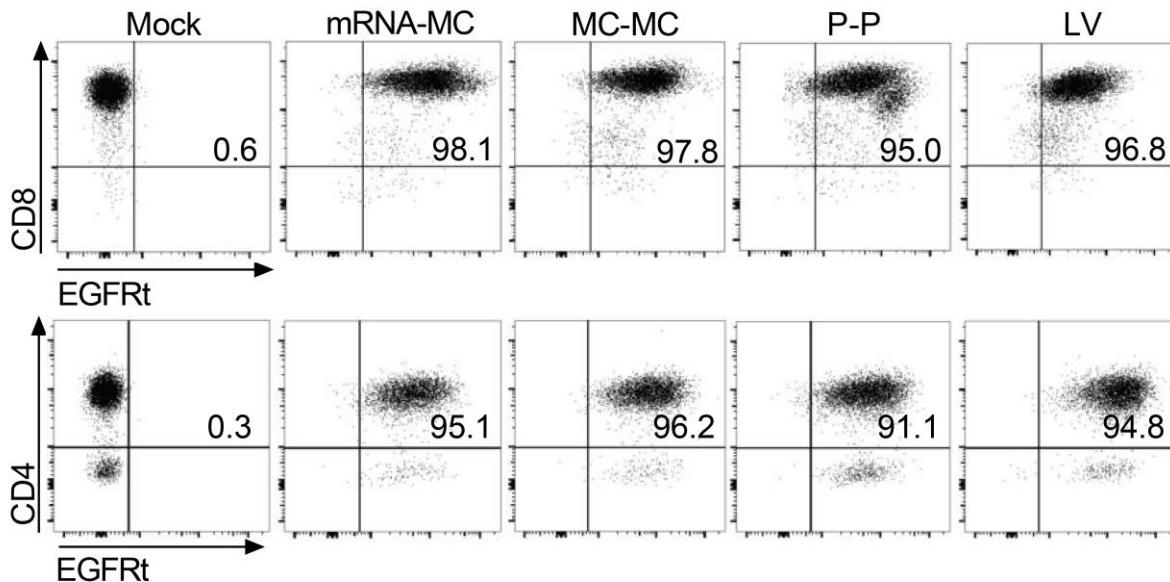


Figure 4.8. Phenotype of CD8+ and CD4+ CD19-CAR T cell lines prior to functional assays.

Flow cytometry dot plots show EGFRt expression after EGFRt-specific enrichment and expansion with TM-LCL (CD19+ feeder cells) for 7 days. The EGFRt marker is encoded *in cis* with the CD19-CAR in SB-transposon donor and lentiviral vectors. P-P: transposon and transposase encoded both by plasmids; MC-MC: transposon and transposase encoded both by MCs; mRNA-MC: SB100X mRNA and minicircle transposon donor; Mock: no mRNA and vector; LV: lentiviral transduction.

T cells that were selected for EGFRt and expanded with CD19+ feeder cells showed stable transgene expression over multiple expansion cycles and for at least another 6 weeks in culture.

First, we evaluated cytolytic activity using K562 cells stably expressing CD19, Raji and JeKo-1 lymphoma cells as targets, which all stably express firefly luciferase. The CD8+ CD19-CAR T cell lines generated by mRNA-MC, MC-MC, P-P transposition or LV transduction conferred similar potent and specific lysis (Figure 4.9).

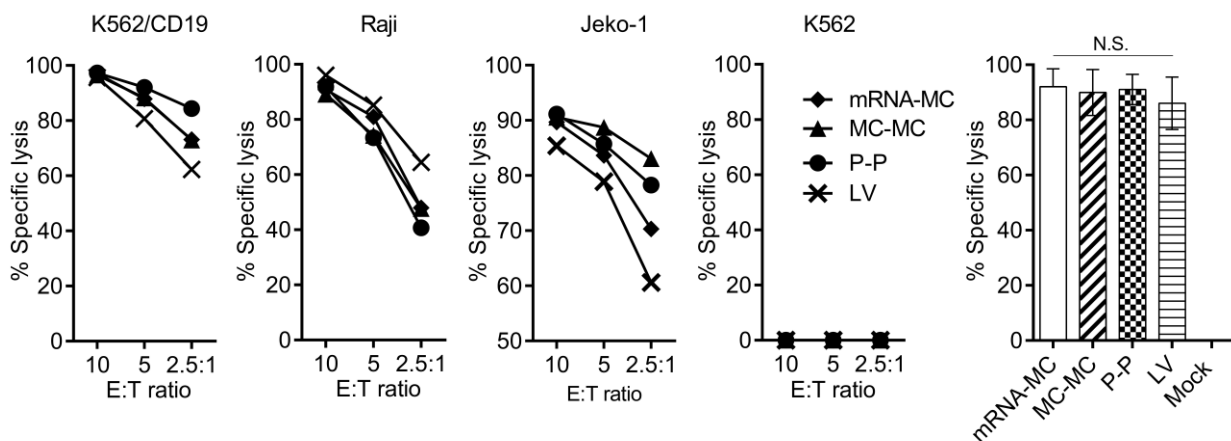


Figure 4.9. Specific cytolytic activity of CD8+ CD19-CAR T cells within 4 hours.

CD8+ T cells were co-cultured with target cells stably expressing firefly luciferase. 4 hours later luciferin was added to the culture and the cytotoxicity was evaluated with a bioluminescence-based assay. Right diagram: specific lysis of K562/CD19 target cells (E:T=10:1) by T cell lines prepared from $n=3$ different donors were compared by one-way ANOVA. No statistically significant difference in lytic activity was detected. P-P: transposon and transposase encoded both by plasmids; MC-MC: transposon and transposase encoded both by minicircles; mRNA-MC: SB100X mRNA and minicircle transposon donor; Mock: no mRNA and vector; LV: lentiviral transduction.

Quantitative cytokine analysis after co-culture with CD19+ lymphoma cell lines also showed similar production of IFN- γ and IL-2 in all CD8+ and CD4+ CD19-CAR T cell lines (Figure 4.10).

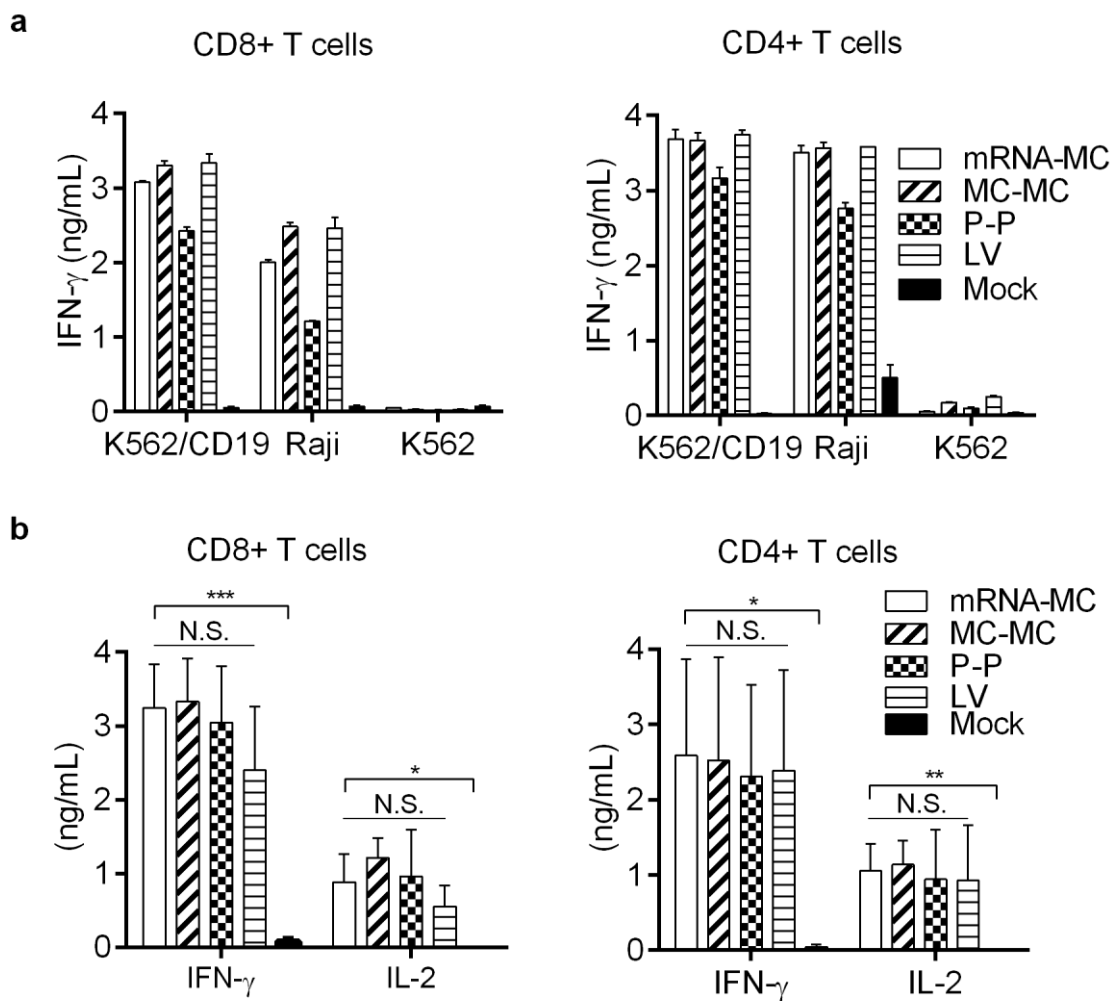


Figure 4.10. Cytokine production of CD8+ and CD4+ CD19-CAR T cells.

(a) CD19-CAR T cells were co-cultured with target cells for 24 hours. Cytokine levels in supernatants were measured by ELISA (assay performed in triplicates). Data show mean values \pm SD of one representative experiment. **(b)** IFN- γ and IL-2 production of CD8+ and CD4+ T cells from three different donors were analyzed by one-way ANOVA. No statistically significant difference in cytokine production was detected. P-P: transposon and transposase encoded both by plasmids; MC-MC: transposon and transposase encoded both by minicircles; mRNA-MC: SB100X mRNA and minicircle transposon donor; Mock: no mRNA and vector; LV: lentiviral transduction.

Further, we found similar proliferation levels (≥ 3 cell divisions in 72 hours) in all CD8+ and CD4+ CD19-CAR T cell lines by CFSE dilution assay, regardless whether the cells had been gene-modified by SB-transposition or LV transduction (Figure 4.11).

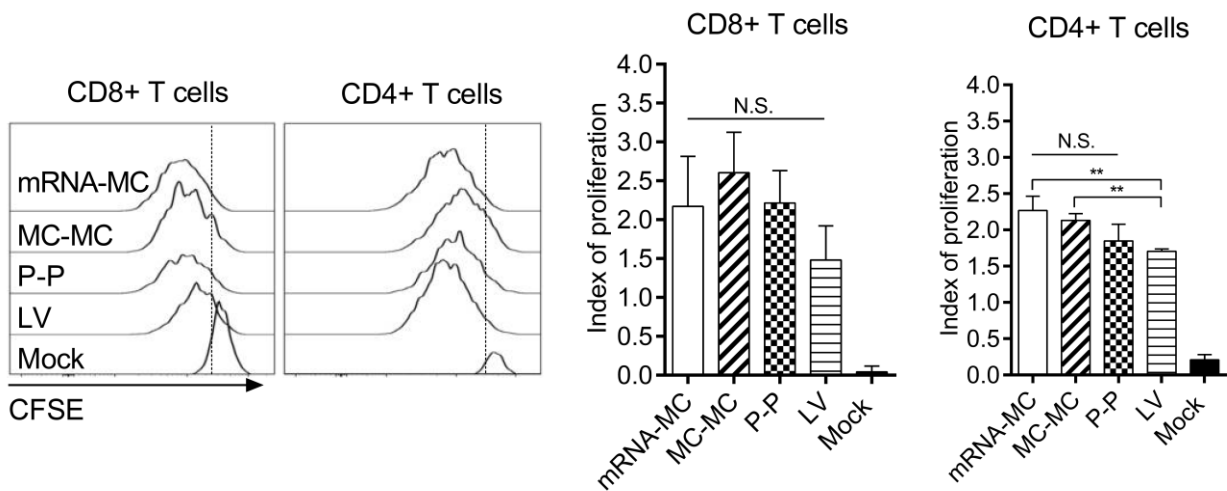


Figure 4.11. Proliferation of CD19-CAR T cells within 72 hours.

CFSE labeled T cells were co-cultured with K562/CD19+ target cells. Number of proliferation cycles was assessed by CFSE dye dilution. No exogenous cytokines were added to the assay medium. The index of cell proliferation (i.e. average number of cell divisions) was calculated from data obtained in $n=3$ independent experiments using FlowJo software. Data were analyzed by one-way ANOVA and Student's t test (** $p < 0.005$). P-P: transposon and transposase encoded both by plasmids; MC-MC: transposon and transposase encoded both by minicircles; mRNA-MC: SB100X mRNA and minicircle transposon donor; Mock: no mRNA and vector; LV: lentiviral transduction.

4.7 CD19-CAR T cells generated via MC transposition show potent antitumor activity *in vivo*

Next, we analyzed antitumor efficacy of generated CAR T cells in a systemic CD19+ lymphoma xenograft model (NSG/Raji-ffLuc). We focused on CAR T cells that were modified with SB100X mRNA and CD19-CAR MC, as this would be the most relevant combination for clinical translation. A potent antitumor effect was mediated by a single dose of SB-modified CD8+ and CD4+ CD19-CAR T cells. These cells rapidly eradicated tumor cells in all treated mice ($n=5$), whereas the mice receiving control T cells showed progressive, deleterious lymphoma (Figure 4.12a,b).

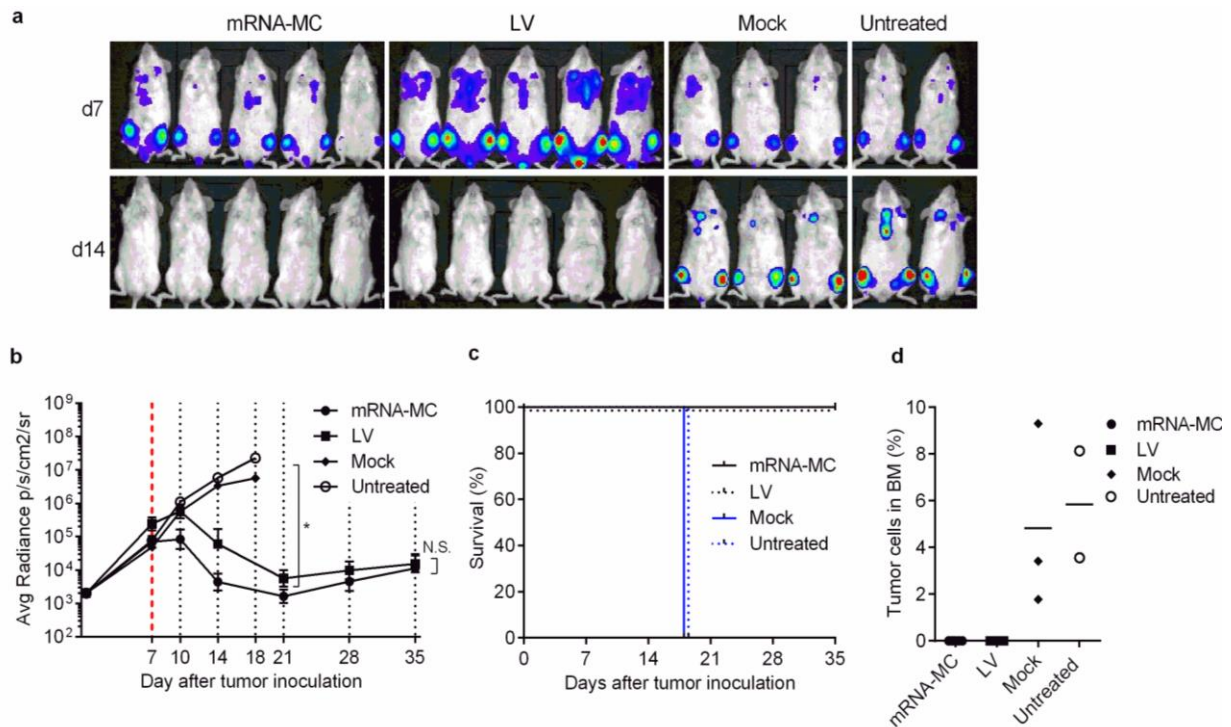


Figure 4.12. *In vivo* antitumor reactivity of CD19-CAR T cells prepared by SB-transposition.

(a) NSG mice were inoculated with Raji-ffluc/eGFP cells and 7 days later treated with 5×10^6 CD19-CAR T cells (1:1 ratio of CD8+ and CD4+ T cells, 2.5×10^6 each), unmodified control T cells (mock) or left untreated. CD19-CAR T cells were generated by transfection with SB100X mRNA and CD19-CAR MC (4:1 ratio) or by LV transduction. Bioluminescence images were obtained on day 7 (before T-cell infusion, upper row) and on day 14 (7 days after T-cell infusion, lower row). **(b)** Mean values of bioluminescence signals obtained from regions of interests encompassing the entire body of each mouse are plotted for each group at each time point. The red line marks the day of T-cell infusion. Data were analyzed using the Mann-Whitney test (* $p < 0.05$). **(c)** Kaplan-Meier analysis of survival in groups of mice treated with CD19-CAR T cells that had been prepared by SB-transposition (SB100X mRNA and CD19-CAR MC) ($n=5$) and LV transduction ($n=5$), mock T cells ($n=3$), or that had received no treatment ($n=2$). **(d)** Detection of tumor cells in the bone marrow of sacrificed mice by flow cytometry analysis. Tumor cell lines were checked for eGFP expression. **(a-d)** Data are representative for results obtained in at least 2 independent experiments with T cells prepared from different healthy donors.

The mice treated with SB CD19-CAR survived until the end of the observation period, as did the mice that were treated with LV-transduced CD19-CAR (Figure 4.12c). We confirmed complete lymphoma eradication from bone marrow in these mice by flow cytometry (Figure 4.12d).

SB-modified CAR T cells were detected in the peripheral blood of treated mice at the peak of response (7 days after T cell infusion), and persisted in the bone marrow of all mice after tumor clearance (Figure 4.13a,b). Collectively, our data demonstrate that CD19-CAR T cells generated through SB-transposition from MC transposon donor vectors are highly potent *in vitro* and *in vivo*, and mediate equally effective antitumor responses as CD19-CAR T cells generated by LV transduction.

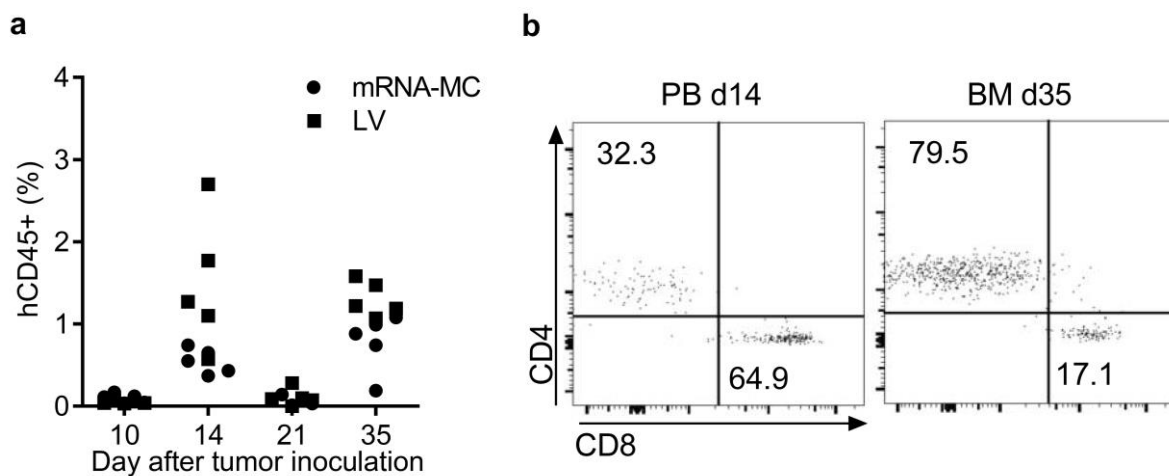


Figure 4.13. *In vivo* persistence of CD19-CAR T cells prepared by SB-transposition.

(a) Frequency of human T cells in the peripheral blood (PB) and bone marrow (BM) of mice treated with CD19-CAR T cells. Blood samples were obtained 3, 7 and 14 days after T cell transfer (i.e. day 10, 14, 21 after tumor inoculation), and bone marrow harvest upon termination of the experiment on day 35 after tumor inoculation. **(b)** Representative flow cytometry dot plots show CD8+ and CD4+ T cells (gated on living i.e. 7-AAD negative, CD45+ cells) in the peripheral blood and bone marrow of mice treated with SB100X mRNA and CD19-CAR MC.

4.8 Transposon insertion site analysis reveals a close-to-random genomic integration pattern in the genome of CD19-CAR T cells

We constructed an insertion site library from polyclonal CD8+ CD19-CAR T cells for massive parallel sequencing on the Illumina MiSeq platform. We mapped and characterized 26,834 unique insertion sites of our MC-derived CAR transposons. A

database of LV integration sites in human CD4+ T cells served as a reference and for comparison¹¹⁷.

Analysis of nucleotide frequencies in a 20-kbp window around the transposon insertion sites revealed that transposition from our MC had occurred into regions with close to random nucleotide frequency. In contrast, LV insertions were biased towards GC-rich chromosomal segments (Figure 4.14a). However, in a smaller, 1.5-kbp window around the insertion sites, both vector systems exhibited a preference for AT-rich DNA (Figure 4.14b). We detected the palindromic ATATATAT motif, which contains the TA dinucleotide target sequence of SB adjacent to all our MC-derived transposons. This observation is in accordance with what has been found for transposons mobilized from conventional donor plasmids⁴² (Figure 4.14c).

We then analyzed whether there was a preference of CD19-CAR transposon insertions into distinct sites of the genome, e.g. exons and introns, genes and cancer related genes. We found that transpositions from MCs had occurred with only a modest, yet statistically significant ($p < 0.001$) bias towards genic categories; however, in all evaluated categories this preference was substantially smaller than what we found for LV integrations (Figure 4.15a).

Importantly, transposon insertions showed only a 1.15-fold enrichment in genes and a 1.29-fold enrichment in cancer-related genes relative to the expected random frequency, whereas there was a 2.11-fold and a 2.64-fold enrichment of LV-associated insertions in these categories, respectively ($p < 0.01$ and $p < 0.05$).

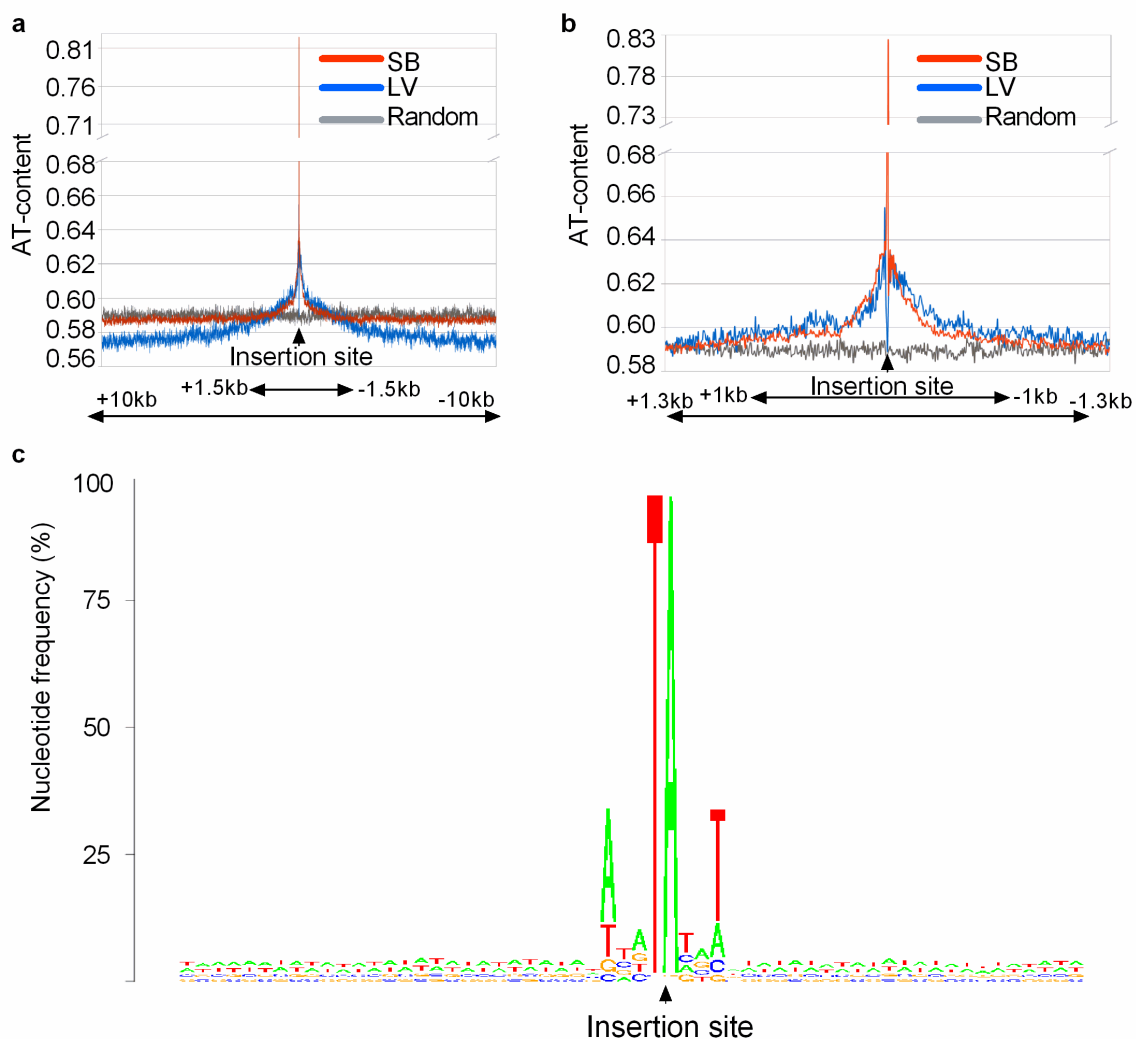


Figure 4.14. Nucleotide composition of chromosomal DNA around SB and LV insertion sites in T cells.

Each data point represents the average TA-content of 5 nucleotide bins in the chromosomal DNA around SB and LV insertion sites in T cells. Depicted are analysis windows of 20 kbp (a) and 2.6 kbp (b). The random dataset depicts the TA content around 10,000 computationally generated arbitrary loci of human chromosomes. (c) Base composition of SB target sites on human T cell chromosomes. The 60 nucleotide long nucleotide frequency matrix was plotted using the SeqLogo tool in R software. The triangle marks the insertion site of integrants. The degree of base conservation is depicted by the height of the letters.

Concordantly, CD19-CAR transposons were also inserted into non-genic regions in a close-to-random manner (0.89-fold compared to random), while LV transgenes were found to be underrepresented in these regions (0.23-fold compared to random) (Figure 4.15a).

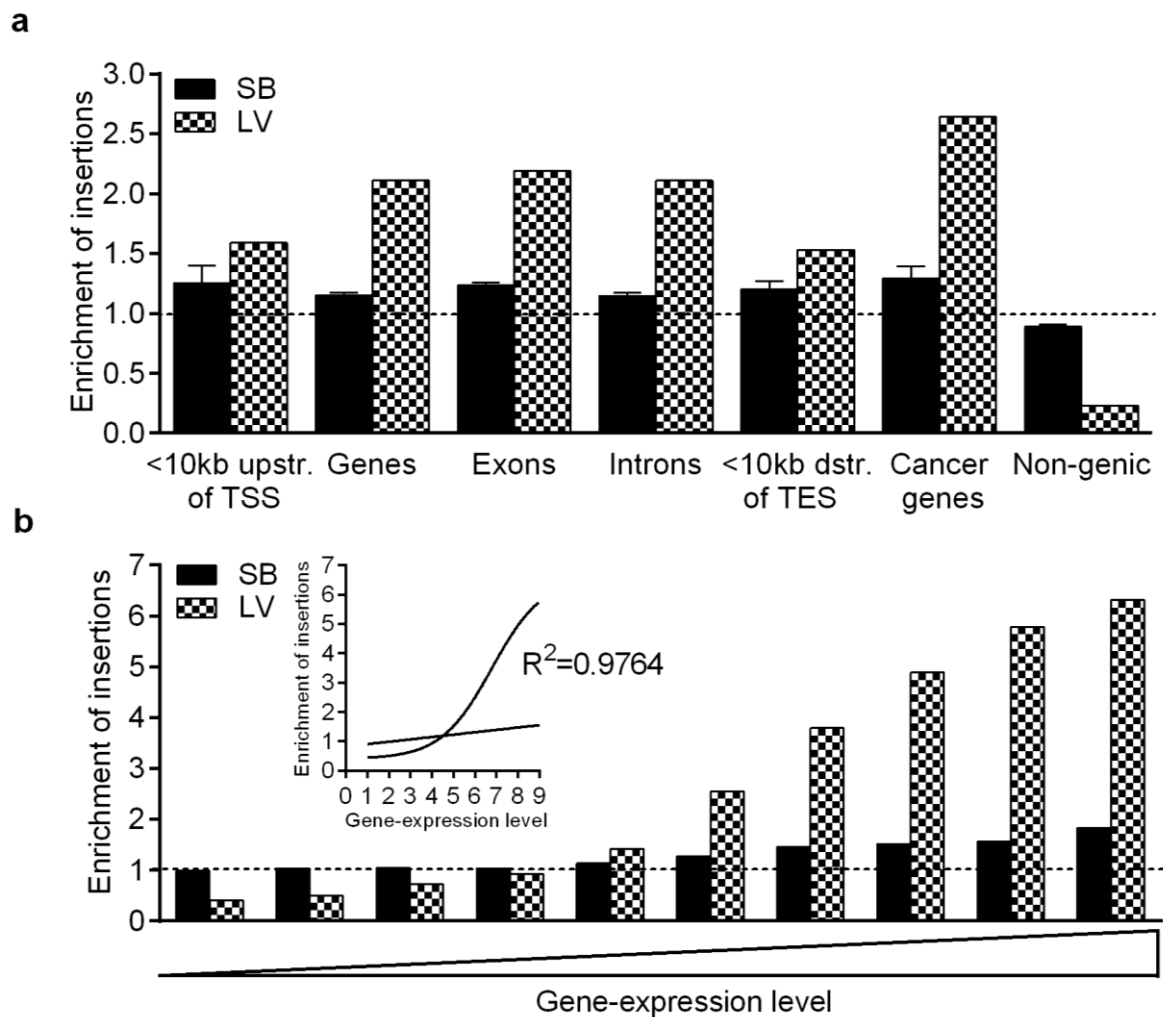


Figure 4.15. Insertion site properties of SB and LV in human T cells.

(a) Comparison of LV and SB insertion frequencies in gene-associated features of the human genome. Fold-enrichment of SB and LV insertion sites over the random expected frequency are plotted. The dashed line stands for fold-enrichment of 1 over the insertion frequency expected by random chance in the categories on the x-axis. TSS and TES: transcriptional start and end sites, respectively. **(b)** Correlation between genic insertion site frequencies and transcriptional status of the genes. Genes of activated T cells were clustered into 10 groups of equal size based on their growing expression levels (from left to right). The dashed line marks the expected random insertion frequencies normalized to 1. The trend line for SB was fitted using linear settings. Exponential setting was used to fit the trend line for the first 9 data points of LV dataset ($R^2=0.9764$). The increase of insertion frequencies in the group of most active genes does not follow the exponential trend.

Further, we determined whether there was an association between intragenic transposon insertion frequency and gene expression level. We used available transcriptome profiles for activated human T cells¹¹², clustered genes according to

their expression levels into ten groups of equal size and counted transposon and LV insertions in each group. The data show that MC-derived transposons were integrated into both low and highly-expressed genes in a close-to-random manner, and only displayed a minute preference for highly-expressed genes (Figure 4.15b). In contrast, lentiviral vector showed a strong preference for integration into highly-expressed genes, and there was an exponential correlation between insertion frequency and expression level of the respective gene ($R^2 = 0.976$) (Figure 4.15b).

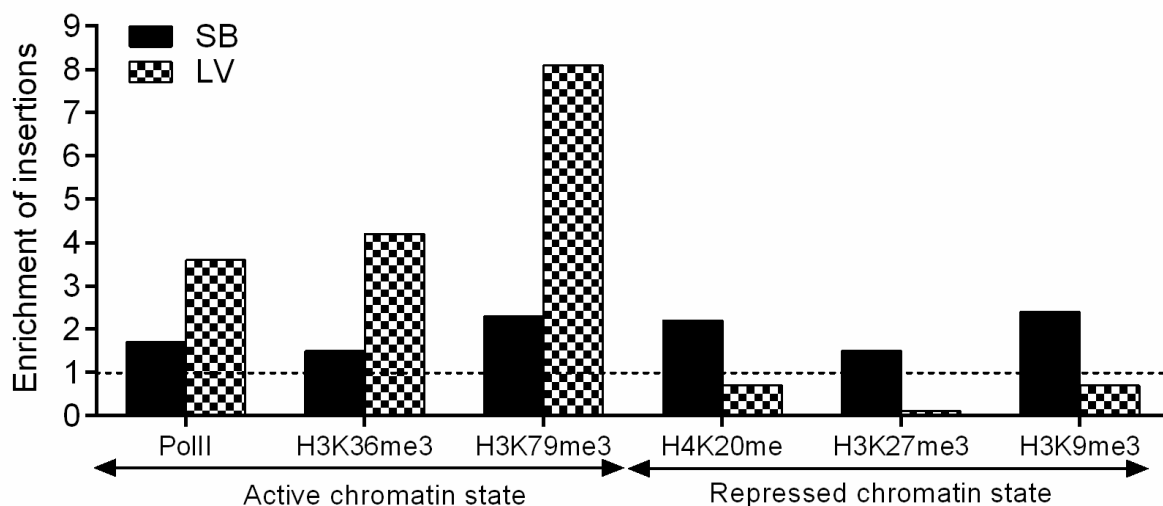


Figure 4.16. Representation of SB and LV insertion sites in transcriptionally active and repressed chromatin of T cells.

Chromosomal regions covered by RNA polymerase II (PolII), or possessing specific histone modifications (listed on the x-axis) were determined from available datasets obtained on activated human T cells. Fold changes in the representation of integration sites in the ChIP-Seq peaks compared to random control (dashed line) are shown on the y-axis.

We also found a strong enrichment of LV insertions in chromosome regions with H3K36- and H3K79-trimethylation and RNA polymerase II tags, all of them being chromatin marks for highly-expressed genes. LV insertions were underrepresented in transcriptionally inactive and heterochromatic chromosomal segments, signified by

H4K20-, H3K27-, and H3K9-trimethylation (Figure 4.16). In contrast, transposon insertions showed only a slight affinity towards markers of active transcription and equally favored integrating into transcriptionally-silenced chromatin domains (Figure 4.16). These data show that SB-transposons mobilized from MCs display a near-random integration pattern in the genome of human T cells, and in contrast to LVs do not have a preference for highly-expressed or transcriptionally active genes.

4.9 CD19-CAR transposons mobilized from MCs are frequently integrated into genomic safe harbors

Ideally, transposition would occur into genomic regions where insertion of the CAR transgene would not compromise the transcriptional integrity of the gene-modified T cell. We applied criteria that have been established to define such genomic safe harbors (GSH)^{111, 118} to our insertion site library of MC-modified CD19-CAR T cells, and compared them to the LV insertion site dataset. Computer-generated random positions in the genome map to GSHs at a frequency of 28%. We found that 20.8% of CD19-CAR transposon insertion sites but only 3% of the LV integration sites fulfilled all of the 5 GSH criteria (Figure 4.17b). In particular, a significantly higher proportion of transposon insertion sites compared to LV was located >300 kbp outside of cancer related genes (59% vs. 38%) and outside of genes (48% vs. 12%) which constitute the two paramount criteria (Figure 4.17a). In our analysis, none of the SB-transposon and LV insertions occurred in known oncogenes¹¹¹, and no insertion occurred in ultraconserved genomic regions which constitute only a minor fraction of the genome. In summary, we demonstrate for the first time that functional CAR T cells can be generated by SB-mediated transposition from MC DNA. MC-

derived transposons possess a highly favorable genomic integration profile, strongly suggesting that our enhanced SB-transposition strategy provides a safety advantage over LV-based gene transfer.

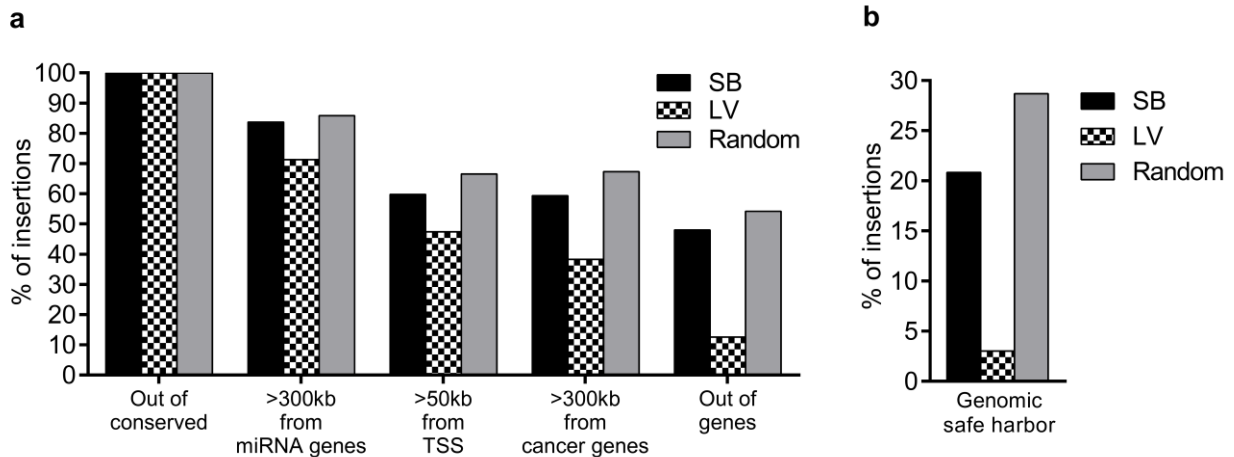


Figure 4.17. Integration frequencies of SB and LV in genomic safe harbors of T cells.

Genomic safe harbors are regions of the human chromosomes that concurrently meet the following 5 criteria of the x-axis: not ultraconserved, more than 300 kb away from microRNA genes, more than 50 kb away from transcriptional start sites (TSS), more than 300 kb away from genes involved in cancer and outside transcription units. **(a)** Percentage of SB, LV and random insertions fulfilling each criterion. **(b)** Percentage of insertions fulfilling all 5 criteria.

4.10 CD19-CAR MC transposon copy number analysis in the genome of T cells

The biosafety of an integrative gene delivery system is usually assessed based on its integration site profile as well as the transgene copy number analysis¹¹⁹. Therefore, we performed copy number analysis in T cells that had been modified with SB100X mRNA and CD19-CAR MC. We performed the copy number analysis on single cell T-cell clones obtained by limiting dilution using two different methods. First we performed a linker-mediated based PCR assay. Although this method is cost-effective for research based analysis but it is a laborious and time-consuming

procedure. On the other hand, the accuracy of its results depends on generation of TA overhang and their ligation to TA-specific linker oligos and sensitivity of gel electrophoresis detection. This limitation led us to develop a rapid and precise TaqMan-based droplet digital PCR (ddPCR) assay. This assay can be easily integrated into the time flow of assessment and producing CAR T cells for clinical applications. The linker-mediated PCR showed an average of $n=5$ (range 3–8) CD19-CAR transposon copies in CD8+ T-cell clones, and $n=6$ (range 3-12) transposon copies in CD4+ T-cell clones (Figure 4.18a,b).

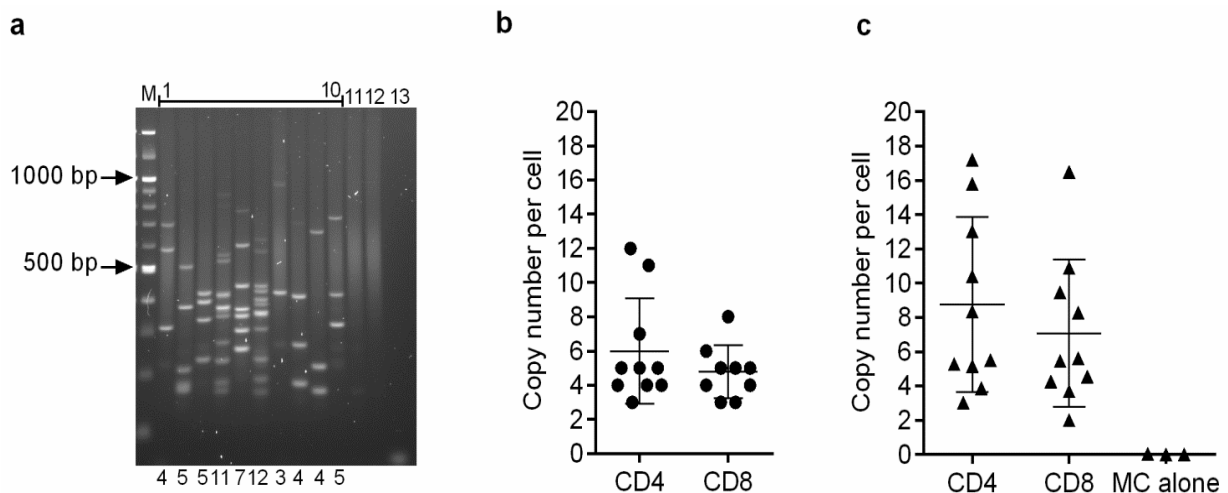


Figure 4.18. Determination of CAR copy number in CAR T cells.

(a) Linker-mediated PCR was performed on genomic DNA (gDNA) obtained from CD19-CAR expressing CD8+ and CD4+ T-cell clones (modified with SB100X mRNA and CD19-CAR MC at 4:1 ratio) using specific primers anchoring in the transposon left terminal inverted repeats (forward) and at the T-cell genome junction site (reverse). CAR copy numbers were determined by gel electrophoresis analysis. Lane M: 100 bp DNA ladder; lane 1-10: PCR product obtained from 10 distinct CD19-CAR expressing CD4+ T-cell clones; lane 11 and 12: input gDNA from samples nucleofected with CD19-CAR MC alone (no SB100X mRNA) and mock nucleofected samples (no MC, no SB100X mRNA); lane 13: no DNA control. Numbers below the gel image correspond to number of bands and gene copy numbers. **(b)** Gene copy number of CD4+ ($n=10$) and CD8+ ($n=9$) CD19-CAR T cell clones, modified with SB100X mRNA and MC CD19-CAR (4:1 ratio) determined by linker-mediated PCR. **(c)** ddPCR was performed on same clones using specific primers anchoring in inverted repeat region (forward) and CAR region (reverse). Inside each amplicon there is a fluorescent TaqMan probe for target detection in the Droplet Reader. MC alone shows the result from samples nucleofected with CD19-CAR MC alone without SB100X mRNA.

Next, we determined CAR copy numbers in same clones using our established TaqMan-based ddPCR assay. We used specific primers anchoring in inverted repeat region, which indicates random integration, and in the CAR region, indicating the CAR transposition events. We found that CAR copy numbers determined based on ddPCR were directly correlated to the ones determined by linker-mediate PCR. However, because of the higher sensitivity of the ddPCR compared with linker-mediated PCR which relies on gel electrophoresis detection, an average of $n=7$ (range 3-16) CD19-CAR transposon copies in CD8+ T-cell clones, and $n=9$ (range 4-17) transposon copies in CD4+ T-cell clones were determined (Figure 4.18c). Importantly, using ddPCR we could detect the SB100X-independent CD19-CAR integration into the gDNA of T cells that were nucleofected with CD19-CAR MC without the SB100X with an average $n=0.02$.

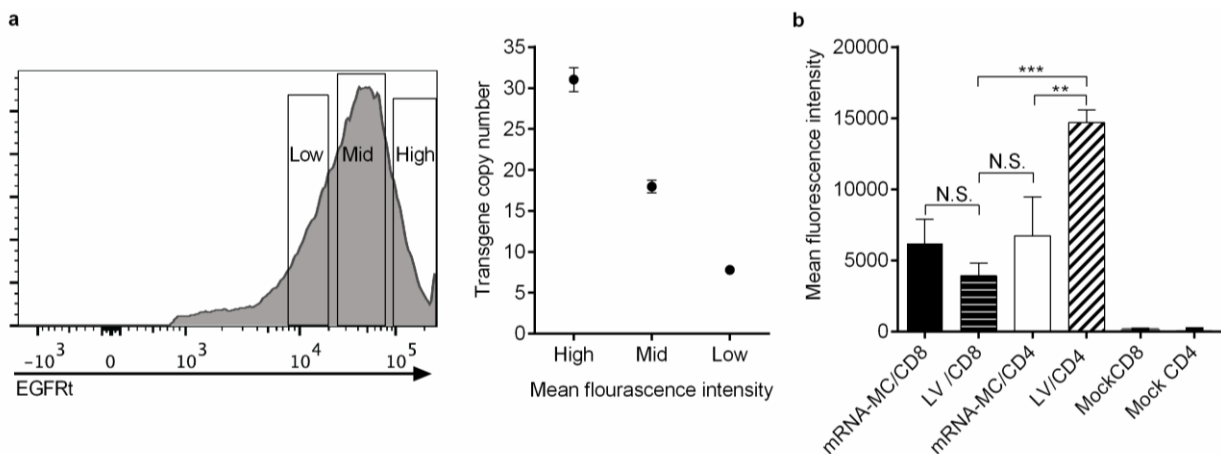


Figure 4.19. Absolute level of transgene expression in CD8+ and CD4+ T cells generated by SB or LV system.

(a) Correlation of mean fluorescent intensity (MFI) and transgene copy number. EGFRt+ CD8+ T cells were sorted into 3 fractions with either high, medium (mid) or low EGFRt expression level and the CAR copy number was determined by ddPCR assay. **(b)** Transgene expression was evaluated using the EGFRt marker encoded *in cis* with the CD19-CAR in SB-transposon donor and lentiviral vectors. CD8+ and CD4+ T cells were transfected with CD19-CAR MC and SB100X mRNA or transduced with LV. T cells were enriched for EGFRt expression and expanded with TM-LCL (CD19+ feeder cells) for 7 days. MFI was calculated based on FACS data analysis. mRNA-MC: SB100X mRNA and minicircle transposon donor; LV: lentiviral transduction. Data shown are mean values \pm SD obtained from three different donors. Statistical analysis was performed using Student's t test.

Nevertheless, CD19-CAR protein was not detectable on T-cell surface after 5 days as shown by flow cytometry analysis (Figure 4.18c, Figure 4.4b).

Moreover, we observed that there is a direct correlation between the mean fluorescence intensity (MFI) measured with flow cytometry analysis and the CAR copy numbers. The CAR T cells sorted for high EGFRt expression (higher MFI) showed dramatically higher CAR copy numbers ($n=31.1$) compared with CAR T cells sorted for medium ($n=17.9$) or low ($n=7.7$) MFI (Figure 4.19a). Consequently, we determined the absolute level of transgene expression base on MFI measurement by flow cytometry on polyclonal CD8+ and CD4+ CAR T-cell lines, which correlated well with the copy number analysis data (Figure 4.18, Figure 4.19b). Collectively, these data reveal that the average number of CAR transposon copies in both CD4+ and CD8+ T cell population at single cell level is in the range ($n<20$) that is accepted by regulatory authorities for clinical application at Paul-Ehrlich-Institute (PEI).

4.11 CAR transposon copy numbers can be modulated using titrated amounts of MC DNAs

The prevailing paradigm is that a higher number of a transgene genomic integration is correlated with the better functional efficiency of the modified cells; however, it may also increase the risk of insertional mutagenesis. Consequently, a lower copy number as far as it does not impair with functional efficiency of the engineered cells is preferable. In order to achieve lower CAR copy numbers, we reduce the amount of MC DNA vectors. CD8+ T cells were transfected with 2-fold serial dilutions of CD19-CAR MC and MC-SB100X vectors, from the optimal amount of 600 ng to 37.5 ng for CD19-CAR MC and from the optimal amount of 500 ng to 31 ng for

SB100X MC (no CAR expression was detectable with lower DNA amounts). On day 14 after transfection, CAR expression was determined by flow cytometry (Figure 4.20a). As expected, CAR expression directly correlated with the amount of vectors used, as well as with the measured MFI (Figure 4.20b). To avoid the possibility of enriching highly EGFRt+ T cells with biotin-conjugated anti-EGFR mAb and anti-biotin MicroBeads, this time, the CD8+ T cells were sorted for EGFRt+ cells using FACS sorting to a purity of approximately 90%.

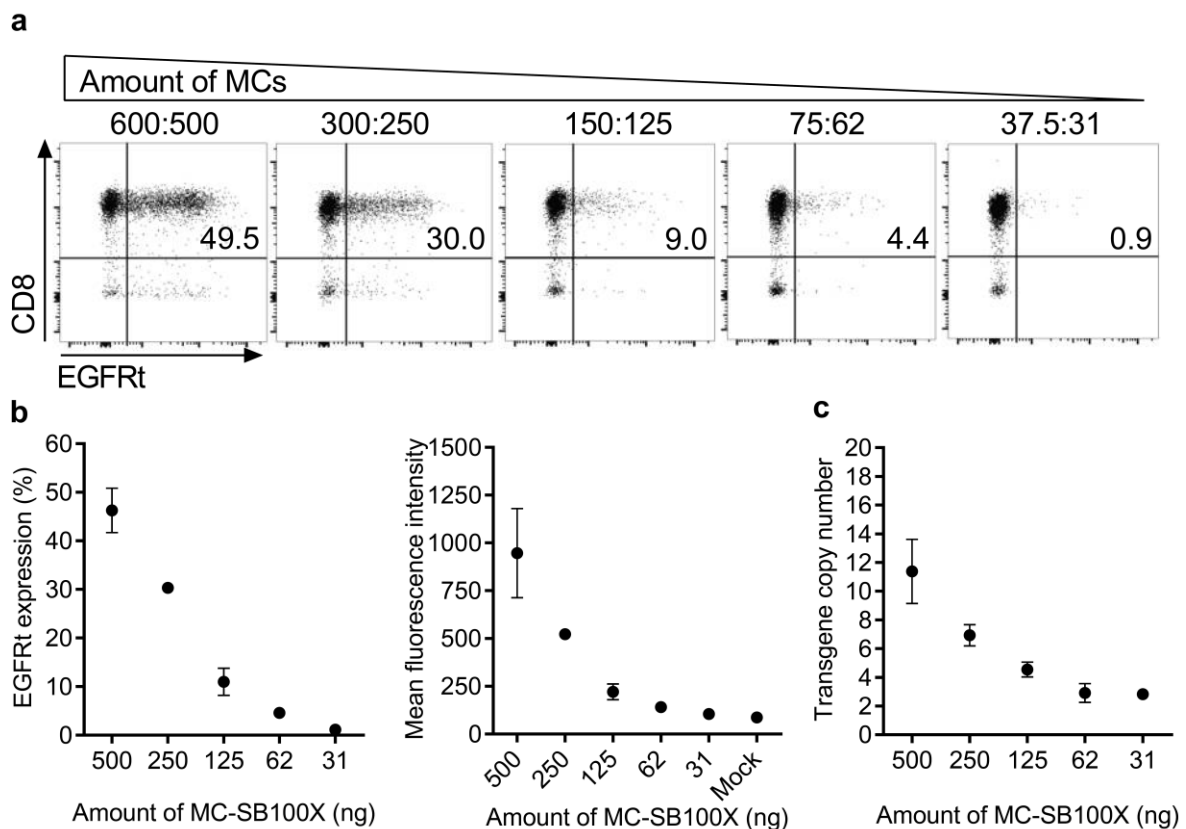


Figure 4.20. Correlation between MC DNA vector amounts and copy number.

(a) A representative flow cytometry analysis of EGFRt expression on day 14 post-transfection (gated on living, i.e. 7-AAD negative cells, gating is done based on mock cells). CD8+ T cells were nucleofected with 600 ng of CD19-CAR MC DNA and 500 ng of SB100X MC DNA, these optimal amounts were 2-fold serially reduced until EGFRt expression was no longer detectable. The amount of each vector in ng is shown at the top of each dot plot. **(b)** EGFRt expression (left graph) and mean fluorescence intensity (right graph) of CD8+ T cells were measured by flow cytometry analysis. **(c)** gDNA of the polyclonal EGFRt+ CD8+ T cells was used for copy number analysis using ddPCR. **(b, c)** Data represent mean values \pm SD of two independent experiments.

The gDNA of polyclonal EGFRt+ T cells was isolated, fragmented and used for the copy number analysis by ddPCR. As expected, we observed a direct correlation between the amount of transfected MC vectors into T cells and copy number variation.

The copy number was decreased from an average of 11.3 for the highest amount of MC DNA vectors to an average of 2.8 for the lowest amount of MC DNA vectors used (Figure 4.20c). Notably, reducing optimal amount of MC vectors to half decreased average CAR copy number from 11.3 to 7 while a transfection rate of approximately 30% was achieved. Therefore, when lower transgene copy number is mandatory for clinical application, half of the optimal amount of MC vectors could be potentially used. In summary, these data show that the CAR copy number can be modulated by the amount of MC vectors used. Hence, we are able to generate CAR T cell with lower CAR transgene copy numbers as may be required for particular applications.

4.12 Interim conclusion for first aim

In summary, our data demonstrate that CAR T cells can be engineered through non-viral SB transposition of CAR transgene from MC vectors. We observed that electroporation of SB MCs is substantially more effective and less toxic compared to conventional plasmids, and enables rapid generation of therapeutic CAR T-cell doses. CD19-CAR T cells engineered with our enhanced SB approach conferred potent reactivity *in vitro* and eradicated lymphoma in a xenograft model *in vivo*. Next, we analyzed genomic distribution of SB and LV integrations and showed that a significantly higher proportion of MC-derived CAR transposons compared to LV integrants had occurred outside of highly-expressed and cancer-related genes into

genomic safe harbor loci that are not expected to cause mutagenesis or genotoxicity. Moreover, we developed a rapid and precise TaqMan-based ddPCR assay for CAR transposon copy number analysis. We determined CAR copy numbers in both CD8+ and CD4+ CAR+ T cells which were in the acceptable range determined by regulatory authorities for clinical application. Finally, we showed that CAR transposon copy number can be fine-tuned using titrated amounts of MC DNAs.

In conclusion, we enhanced engineering of CAR T cells using non-viral SB transposition from MC DNAs with a superior biosafety profile compared with lentiviral gene delivery approach, which resulted in accomplishment of our first objective. In the second part of this chapter, we focus on the second aim of this study, which was the establishment of a single-step and fully non-viral T-cell engineering strategy for generating *PD-1* knockout CAR+ T cells with improved therapeutic index.

4.13 Editing of human *PD-1* in Jurkat cells using lentiCRISPR/Cas9

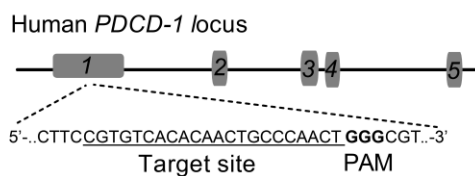
Blockade of key immune checkpoints such as PD-1 may enhance function of CD19-CAR T cells¹⁰². Here, we used RNA guided endonuclease (RGEN) CRISPR/Cas9 system for deleting *PDCD-1* (*PD-1*) in T cells. Knockout (KO) of *PD-1* is anticipated to be synergistic with the function of CD19-CAR T cells. In order to genetically knock out *PDCD1* (*PD-1*), we used an *in silico* prediction tool to design a panel of single guide RNA (sgRNA) candidates to guide Cas9 to this locus. One previously designed sgRNA targeting *PD-1* was used as a positive control⁹⁹. We directed our sgRNAs to loci that correspond to exons of *PD-1* and at N-terminus of PD-1 protein to avoid creating a truncated but functional PD-1 protein. sgRNAs with higher quality score ($\geq 90\%$) were selected for assuring the highest editing efficiencies

and lower off-target effects (Figure 4.21a,b,d). The sgRNAs were then cloned into a lentiviral vector (lentiCRISPR v2) encoding Cas9 and puromycin, which the latter serves as a selection marker (Figure 4.21c). To test the ability of each sgRNA to direct Cas9-mediated ablation of *PD-1*, we transduced Jurkat cells that are PD-1+ (>70%) with sgRNA-encoding viral vectors. Three days after viral transduction, cells were treated with puromycin (1µg/mL) to select successfully transduced cells. At this puromycin concentration, the cells that have not been transduced and are not resistant to this antibiotic will die.

a

sgRNA No.	Target sequence	PAM	Target site	Quality score
1	CGTCTGGGCGGTGCTACAAC	TGG	Exon1 (100-122)	93%
2	GTCTGGGCGGTGCTACAAC	GGG	Exon1 (101-123)	90%
3	CACGAAGCTCTCCGATGTGT	TGG	Exon2 (6022-6044)	93%
0	CGACTGGCCAGGGCGCCTGT	GGG	Exon1 (83-103)	Positive control sgRNA

b



c



d

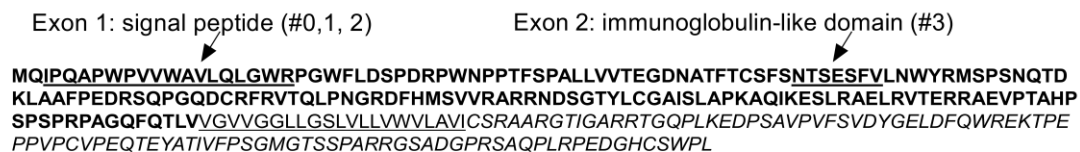


Figure 4.21. Selection of sgRNAs in the human *PD-1* locus.

(a) Designed sgRNAs and their criteria. A protospacer adjacent motif (PAM) domain at the 3' end of the target site is required for Cas9 function. Quality score shows the accuracy of on-target activity computed as 100% minus sum of off-target hit-scores in the target genome. **(b)** Schematic of human *PDCD-1* locus with 5 exons shown as grey boxes. Target site of sgRNA #2 is shown as an example which is underlined, PAM is shown in bold. **(c)** Schematic of bicistronic viral expression vector (lentiCRISPR v2) for U6 promoter-driven sgRNA and EFS promoter-driven human codon-optimized *S.pyogenes* Cas9 (*SpCas9*) with puromycin (*puro*) selection marker. **(d)** Amino acid sequence and targeted domain in PD-1 protein by sgRNA. Targeted sites in extracellular domain of PD-1 are shown with arrows. sgRNA #1 and #2 target signal peptide within exon 1 and #3 targets immunoglobulin-like domain within exon 2. Grey underlined: transmembrane domain; grey italic: cytoplasmic domain.

Next, we performed T7 endonuclease I (T7EI) assay to measure insertions or deletions (indels) at *PD-1* locus and observed that *PD-1* was significantly abrogated up to 58-66% in Jurkat cells depending upon the sgRNA used (Figure 4.22a). To further evaluate the efficiency of sgRNA-mediated *PD-1* disruption in Jurkat cells, we analyzed PD-1 protein level by flow cytometry and MFI measurement. We found that PD-1 expression was reduced from 88% in Jurkat cells treated with Cas9 alone to 36.1%, 24% and 39% after treatment with sgRNA #1, #2 and #3, respectively. Moreover, we observed 4-fold reduction in MFI of PD-1 expression when Jurkat cells were treated with sgRNA #2 (Figure 4.22b). Consequently, sgRNA #2, which showed the highest editing efficiency among all the sgRNAs including the positive control sgRNA, was used in following experiments.

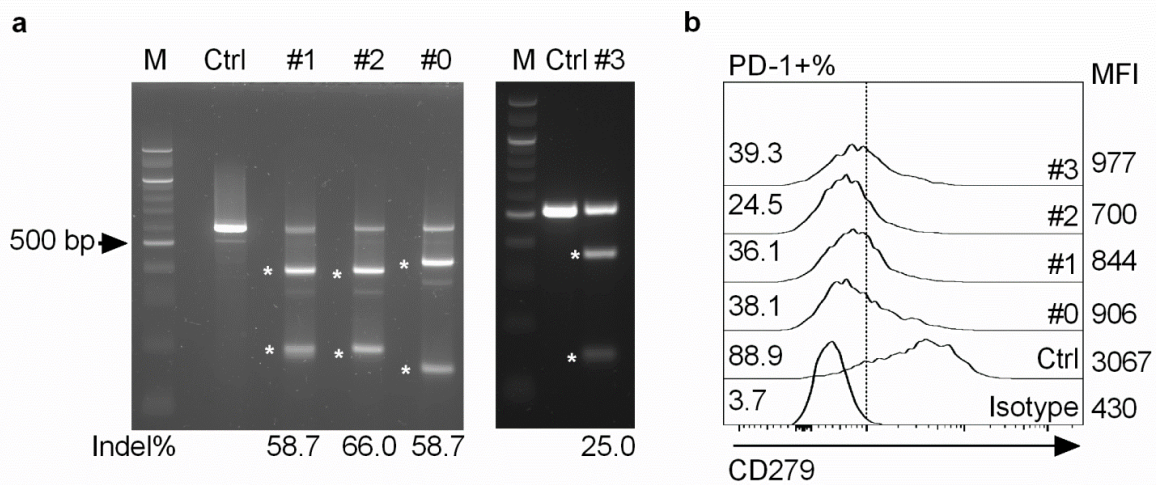


Figure 4.22. Modification efficiencies of different sgRNAs targeting *PD-1* in Jurkat cell line

(a) A representative of T7 endonuclease I (T7EI) assay. T7EI assay was used to estimate sgRNA #1, #2, #3 and control sgRNA editing efficiency in Jurkat cells. gDNA from the transduced cells was extracted. The target sites were PCR amplified to test *PD-1* disruption. The two T7EI digested fragments are indicated by stars. Intensity of each band was measured by Image Lab™ Software. Indel% was measured using the standard formula. Lane M, 100bp DNA ladder; lanes Ctrl, #1, #2, #3 and #0, Jurkat cells transduced with Cas9 alone or sgRNA #1, 2, 3; and positive control sgRNA, respectively. **(b)** PD-1 (CD279) surface expression analysis by flow cytometry. PD-1 expression percentage and MFI are shown at left and right site of the histogram, respectively. Jurkat cells stained with a corresponding isotype antibody were considered as a negative control for staining. Flow cytometry analysis was done using FlowJo software.

4.14 Editing of human *PD-1* in CD8+ T cells using lentiCRISPR/Cas9

Next, to check the efficiency of sgRNA #2 in primary T cells, we transduced CD8+ T cells with this sgRNA. We could successfully achieve *PD-1* KO in T cells. Although the cleavage efficiency of the sgRNA was dramatically reduced from 66% in Jurkat cells to 9.8 % (mean of n=2) in primary CD8+ T cells (Figure 4.23a). Moreover, we observed 1.4-fold reduction (mean of n=2) in MFI of PD-1 expression in *PD-1* KO T cells as compared with control CD8+ T cells (Figure 4.23b).

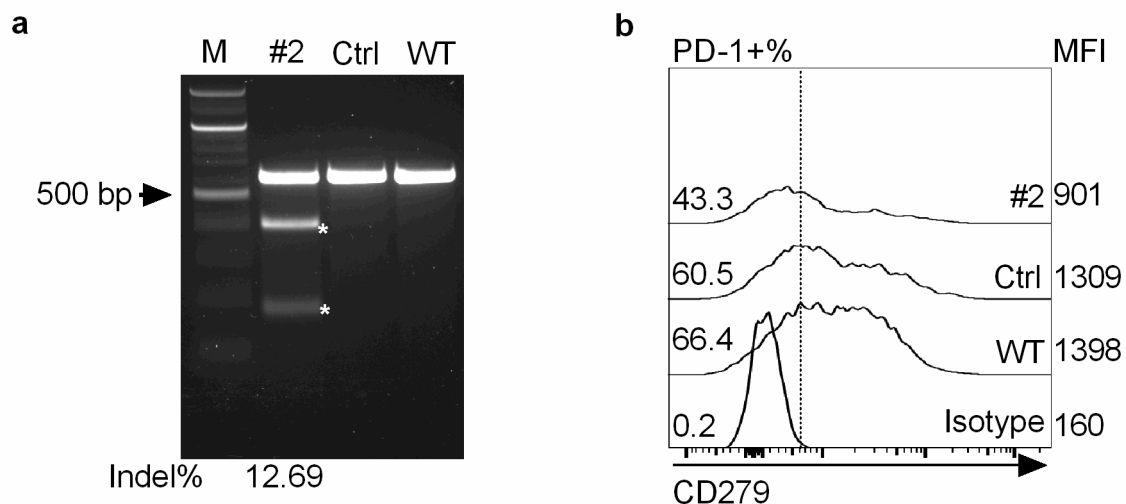


Figure 4.23. LentiCRISPR/Cas9 mediated ablation of *PD-1* locus in CD8+ T cells.

(a) A representative T7EI assay in CD8+ T cells for estimation of sgRNA #2 cleavage efficiency. CD8+ T cells were transduced with lentiCRISPR v2 encoding sgRNA #2. gDNA from the cells was extracted and target site was PCR amplified to test *PD-1* disruption by T7EI assay. The two T7EI digested fragments are indicated by stars. Lane M, 100bp DNA ladder; lanes #2, Ctrl, WT, CD8+ T cells transduced by sgRNA #2, Cas9 alone or left untransduced, respectively. **(b)** A representative PD-1 (CD279) surface expression analysis by flow cytometry (n=2). CD8+ T cells were transduced with lentiCRISPR v2 viral vectors encoding sgRNA #2, Cas9 alone (Ctrl) or left untransduced (WT). PD-1 expression percentage and MFI are shown at left and right site of the histogram, respectively. The cells stained by a corresponding isotype antibody were considered as a negative control for staining. Flow cytometry analysis was done using FlowJo software.

We had observed that T cells upregulate PD-1 after stimulation with PMA/Ionomycin (PMA/Iono). We decided to use this as a maneuver for distinguishing and isolating *PD-1* KO T cells from unmodified cells. This will facilitate the assessment of PD-1 expression by flow cytometry analysis or *PD-1* KO effect on functional potency of edited cells compared with wild type T cells. We enforced T cells to display PD-1 on their surface through unspecific PMA/Iono stimulation¹²⁰. Wild type T cells displayed PD-1 up to 90% which confirms the efficiency of PMA/Iono stimulation for PD-1 upregulation (Figure 4.24a).

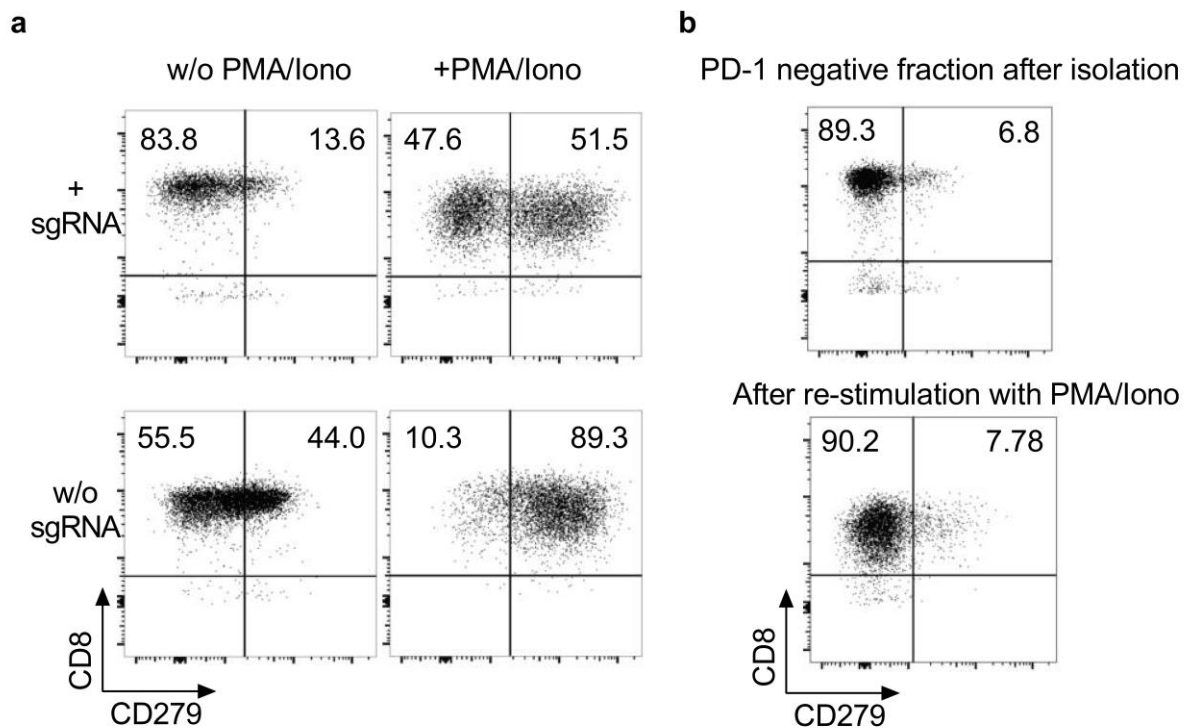


Figure 4.24. Enrichment of *PD-1* knockout T cells.

(a) Upregulation of PD-1 on T cell surface using PMA/Ionomycin (PMA/Iono). Prior to enrichment, CD8+ T cells transduced with lentiCRISPR v2 sgRNA#2 (upper panel) or lentiCRISPR v2 without sgRNA were stimulated with 1 μ L of each PMA (1 mg/mL) and ionomycin (1 mM) per 1 x10⁶ cell/mL for 24-36 hours. **(b)** Enrichment of *PD-1* knockout T cells. 24-36 hours post-stimulation with PMA/Iono. *PD-1* knockout T cells were enriched using anti-PD-1 PE antibody and Anti-PE MicroBeads (Miltenyi) via Macs magnetic procedure and negative selection (upper panel) and were re-stimulated similarly with PMA/Iono to confirm the efficiency and accuracy of enrichment (lower panel).

Post-stimulation with PMA/Iono, *PD-1* KO CD8+ T cells were enriched to approximately 90% purity via staining with anti-*PD-1* mAb conjugated to PE and anti-PE MicroBeads (Miltenyi). We next re-stimulated the resting enriched *PD-1* KO cells with PMA/Iono to check their purity. The cells did not display *PD-1* surface expression, which confirms that the isolation protocol results in selection of *PD-1* KO T cells with high purity.

4.15 Non-viral ablation of *PD1* in CD8+ T cells via Cas9 RNP

Persistence of Cas9 when is delivered as DNA plasmid or its stable integration into the T cells genome via viral vectors has been shown to increase the off-target activity of the system and may increase the risk of genotoxicity⁹⁸. Consequently, we investigated whether performing *PD-1* ablation via delivery of pre-assembled recombinant Cas9 protein and *in vitro*-transcribed sgRNA as a ribonucleoprotein complex (Cas9 RNP) instead of viral delivery is sufficient for accomplishing *PD-1* KO in CD8+ T cells. We cloned sgRNA #2 and its scaffold into a plasmid which contained a T7 promoter and produced the *in vitro*-transcribed sgRNA that has a size of 120 bp after agarose gel electrophoresis (Figure 4.25a). Next, we used two different molar ratios of Cas9 to sgRNA (1:6 and 1:3) to determine the optimal ratio for nucleofection. On day 12 post-nucleofection, cleavage efficiency and *PD-1* surface expression were analyzed by T7EI assay and flow cytometry, respectively. Delivery of *PD-1* specific Cas9 RNP with molar ratios of 1:6 and 1:3 induced indels at frequencies of 27% and 22% in CD8+ T cells, respectively, which was approximately 2-fold higher than what observed with virally modified CD8+ T cells (Figure 4.25b).

Moreover, MFI of PD-1 expression was reduced 3.5-fold as compared with wild type unmodified CD8+ T cells based on flow cytometry analysis (Figure 4.25c).

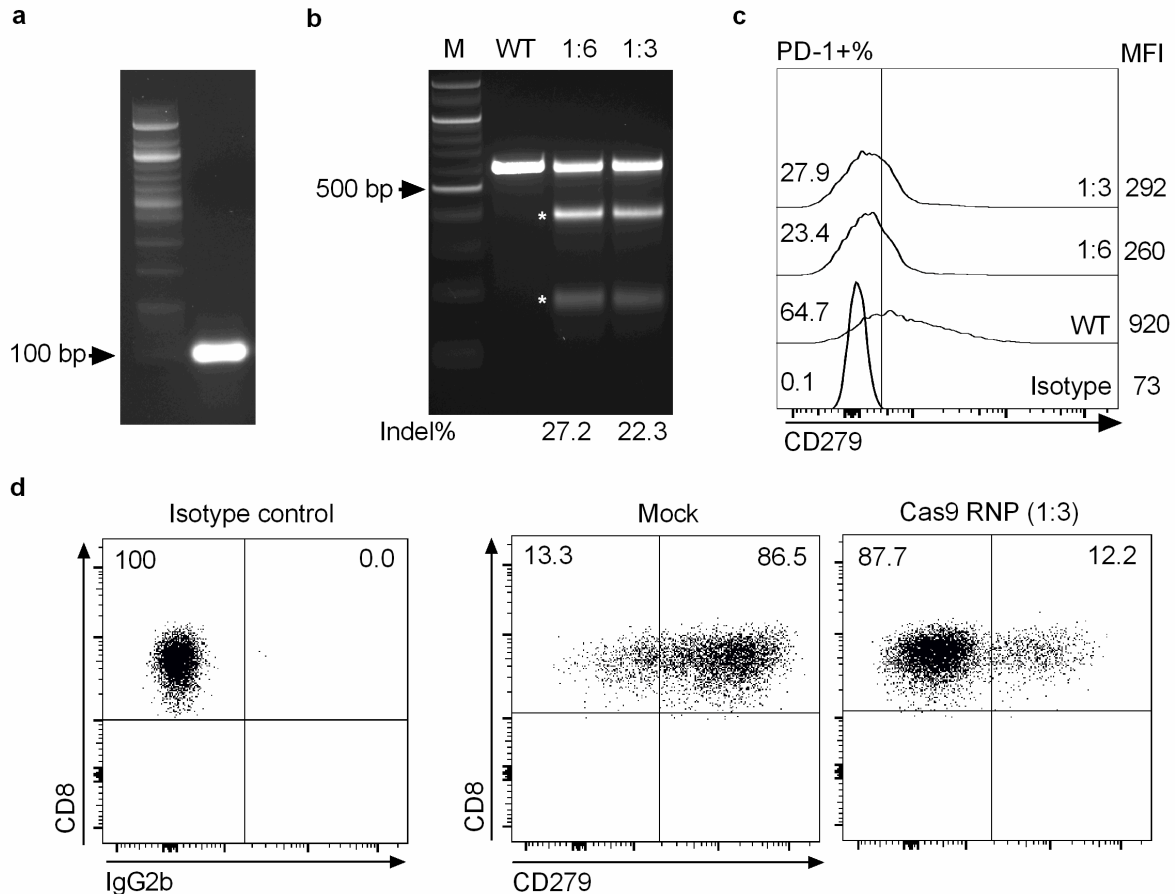


Figure 4.25. Disruption of *PD-1* in CD8+ T cells via delivery of Cas9 RNP.

(a) sgRNA #2 and its scaffold were cloned into a pCRTM-Blunt vector which contains a T7 promoter and *in vitro*-transcribed sgRNA was produced. The sgRNA has a size of 120 bp after agarose gel electrophoresis. (b) A representative T7EI assay for estimation of cleavage efficiency in CD8+ T cells (n=2). 1×10^6 cells CD8+ T cells from healthy donor were nucleofected with $0.75 \mu\text{g}/\mu\text{L}$ cas9 protein (15 μg) premixed with $1 \mu\text{g}/\mu\text{L}$ of *in vitro*-transcribed sgRNA, 20 μg , (Cas9: sgRNA molar ratio of 1:6) or $0.5 \mu\text{g}/\mu\text{L}$ *in vitro*-transcribed sgRNA, 10 μg , (Cas9: sgRNA molar ratio of 1:3) in 20 μL of nucleofection solution. gDNA from the cells was extracted on day 12 after transfection. The target site was PCR amplified to test *PD-1* disruption by T7EI assay. The two T7EI digested fragments are indicated by stars. Lane M, 100bp DNA ladder; lane WT, gDNA from mock CD8+ T cells, lane 1:6 and 1:3 show the two different Cas9:sgRNA molar ratios used. (c) PD-1 (CD279) surface expression analysis by flow cytometry in CD8+ T cells. PD-1 expression percentage and MFI are shown at left and right site of the histogram, respectively. The cells stained by a corresponding isotype antibody were considered as a negative control for staining. Flow cytometry analysis was done using FlowJo software. (d) A representative flow cytometry analysis of PD-1 expression in CD8+ T cells after PMA/Ionomycin stimulation. CD8+ T cells nucleofected with Cas9 RNP complex in a Cas9: sgRNA molar ratio of 1:3 are shown.

Stimulation of T cells with PMA/Iono also confirmed the efficient KO of *PD-1* in transfected cells with Cas9 RNP complex. CD8⁺ T cells that were modified via Cas9 RNP dramatically expressed lower percentage of PD-1 (12%) on their surface while wild type cells showed 86% PD-1 expression based on flow cytometry analysis (Figure 4.25d). Notably, RGEN via Cas9 RNP delivery was less toxic to the cells than the viral delivery. The latter requires selection of transduced cells by puromycin treatment, which needs to be followed by an expansion cycle with feeder cells for obtaining required T cell number for analyses.

4.16 Single-step fully non-viral generation of *PD-1* KO CD19-CAR⁺ T cells via MC-based CAR transposition and Cas9 RNP

Finally, we combined the SB-mediated CAR transposition from minicircles (Aim 1 of the study) with *PD-1* disruption via Cas9-RNP to generate *PD-1* KO CAR⁺ T cells through a complete non-viral strategy (Aim 2). To achieve this goal, CD8⁺ T cells were nucleofected with MC-derived CD19-CAR transposon donor vector, SB100X MC or SB100X mRNA and in the same reaction, the cells were additionally nucleofected either with Cas9 RNP complex targeting *PD-1* or without Cas9 RNP. CD19-CAR and PD-1 expression were analyzed on day 14 post-nucleofection by flow cytometry. To assess PD-1 expression the cells were stimulated for 24-36 hours with PMA/Iono before analysis. PD-1 expression was dramatically reduced from 86% to 13% in CAR⁺ CD8⁺ T cells when the cells were nucleofected in combination with Cas9 RNP. Of note, CD19-CAR expression was reduced approximately 2 times as compared with the CD8⁺ T cells that were nucleofected with CD19-CAR MC and SB100X MC without Cas9 RNP complex (Figure 4.26a). Since the use of SB100X

mRNA rather than SB100X MC increases the safety of cell products for clinical application, we replaced SB100X MC with SB100X mRNA. Similar results were achieved when SB100X mRNA was used as a transient source of SB100X (Figure 4.26b).

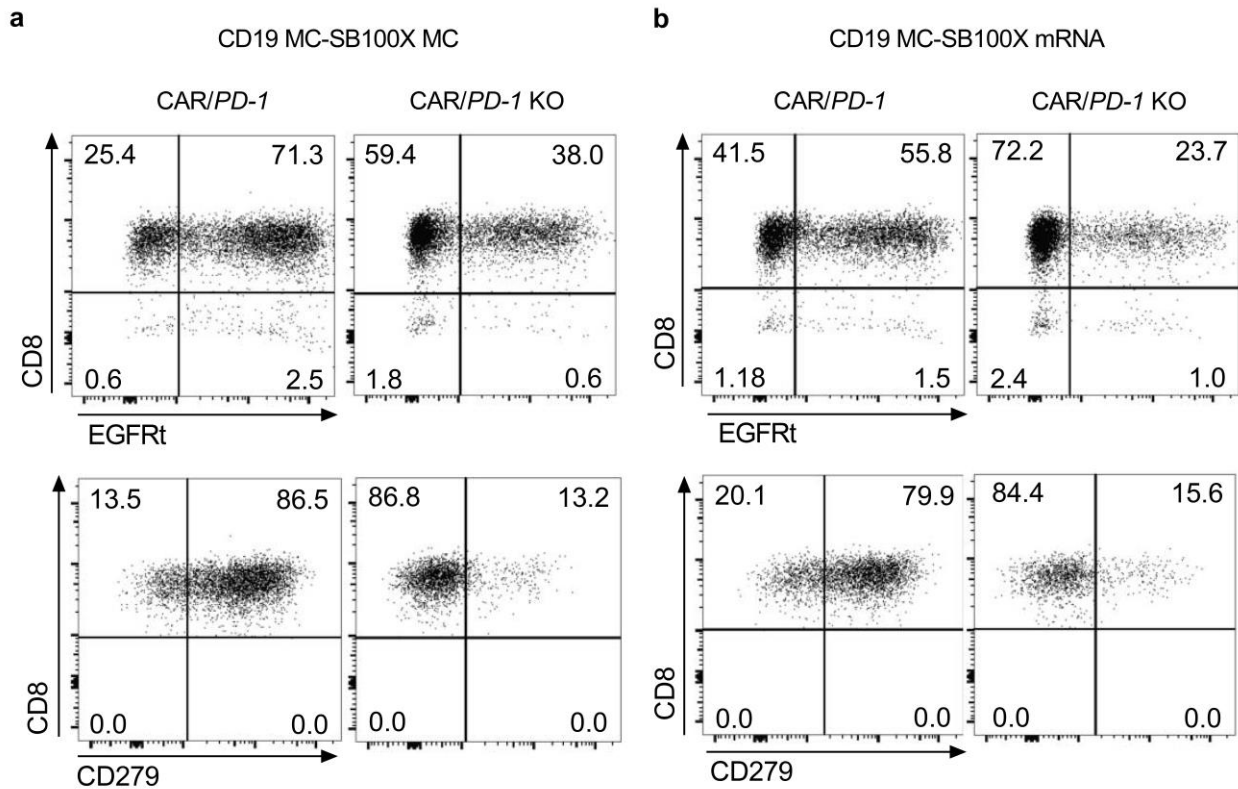


Figure 4.26. Generation of *PD-1* KO CD19-CAR⁺ CD8⁺ T cells using a complete non-viral system.

(a) Generation of *PD-1* KO CAR⁺ T cells using MC vectors encoding CAR transposon and SB100X transposase in combination with Cas9 RNP targeting *PD-1*. CD8⁺ T cells were nucleofected with 0.6 μ g and 0.5 μ g of each CD19-CAR transposon and SB100X transposase donor MC DNA (left dot plot) or in combination with Cas9 RNP complex, molar ratio of 1:3, 15 μ g Cas9 protein: 10 μ g *in-vitro* transcribed sgRNA, (right dot plot) in 20 μ L of nucleofection buffer. **(b)** Replacement of SB100X MC DNA with SB100X mRNA as transient source of transposase. Cells were nucleofected with CD19-CAR MC DNA (0.6 μ g) and SB100X mRNA (2.4 μ g, ratio of 1:4, left dot plot) or in combination with Cas9RNP complex, molar ratio of 1:3 (right dot plot). The cells were gated on living, i.e. 7-AAD negative cells for EGFRt analysis (upper panels) and were gated on EGFRt⁺ cells for CD279 (*PD-1*) expression analysis (lower panels). The results are the representative of two separate experiments.

Next, we sought to confirm the efficiency of our novel fully non-viral T-cell engineering strategy for generating genome edited CAR T cells other than CD19-specific CAR T cells. In this regard, we replaced the CD19-CAR MC with SLAMF7-CAR MC. We have previously observed that SLAMF7 is highly expressed in multiple myeloma cells, which is among malignancies that our group is interested in for future clinical trials. We successfully generated *PD-1* KO SLAMF7-CAR+ CD8+ T cells by the combination of SLAMF7-CAR transposition from MC with *PD-1* KO via Cas9 RNP (Figure 4.27).

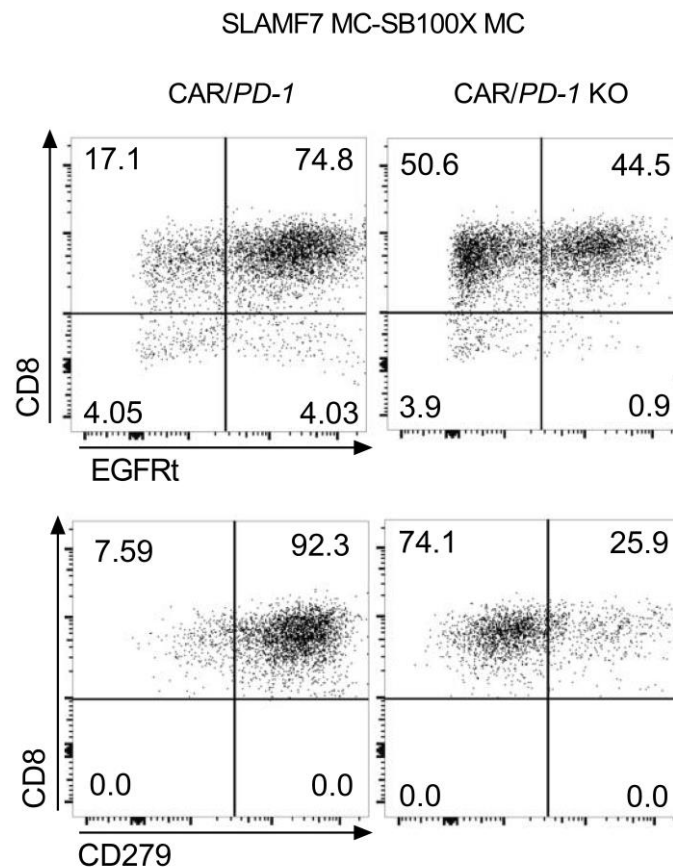


Figure 4.27. Generation of *PD-1* KO SLAMF7-CAR+ CD8+ T cells using a fully non-viral system.

CD8+ T cells were nucleofected with 0.6 μg and 0.5 μg of each SLAMF7-CAR transposon and SB100X transposase donor MC DNAs (left dot plot) or in combination with Cas9 RNP complex, molar ratio of 1:3, 15 μg Cas9 protein : 10 μg *in-vitro* transcribed sgRNA, (right dot plot) in 20 μL of nucleofection buffer. The results are a representative of two separate experiments.

Collectively, our data demonstrate that SB transposition when CAR transgene is transposed from a minicircle vector in combination with CRISPR/Cas9 genome editing tool when Cas9 RNP complex is used to target *PD-1* is a powerful strategy for generating *PD-1* KO CAR+ T cells. This single-step and fully non-viral gene transfer and genome editing strategy will pave the way for stable, fast and efficient genetic modification of T cells for various T-cell therapy approaches and addresses the biosafety concerns related to viral-based gene transfer strategies to a great extent.

4.17 Interim conclusion

In this study, we had two different but related objectives to improve non-viral gene transfer and genome editing tools as an alternative to viral gene delivery strategies for engineering of CAR T cells. As the first objective, we aimed to address three problems related to CAR transposition from conventional SB plasmids into T cells: **(1)** low CAR transfer rate, **(2)** high T-cell toxicity and **(3)** long *ex vivo* culturing time due to low CAR transfer rate and T-cell toxicity, which has led to T cell exhaustion as well⁴⁸. We hypothesized that SB transposition of CAR transgene from smaller sized vectors called minicircle vectors (MCs) may solve these problems. Our data revealed that SB transposition from MC vectors is substantially more effective and less toxic compared to conventional plasmids, and enables rapid generation of therapeutic CAR T-cell doses. CD19-CAR T cells engineered with our enhanced SB approach conferred potent reactivity *in vitro* and eradicated tumor in a xenograft mouse model *in vivo*. Next, we analyzed genomic distribution of SB and LV integrations and showed that a significantly higher proportion of MC-derived CAR transposons compared to LV integrants had occurred outside of highly-expressed and

cancer-related genes and into genomic safe harbor loci that are not expected to cause mutagenesis or genotoxicity.

As the second objective of this study we aimed to knock out *PD-1* in CAR+ T cells and accomplished CAR gene transfer and *PD-1* KO through a single-step and fully non-viral strategy. Generation of *PD-1* KO CAR+ T cells may address some problems associated with combined CAR and antibody therapies: **(1)** the need for sequential administration of anti-PD-1 antibody due to rapid expansion of PD-1 expressing CAR T cells after encountering their specific antigens, **(2)** induction of severe immune-related adverse events due to sequential systematic administration of anti-PD-1 antibody and **(3)** high expenses of long-term administration of anti-PD-1 antibodies. By combining CAR transposition from MC vector with *PD-1* disruption via Cas9 RNP we managed to knock out *PD-1* in CAR+ T cells in a fast and single-step protocol.

In conclusion, we designed a novel and cutting-edge T cell genetic engineering platform, which can be applied for introducing other CARs or transgenes of interest into T cells. It is also applicable for edition of other target genes deemed suitable to enhance T-cell therapeutic index. Our developed strategies pave the way for broader and advanced clinical application of T-cell therapies for treatment of cancers and other diseases.

5 Discussion

5.1 Efficiency of SB transposition from MC DNAs for generating CAR T cells

CAR T-cell therapy is a transformative novel way for treating advanced malignancies. Prior work has shown that CAR T cells can be generated by *Sleeping Beauty* (SB) transposition⁴⁹. In this study, we aimed to enhance the SB transposition of CAR transgene into T cells. During the last years, SB has gone through a number of modifications in order to enhance the potency of the system for gene engineering of primary cell types³⁸. These include molecular evolution of the hyperactive SB100X transposase. SB100X shows about 100-fold enhancement in transposition as compared with first-generation transposases. However, despite the use of hyperactive SB100X transposase, low gene transfer rates and severe T-cell toxicity associated with electroporation of plasmid DNAs to deliver transposase and transposon have impeded its use in the field^{45, 48, 49, 121, 122}. Prior work showed that minicircle DNAs (MCs) when are used as SB-transposon donors increase stable expression of eGFP in mammalian cell lines as compared with conventional SB plasmids⁵³. However, transposition-mediated stable delivery for a therapeutically relevant gene out of MC vectors in primary human cells has to date not been explored. In this study, we show for the first time that CAR transposons can also be mobilized from MCs instead of plasmids and the CAR encoding gene is stably integrated into the genome of primary human T cells. Our data demonstrate that SB-transposition from MC transposon donor vectors through MC- or mRNA-encoded SB100X transposase is significantly more effective, and less toxic to T cells

compared to the current plasmid-based approach. This advance leverages non-viral SB-transposition to provide an effective and broadly applicable gene-transfer strategy, which might be preferable alternative to viral vectors because of its superior safety profile (see section 5.2). Several mechanisms likely contribute to the higher transposition rate from MCs compared to plasmids, including better transfection, longer half-life and easier migration through cytoplasm and into the nucleus, as well as easier mobilization of the transposon from small supercoiled MCs compared to large circular plasmids^{36, 54, 123}.

The reduction in toxicity correlates proportionally with lower amounts of transfected DNA. Most prior studies do not report the actual SB-transposition rate after transfection and use repetitive expansion cycles with antigen-positive feeder cells to rescue CAR-modified T cells that survived the gene-transfer procedure⁴⁹. This long *ex vivo* culturing is time and cost intensive and even more important, may lead to progressive T-cell exhaustion. Moreover, for generating good manufacturing practice (GMP) grade CAR T cells, use of feeder cells increases the regulatory requirements and the risk of contamination of CAR product during the long manufacturing process⁴⁸. Due to the higher transposition rate and lower toxicity, no feeder cell expansion is required to obtain therapeutically relevant CAR T cell numbers with our novel MC-based approach⁷. Protocols that enable MC production of clinical grade and quantity have been established⁵⁷.

A relevant advantage of MCs compared to plasmids is the lack of antibiotic resistance genes, which excludes the potential for horizontal transfer of these genes to host bacteria and unintended integration into the host genome. Importantly, our data also show that mRNA can serve as a transient source of SB100X transposase

and in combination with MC-encoded CD19-CAR transposons achieves near-equivalent levels of gene transfer in comparison to MC-encoded SB100X. The use of mRNA rather than MC- or plasmid-encoded SB100X transposase is preferable for at least two reasons. First, because transposase is short-lived, there is a much lower risk that already integrated transposons are 're-mobilized'. Second, supply of the transposase as mRNA eliminates the risk of unintentional integration of a transposase expression cassette into the host genome, which could lead to uncontrollable, continuous transposition of genomically integrated transposons^{37, 122}.

5.2 Biosafety aspects of SB transposon insertions mobilized from MCs

Genotoxicity through inadvertent activation or disruption of host genes, leading in the worst case to malignant transformation, is a concern associated with gene-modified cell products²¹. Prior work in mammalian cells has shown that SB integrates with an almost random pattern into the host genome, and in comparison to lentiviral (LV) and γ -retroviral vectors (RV) has a lower preference for integration into highly-expressed genes and oncogenes^{46, 124, 125}. Our analysis of SB chromosomal target sites and genomic distribution is the most comprehensive study of SB integrations in human T cells performed so far, and the first study to analyze SB insertions after mobilization from MCs. Despite substantially higher transposition rates from MCs, CD19-CAR transposon integrations remained close-to-random and neither acquired a preference for highly-expressed, transcriptionally active nor cancer-related genes. We analyzed the number of transposon integrations into genomic safe harbor (GSH) sites, which fulfill five criteria based on their position relative to coding genes, microRNAs and

ultraconserved regions^{111, 118, 126}. Intriguingly, we found 7 times more (21% of all integrants) insertion sites of SB in GSHs than for LV (3%), coming close to the 28% of GSH integrations assuming completely random integration. We hypothesize that enhanced transposition from MCs can also be accomplished with other transposon systems such as *piggyBac* (PB) and Tol2. However, each transposase demands a separate GSH assessment, as prior data have shown that e.g. PB integrations are per se less favorable than SB^{127, 128}. To date, no case of malignant transformation has been reported with T cells modified by viral or non-viral gene transfer. However, preferential growth and expansion of selected T-cell clones carrying HIV integrants has nurtured the notion that albeit low risk for transformation may originate from integrating viral vectors also in terminally differentiated T cells¹²⁹. Based on our integration data and an extensive body of prior work, SB may be considered as a 'safer' and therefore more preferable gene transfer system compared to LV and RV.

A prime future goal is to increase the safety of the SB system by targeting GSH or a defined locus in the T cell genome. The first attempts to combine the DNA targeting ability of zinc finger nucleases with SB transposons gene insertion consisted of adding a zinc finger DNA-binding domain to SB transposase^{130, 131}. These approaches resulted in diminished transposition activity and marginal targeting. As an alternative, we have prepared the platform for combining CRISPR/Cas9 DNA targeting feature with SB via a peptide linker for targeted integration of CAR transgene.

5.3 Compatibility of CAR transposon copy numbers with clinical application

Apart from the integration site profile, the number of CAR transposon integrations in T cell genome is an important biosafety criterion for assessment of potency and risk of genotoxicity and malignant transformation for clinical application.

Here, we developed a precise TaqMan-based droplet digital PCR (ddPCR) assay for determination of CAR copy number using a single-copy endogenous reference gene as a control. Our copy number analysis on CAR T cells generated through MC transposition confirmed that the average number of CAR copies in both CD4+ and CD8+ T cell population at single cell level is in the acceptable range ($n < 20$). This range of CAR copy numbers has been confirmed to be satisfactory by Paul-Ehrlich-Institute (PEI) scientific advisory board for the clinical trial (personal communication with Dr. Michael Hudecek).

It would be desirable to be able to fine-tune CAR copy number based on each patient's specific treatment requirements. In this case, patients with high and low tumor burden can receive the CAR T cell with higher and lower potency and CAR copy numbers, respectively. We found that the CAR copy number can be modulated by the amount of vectors transfected into the cells. Two-fold reduction in optimal amount of MC DNAs that led to the highest CAR expression, dramatically reduced CAR copy numbers (from 11.7 to 7, approximately 1.6-fold reduction) in polyclonal CAR+ T cell population while nearly equivalent gene transfer rate was achieved (10% less than optimal condition). Consequently, half of the optimal amount of MC vectors could be potentially used for clinical application when lower transgene copy number is desired. In this regards, functional assays have yet to be performed to assess the

impact of CAR copy number variation on the antitumor reactivity of CAR⁺ T cells in terms of killing, cytokine production and proliferation.

Moreover, a rapid and easy protocol for CAR copy number determination is preferable for broad clinical application. In ddPCR the sample is fractionated into 20,000 droplets and PCR amplification of the template molecules occurs in each individual droplet. As a result, this method is not only sensitive for copy number determination in single cell clones but also allows estimation of transgene copy number from polyclonal cell population. Since no single cell clone preparation is needed, required time for copy number analysis will be substantially reduced. Hence, CAR copy numbers can be determined rapidly before infusion into patients when fast turnaround time is needed in routine and clinical application.

Furthermore, we found that there is a direct correlation between the mean fluorescence intensity (MFI) of CAR expression measured by flow cytometry analysis and copy number variation. However, there are some considerations that we should take into account for estimation of CAR copy numbers based on MFI measurements. First, in a very high and low transgene expression level FACS-based method may lose its precision. Therefore, it is necessary to determine the highest and lowest copy number that can be determined based on MFI measurements. On the other hand, one should consider that the cell machinery cannot handle unlimited CAR transgene insertions and infinite amount of CAR protein expression probably due to genomic instability and limitation in protein production, respectively. Hence, the protein expression will reach a saturation point when certain amount of vectors is used. This saturation point needs to be determined as well. Consequently, more analyses and statistical data are required to formulate and standardize the estimation of CAR copy numbers based on MFI measurements. This method may lead to estimation of CAR

copy numbers based on a fast, simple and more cost-effective flow cytometry analysis compared with ddPCR. However, this MFI-based assay may be less accurate than ddPCR, but when it is carefully standardized it can be potentially sufficient for estimation of CAR copy numbers and rapid release of CAR T cell products for clinical use.

5.4 Generation of CD19-CAR T cells using MC-mediated transposition for clinical application

Clinical trials with CD19-CAR T cells are currently ongoing at several institutions. It has been noted that studies employing SB-transposition for gene-modification have thus far not reported as impressive results as those with LV and RV gene transfer⁴⁸. However, comparisons between trials are difficult due to variations in multiple parameters, including patient population and disease entity, prior treatment and conditioning^{132, 133}. In addition, we have shown in our own prior work that CAR design and subset composition of CAR T-cell products - that differ extensively between trials - profoundly influence efficacy^{105, 106, 134}. In the work presented here, we used a CD19-CAR that has been functionally optimized¹⁰⁶ and conferred durable complete remissions in a clinical trial of LV-based CAR T-cell therapy⁵¹. We demonstrate that our novel MC-based transposition strategy is equally effective in CD8+ and CD4+ T-cell subsets and supports formulating CAR T-cell products with defined cell composition^{105, 135}. Our study is the first to perform a head-to-head comparison of SB-modified and LV-transduced CAR T cells and to demonstrate equivalent antitumor function and potency *in vitro* and *in vivo*.

In conclusion, we anticipate that CD19-CAR T cells generated by SB-transposition from MCs will also be effective in a clinical setting. Based on our discussions with PEI clinical trials advisory committee, we are confident that our non-viral gene transfer strategy will facilitate clearance of regulatory hurdles and accelerate clinical translation to increase access of patients to CAR T-cell therapy.

5.5 Non-viral KO of *PD-1* using Cas9 RNP to improve the therapeutic index of CAR T cells

Though adoptive transfer of CAR T cells has shown significant success in treating acute lymphoblastic leukemia (CR $\geq 70\%$) by CD19-specific CAR T cells, unfortunately, the clinical results have been less promising in treatment of chronic lymphoblastic leukemia, lymphomas (CR $\approx 50-60\%$) and solid tumors¹³⁶⁻¹³⁸. There are studies demonstrated that utilization of checkpoint blockade antibodies targeting PD-1/PD-L1 immune inhibitory axis enhances antitumor effects of CAR T cells in the treatment of solid tumors and B-cell lymphoma^{65, 85, 102}. However, rapid expansion of PD-1 expressing CAR T cells by the stimulation of tumor antigens may require sequential administration of anti-PD-1 antibody. The long-term systematic administration of the blocking antibodies is costly and carries the risk of severe immune-related adverse events. These side effects include breaking of immune tolerance that may cause immune attack of normal tissues, severe diarrhea, skin rash and mucosal irritations^{139, 140}. Due to the severe side effects, the administration of immune checkpoint blocking antibodies needs to be discontinued in a substantial number of patients. Consequently, specific disruption of *PD-1* in CAR+ T cells may be a strategy to avoid these side effects. In this study, for the first time, we managed

to generate *PD-1* knockout (KO) CAR+ T cells in a complete non-viral format. We combined the SB-mediated CAR transposition from MC vectors with RNA guided endonuclease Cas9 (RGEN) system for editing *PD-1* via transient delivery of Cas9 protein complexed with *in vitro*-transcribed sgRNA (Cas9 RNP). The sgRNA used in this study resulted in more efficient disruption of *PD-1* compared with two previously reported studies that have used RGEN system for disruption of *PD-1* in human T cells and in CD4+ T-cell subsets via plasmid DNA delivery and Cas9 RNP, respectively^{4, 99}. Besides, transient delivery of Cas9 and sgRNA via Cas9 RNP has some advantages over plasmid-mediated or viral delivery of RGEN. First, delivery of RGEN via plasmid DNA is often inefficient and stressful in primary T cells⁹⁶. Secondly, unwanted integration of plasmid DNA sequences can cause host immune responses¹⁴¹. Finally, prolonged expression of RGENs from plasmid DNA, which can persist in cells for several days post-transfection, can increase Cas9 off-target activities^{98, 142}. Viral delivery of RGEN is more efficient in T cells compared with plasmid based gene delivery. However, it substantially aggravates the risk of off-target mutation at sites that are highly homologous to on-target sites by persistence expression of the Cas9 and sgRNA¹⁴³. In this regard, further analyses are required to assess the potential off-target effect of our developed Cas9 RNP system. However, Cas9 RNP has a fast editing action and rapid protein turnover in the cells as it is degraded within 24 hours of delivery⁹⁸. As a result, delivery of RGEN via short-lived Cas9 RNP addresses the biosafety issues largely.

Apart from the genome engineering side, there are safety aspects that need to be carefully addressed when *PD-1* KO CAR+ T cells are administrated in a clinical setting. Deletion of PD-1/PD-L1 pathway as one of the immune inhibitory strategies

in T cells may lead to prolonged activation of CAR T cells, though the cells still are equipped with other immune checkpoint mechanisms. To address this issue the suicide genes like inducible caspase9 or depletion markers like EGFRt can be expressed on CAR T cells for eliminating the cells when is needed^{16, 61}. The EGFRt depletion marker is included in the CD19-CAR cassette we used in this study and its ability to deplete CAR T cells has been demonstrated¹⁶. Another possible strategy would be simultaneous KO of endogenous *TCR* and *PD-1* to avoid uncontrolled T cell responses to other unwanted antigen peptides through binding to endogenous TCR.

Furthermore, checking the efficiency of genome editing is challenging in context of PD-1 expression that varies depending on the activation status of T cells. Here, we observed that stimulation of T cells with PMA/Ionomycin leads to PD-1 upregulation on T-cell surface. In this method, following the stimulation, PD-1+ T cells can be easily distinguished from edited cells and editing efficiency on protein level can be determined by flow cytometry. Moreover, the PD-1+ T cells can be removed by FACS or MACS based separation procedures post-stimulation. This will facilitate future studies, which are necessary to be performed for analyzing the functional characterization of *PD-1* KO CAR+ T cells and unmodified control CAR+ T cells in terms of tumor eradication. Of note, because of the high efficiency of *PD-1* KO ($\approx 80\%$) in CAR+ T cells, the pool of the edited and non-edited CAR+ T cells can potentially be infused into the patients in a clinical setting.

5.6 Conclusion and perspective: roadmap to clinical translation

In this study, we successfully developed a non-viral gene engineering strategy with two essential components for effective and stable genetic manipulation of T cells for cancer immunotherapy. First, we leveraged the *Sleeping Beauty* transposon system via transposition from minicircle DNA vectors to a level that now is efficient for generation of CAR T cells. Our comprehensive genomic insertion site analysis showed a close-to-random integration profile of MC-derived CD19-CAR transposons with a significantly higher proportion of SB integrations in genomic safe harbors as compared to LV integrations.

In the second step, we successfully combined the established SB-mediated CAR transposition from MC vectors with Cas9 RNP complex for generating *PD-1* KO CAR⁺ T cells. For the first time, we managed to generate *PD-1* KO CAR⁺ T cells via a single-step and complete virus-free gene transfer and genome editing.

In conclusion, we demonstrate efficient engineering of T cells using a fully non-viral production procedure with a safer integration pattern as compared with LV gene delivery protocols. The developed strategy in this study yield therapeutic doses of T cells with desired phenotype (i.e. *PD-1* KO CAR⁺ T cells). Use of *PD-1* KO CAR⁺ T cells instead of systematic administration of blocking antibodies is cost and time effective. Besides, patients will not require sequential administration of antibody and hospitalization. Moreover, the ease-of-handling of non-viral systems and their shorter production time is anticipated to reduce the cost and lengthy regulation procedure required for clinical approval. Hence, it may facilitate the access of large cohort of patients to T-cell immunotherapies via gene engineered T cells not only in developed

countries but worldwide. The developed strategies in this study can serve as a preferred genome engineering tools in advanced cellular and gene therapy for treatment of broad spectrum of cancers, autoimmune and infectious diseases.

The achieved results as well as the established T-cell engineering tools in this study set new directions for future research. Studies assessing off-target activities of Cas9 RNP and functional efficacy of *PD-1* KO CAR⁺ T cells have to be performed. The next anticipated goal of the study would be precise targeted integration of CAR gene into the *PD-1* locus via homology directed repair mechanism using the Cas9 RNP. This targeted CAR insertion will accelerate both the safety and function of CAR T cells, which is a prime and long-sought objective in the field of gene therapy and CAR T-cell cancer therapy.

List of figures

Figure 1.1. Immunotherapy with chimeric antigen receptor T cells.....	16
Figure 1.2. <i>Sleeping Beauty</i> and its mechanism of transposition.	21
Figure 1.3. Schematic of CRISPR/Cas9 system.....	27
Figure 1.4. Improving non-viral gene delivery and genome editing strategies in T-cell engineering.....	30
Figure 4.1. Titration of transposon and SB100X transposase DNA plasmids.....	63
Figure 4.2. Production of minicircle (MC) vectors.	64
Figure 4.3. SB-transposition of eGFP from MC or plasmid vectors.	65
Figure 4.4. CAR transposition using MC and plasmid-encoded SB-transposase and transposon.....	66
Figure 4.5. SB transposition from MCs in CD4+ T cells.....	67
Figure 4.6. mRNA as the transient source of SB100X transposase.	69
Figure 4.7. SB transposition from MC in CD8+ naïve and memory T-cell subsets... ..	70
Figure 4.8. Phenotype of CD8+ and CD4+ CD19-CAR T cell lines prior to functional assays.	71
Figure 4.9. Specific cytolytic activity of CD8+ CD19-CAR T cells within 4 hours.....	72
Figure 4.10. Cytokine production of CD8+ and CD4+ CD19-CAR T cells.	73
Figure 4.11. Proliferation of CD19-CAR T cells within 72 hours.	74
Figure 4.12. <i>In vivo</i> antitumor reactivity of CD19-CAR T cells prepared by SB-transposition.....	75
Figure 4.13. <i>In vivo</i> persistence of CD19-CAR T cells prepared by SB-transposition.	76

Figure 4.14. Nucleotide composition of chromosomal DNA around SB and LV insertion site in T cells.	78
Figure 4.15. Insertion site properties of SB and LV in human T cells.	79
Figure 4.16. Representation of SB and LV insertion sites in transcriptionally active and repressed chromatin of T cells.....	80
Figure 4.17. Integration frequencies of SB and LV in genomic safe harbors of T cells.	82
Figure 4.18. Determination of CAR copy number in CAR-T cells.	83
Figure 4.19. Absolute level of transgene expression in CD8+ and CD4+ T cells generated by SB or LV system.....	84
Figure 4.20. Correlation between MC DNA vector amounts and copy number.	86
Figure 4.21. Selection of sgRNAs in the human <i>PD-1</i> locus.	89
Figure 4.22. Modification efficiencies of different sgRNAs targeting <i>PD-1</i> in Jurkat cell line.....	90
Figure 4.23. LentiCRISPR/Cas9 mediated ablation of <i>PD-1</i> locus in CD8+ T cells..	91
Figure 4.24. Enrichment of <i>PD-1</i> knockout T cells.....	92
Figure 4.25. Disruption of <i>PD-1</i> in CD8+ T cells via delivery of Cas9 RNP.	94
Figure 4.26. Generation of <i>PD-1</i> KO CD19-CAR+ CD8+ T cells using a complete non-viral system.	96
Figure 4.27. Generation of <i>PD-1</i> KO SLAMF7-CAR+ CD8+ T cells using a fully non-viral system.	97

List of tables

Table 3.1. Primers used for T7 endonuclease I assay.....	53
Table 3.2. Primers and oligos used for integration library preparation.....	56
Table 3.3. Primers used for linker mediated copy number analysis.....	59
Table 3.4. Primers and oligos used for ddPCR copy number analysis.	60

List of abbreviations

μ	micro (10^{-6})
$\times g$	times gravity
μg	microgram
μL	microliter
μM	micromolar
μm	micrometer
$^{\circ}\text{C}$	centigrade
7-AAD	7-aminoactinomycin D
ACT	adoptive cell transfer
ALL	acute lymphoblastic leukemia
bp	base pair
B-CLL	B-cell chronic lymphocytic leukemia
CAR	chimeric antigen receptor
Cas9 RNP	Cas9 ribonucleoprotein complex
CD	cluster of differentiation
cDNA	complementary DNA
CFSE	carboxyfluorescein succinimidyl ester
CO_2	carbon dioxide
CR	complete remission
CRISPR	clustered regularly interspaced short palindromic repeats
ddPCR	droplet digital PCR
DEPC	diethylpyrocarbonate
DMEM	dulbecco's modified eagle medium
DMSO	dimethyl sulfoxide
DNA	deoxyribonucleic acid
dNTPs	2'- deoxynucleoside 5'-triphosphates
DR	direct repeats
DSB	double stranded break
EDTA	ethylenediaminetetraacetic acid
eGFP	enhanced green fluorescent protein
EGFRt	human truncated epidermal growth factor

ELISA	enzyme-linked immunosorbent assay
FACS	fluorescence-activated cell sorting
Fc	fragment crystallizable
FCS	fetal calf serum
ffluc	firefly luciferase
HSC	hematopoietic stem cell
GSH	genomic safe harbor
HDR	homology-directed repair
HEPES	4-(2-hydroxyethyl)-1-piperazineethanesulfonic acid
IFN γ	interferon gamma
IgG	immunoglobulin G
IR	inverted repeats
IRAEs	immune-related adverse events
kbp	kilobase pairs
KO	knockout
LB	luria-bertani
LV	lentiviral
M	molar
m	milli (10^{-3})
mAb(s)	monoclonal antibody(ies)
MACS	magnetic-activated cell sorting
MC	minicircle DNA
MFI	mean fluorescence intensity
mg	milligram
MHC	major histocompatibility complex
min	minute
mL	milliliter
mM	millimolar
MOI	multiplicity of infection
mRNA	messenger RNA
n	nano (10^{-9})
ng	nanogram
NHEJ	non-homologous end joining
NHL	Non-Hodgkin lymphoma

nM	nanomolar
p	pico (10^{-12})
PAM	protospacer adjacent motif
PB	<i>piggyBac</i>
PBMC	peripheral blood mononuclear cells
PBS	phosphate-buffered saline
PCR	polymerase chain reaction
PD-1	programmed cell death protein 1
PD-L1	programmed death ligand 1
PE	phycoerythrin
PMA	phorbol-12-myristat-13-acetate
pmol	picomole
polyA	polyadenylation
RGEN	RNA guided endonucleases
rh IL-2	recombinant human interleukin 2
RNA	ribonucleic acid
RV	γ -retroviral vectors
s	second
SB	<i>Sleeping Beauty</i>
scFv	single-chain variable fragment
sgRNA	single guide RNA
TAE	tris-acetate-EDTA
TALLEN	transcription activator like effector nuclease
TCM	T cell culture medium
TCR	T cell receptor
TE	transposable element
TE buffer	tris-EDTA buffer
TM	transmembrane
TM-LCL	lymphoblastoid cell lines, donor initials: TM
WT	wild type
ZFNs	zinc finger nucleases

References

1. Stewart B, Wild CP. World cancer report 2014. International Agency for Research on Cancer: WHO press; 2014.
2. Vanneman M, Dranoff G. Combining immunotherapy and targeted therapies in cancer treatment. *Nature reviews Cancer* 2012 Mar 22; **12**(4): 237-251.
3. Sadelain M, Riviere I, Brentjens R. Targeting tumours with genetically enhanced T lymphocytes. *Nat Rev Cancer* 2003 Jan; **3**(1): 35-45.
4. Su S, Hu B, Shao J, Shen B, Du J, Du Y, *et al.* CRISPR-Cas9 mediated efficient PD-1 disruption on human primary T cells from cancer patients. *Sci Rep* 2016; **6**: 20070.
5. Torikai H, Reik A, Liu PQ, Zhou Y, Zhang L, Maiti S, *et al.* A foundation for universal T-cell based immunotherapy: T cells engineered to express a CD19-specific chimeric-antigen-receptor and eliminate expression of endogenous TCR. *Blood* 2012 Jun 14; **119**(24): 5697-5705.
6. Berdien B, Mock U, Atanackovic D, Fehse B. TALEN-mediated editing of endogenous T-cell receptors facilitates efficient reprogramming of T lymphocytes by lentiviral gene transfer. *Gene Ther* 2014 Jun; **21**(6): 539-548.
7. Turtle CJ, Hanafi LA, Berger C, Gooley TA, Cherian S, Hudecek M, *et al.* CD19 CAR-T cells of defined CD4+:CD8+ composition in adult B cell ALL patients. *The Journal of clinical investigation* 2016 Apr 25.
8. Billingham RE, Brent L, Medawar PB. Quantitative studies on tissue transplantation immunity. II. The origin, strength and duration of actively and adoptively acquired immunity. *Proc R Soc Lond B Biol Sci* 1954 Dec 15; **143**(910): 58-80.
9. Rosenberg SA, Restifo NP, Yang JC, Morgan RA, Dudley ME. Adoptive cell transfer: a clinical path to effective cancer immunotherapy. *Nat Rev Cancer* 2008 Apr; **8**(4): 299-308.
10. Curran KJ, Pegram HJ, Brentjens RJ. Chimeric antigen receptors for T cell immunotherapy: current understanding and future directions. *J Gene Med* 2012 Jun; **14**(6): 405-415.
11. Maude SL, Frey N, Shaw PA, Aplenc R, Barrett DM, Bunin NJ, *et al.* Chimeric antigen receptor T cells for sustained remissions in leukemia. *The New England journal of medicine* 2014 Oct 16; **371**(16): 1507-1517.

12. Lee DW, Kochenderfer JN, Stetler-Stevenson M, Cui YK, Delbrook C, Feldman SA, *et al.* T cells expressing CD19 chimeric antigen receptors for acute lymphoblastic leukaemia in children and young adults: a phase 1 dose-escalation trial. *Lancet* 2015 Feb 7; **385**(9967): 517-528.
13. Harris DT, Kranz DM. Adoptive T Cell Therapies: A Comparison of T Cell Receptors and Chimeric Antigen Receptors. *Trends Pharmacol Sci* 2016 Mar; **37**(3): 220-230.
14. Zhou G, Levitsky H. Towards curative cancer immunotherapy: overcoming posttherapy tumor escape. *Clin Dev Immunol* 2012; **2012**: 124187.
15. Wang X, Chang WC, Wong CW, Colcher D, Sherman M, Ostberg JR, *et al.* A transgene-encoded cell surface polypeptide for selection, in vivo tracking, and ablation of engineered cells. *Blood* 2011 Aug 4; **118**(5): 1255-1263.
16. Paszkiewicz PJ, Frassle SP, Srivastava S, Sommermeyer D, Hudecek M, Drexler I, *et al.* Targeted antibody-mediated depletion of murine CD19 CAR T cells permanently reverses B cell aplasia. *The Journal of clinical investigation* 2016 Oct 17.
17. Tumaini B, Lee DW, Lin T, Castiello L, Stroncek DF, Mackall C, *et al.* Simplified process for the production of anti-CD19-CAR-engineered T cells. *Cytotherapy* 2013 Nov; **15**(11): 1406-1415.
18. Bushman F, Lewinski M, Ciuffi A, Barr S, Leipzig J, Hannenhalli S, *et al.* Genome-wide analysis of retroviral DNA integration. *Nat Rev Microbiol* 2005 Nov; **3**(11): 848-858.
19. Mitchell RS, Beitzel BF, Schroder AR, Shinn P, Chen H, Berry CC, *et al.* Retroviral DNA integration: ASLV, HIV, and MLV show distinct target site preferences. *PLoS Biol* 2004 Aug; **2**(8): E234.
20. Cavazzana-Calvo M, Hacein-Bey S, de Saint Basile G, Gross F, Yvon E, Nusbaum P, *et al.* Gene therapy of human severe combined immunodeficiency (SCID)-X1 disease. *Science* 2000 Apr 28; **288**(5466): 669-672.
21. Hacein-Bey-Abina S, Von Kalle C, Schmidt M, McCormack MP, Wulffraat N, Leboulch P, *et al.* LMO2-associated clonal T cell proliferation in two patients after gene therapy for SCID-X1. *Science* 2003 Oct 17; **302**(5644): 415-419.
22. Tiscornia G, Singer O, Verma IM. Production and purification of lentiviral vectors. *Nat Protoc* 2006; **1**(1): 241-245.
23. Grimm D, Kern A, Rittner K, Kleinschmidt JA. Novel tools for production and purification of recombinant adenoassociated virus vectors. *Hum Gene Ther* 1998 Dec 10; **9**(18): 2745-2760.

24. Hodges BL, Cheng SH. Cell and gene-based therapies for the lysosomal storage diseases. *Curr Gene Ther* 2006 Apr; **6**(2): 227-241.
25. Ramamoorth M, Narvekar A. Non viral vectors in gene therapy- an overview. *J Clin Diagn Res* 2015 Jan; **9**(1): GE01-06.
26. Al-Dosari MS, Gao X. Nonviral gene delivery: principle, limitations, and recent progress. *AAPS J* 2009 Dec; **11**(4): 671-681.
27. Ivics Z, Hackett PB, Plasterk RH, Izsvak Z. Molecular reconstruction of Sleeping Beauty, a Tc1-like transposon from fish, and its transposition in human cells. *Cell* 1997 Nov 14; **91**(4): 501-510.
28. Izsvak Z, Hackett PB, Cooper LJ, Ivics Z. Translating Sleeping Beauty transposition into cellular therapies: victories and challenges. *Bioessays* 2010 Sep; **32**(9): 756-767.
29. Mc CB. The origin and behavior of mutable loci in maize. *Proc Natl Acad Sci U S A* 1950 Jun; **36**(6): 344-355.
30. McClintock B. Mutable loci in maize. *Carnegie Inst Wash Year Book* 1948; **47**: 155-169.
31. Lander ES, Linton LM, Birren B, Nusbaum C, Zody MC, Baldwin J, *et al.* Initial sequencing and analysis of the human genome. *Nature* 2001 Feb 15; **409**(6822): 860-921.
32. Izsvak Z, Ivics Z. Sleeping beauty transposition: biology and applications for molecular therapy. *Mol Ther* 2004 Feb; **9**(2): 147-156.
33. Cui Z, Geurts AM, Liu G, Kaufman CD, Hackett PB. Structure-function analysis of the inverted terminal repeats of the sleeping beauty transposon. *J Mol Biol* 2002 May 17; **318**(5): 1221-1235.
34. Plasterk RH, Izsvak Z, Ivics Z. Resident aliens: the Tc1/mariner superfamily of transposable elements. *Trends Genet* 1999 Aug; **15**(8): 326-332.
35. Mikkelsen JG, Yant SR, Meuse L, Huang Z, Xu H, Kay MA. Helper-Independent Sleeping Beauty transposon-transposase vectors for efficient nonviral gene delivery and persistent gene expression in vivo. *Mol Ther* 2003 Oct; **8**(4): 654-665.
36. Izsvak Z, Ivics Z, Plasterk RH. Sleeping Beauty, a wide host-range transposon vector for genetic transformation in vertebrates. *J Mol Biol* 2000 Sep 8; **302**(1): 93-102.

37. Wilber A, Frandsen JL, Geurts JL, Largaespada DA, Hackett PB, Mclvor RS. RNA as a source of transposase for Sleeping Beauty-mediated gene insertion and expression in somatic cells and tissues. *Mol Ther* 2006 Mar; **13**(3): 625-630.
38. Zayed H, Izsvak Z, Walisko O, Ivics Z. Development of hyperactive sleeping beauty transposon vectors by mutational analysis. *Mol Ther* 2004 Feb; **9**(2): 292-304.
39. Mates L, Chuah MK, Belay E, Jerchow B, Manoj N, Acosta-Sanchez A, *et al.* Molecular evolution of a novel hyperactive Sleeping Beauty transposase enables robust stable gene transfer in vertebrates. *Nat Genet* 2009 Jun; **41**(6): 753-761.
40. Aronovich EL, Mclvor RS, Hackett PB. The Sleeping Beauty transposon system: a non-viral vector for gene therapy. *Hum Mol Genet* 2011 Apr 15; **20**(R1): R14-20.
41. Izsvak Z, Khare D, Behlke J, Heinemann U, Plasterk RH, Ivics Z. Involvement of a bifunctional, paired-like DNA-binding domain and a transpositional enhancer in Sleeping Beauty transposition. *J Biol Chem* 2002 Sep 13; **277**(37): 34581-34588.
42. Vigdal TJ, Kaufman CD, Izsvak Z, Voytas DF, Ivics Z. Common physical properties of DNA affecting target site selection of sleeping beauty and other Tc1/mariner transposable elements. *J Mol Biol* 2002 Oct 25; **323**(3): 441-452.
43. Lohe AR, Hartl DL. Autoregulation of mariner transposase activity by overproduction and dominant-negative complementation. *Mol Biol Evol* 1996 Apr; **13**(4): 549-555.
44. Mates L, Izsvak Z, Ivics Z. Technology transfer from worms and flies to vertebrates: transposition-based genome manipulations and their future perspectives. *Genome Biol* 2007; **8 Suppl 1**: S1.
45. Singh H, Manuri PR, Olivares S, Dara N, Dawson MJ, Huls H, *et al.* Redirecting specificity of T-cell populations for CD19 using the Sleeping Beauty system. *Cancer Res* 2008 Apr 15; **68**(8): 2961-2971.
46. Field AC, Vink C, Gabriel R, Al-Subki R, Schmidt M, Goulden N, *et al.* Comparison of lentiviral and sleeping beauty mediated alphabeta T cell receptor gene transfer. *PLoS One* 2013; **8**(6): e68201.
47. Peng PD, Cohen CJ, Yang S, Hsu C, Jones S, Zhao Y, *et al.* Efficient nonviral Sleeping Beauty transposon-based TCR gene transfer to peripheral blood lymphocytes confers antigen-specific antitumor reactivity. *Gene Ther* 2009 Aug; **16**(8): 1042-1049.

48. Kebriaei P, Singh H, Huls MH, Figliola MJ, Bassett R, Olivares S, *et al.* Phase I trials using Sleeping Beauty to generate CD19-specific CAR T cells. *The Journal of clinical investigation* 2016 Aug 2.
49. Singh H, Figliola MJ, Dawson MJ, Olivares S, Zhang L, Yang G, *et al.* Manufacture of clinical-grade CD19-specific T cells stably expressing chimeric antigen receptor using Sleeping Beauty system and artificial antigen presenting cells. *PLoS One* 2013; **8**(5): e64138.
50. Davila ML, Riviere I, Wang X, Bartido S, Park J, Curran K, *et al.* Efficacy and toxicity management of 19-28z CAR T cell therapy in B cell acute lymphoblastic leukemia. *Science translational medicine* 2014 Feb 19; **6**(224): 224-225.
51. Turtle CJ, Hanafi LA, Berger C, Gooley TA, Cherian S, Hudecek M, *et al.* CD19 CAR-T cells of defined CD4+:CD8+ composition in adult B cell ALL patients. *The Journal of clinical investigation* 2016 Jun 1; **126**(6): 2123-2138.
52. Kochenderfer JN, Dudley ME, Kassim SH, Somerville RP, Carpenter RO, Stetler-Stevenson M, *et al.* Chemotherapy-refractory diffuse large B-cell lymphoma and indolent B-cell malignancies can be effectively treated with autologous T cells expressing an anti-CD19 chimeric antigen receptor. *Journal of clinical oncology : official journal of the American Society of Clinical Oncology* 2015 Feb 20; **33**(6): 540-549.
53. Sharma N, Cai Y, Bak RO, Jakobsen MR, Schroder LD, Mikkelsen JG. Efficient sleeping beauty DNA transposition from DNA minicircles. *Mol Ther Nucleic Acids* 2013; **2**: e74.
54. Karsi A, Moav B, Hackett P, Liu Z. Effects of insert size on transposition efficiency of the sleeping beauty transposon in mouse cells. *Marine biotechnology* 2001 May; **3**(3): 241-245.
55. Chen ZY, He CY, Ehrhardt A, Kay MA. Minicircle DNA vectors devoid of bacterial DNA result in persistent and high-level transgene expression in vivo. *Mol Ther* 2003 Sep; **8**(3): 495-500.
56. Mayrhofer P, Schleef M, Jechlinger W. Use of minicircle plasmids for gene therapy. *Methods Mol Biol* 2009; **542**: 87-104.
57. Kay MA, He CY, Chen ZY. A robust system for production of minicircle DNA vectors. *Nat Biotechnol* 2010 Dec; **28**(12): 1287-1289.
58. Kobelt D, Schleef M, Schmeer M, Aumann J, Schlag PM, Walther W. Performance of high quality minicircle DNA for in vitro and in vivo gene transfer. *Mol Biotechnol* 2013 Jan; **53**(1): 80-89.

59. Chabot S, Orio J, Schmeer M, Schleef M, Golzio M, Teissie J. Minicircle DNA electrotransfer for efficient tissue-targeted gene delivery. *Gene Ther* 2013 Jan; **20**(1): 62-68.
60. Budde LE, Berger C, Lin Y, Wang J, Lin X, Frayo SE, *et al.* Combining a CD20 chimeric antigen receptor and an inducible caspase 9 suicide switch to improve the efficacy and safety of T cell adoptive immunotherapy for lymphoma. *PLoS One* 2013; **8**(12): e82742.
61. Gargett T, Brown MP. The inducible caspase-9 suicide gene system as a "safety switch" to limit on-target, off-tumor toxicities of chimeric antigen receptor T cells. *Front Pharmacol* 2014; **5**: 235.
62. Newick K, O'Brien S, Moon E, Albelda SM. CAR T Cell Therapy for Solid Tumors. *Annual review of medicine* 2017 Jan 14; **68**: 139-152.
63. Moon EK, Wang LC, Dolfi DV, Wilson CB, Ranganathan R, Sun J, *et al.* Multifactorial T-cell hypofunction that is reversible can limit the efficacy of chimeric antigen receptor-transduced human T cells in solid tumors. *Clin Cancer Res* 2014 Aug 15; **20**(16): 4262-4273.
64. Beatty GL, Moon EK. Chimeric antigen receptor T cells are vulnerable to immunosuppressive mechanisms present within the tumor microenvironment. *Oncoimmunology* 2014 Nov; **3**(11): e970027.
65. Cherkassky L, Morello A, Villena-Vargas J, Feng Y, Dimitrov DS, Jones DR, *et al.* Human CAR T cells with cell-intrinsic PD-1 checkpoint blockade resist tumor-mediated inhibition. *The Journal of clinical investigation* 2016 Aug 1; **126**(8): 3130-3144.
66. Keir ME, Butte MJ, Freeman GJ, Sharpe AH. PD-1 and its ligands in tolerance and immunity. *Annu Rev Immunol* 2008; **26**: 677-704.
67. Jin HT, Ahmed R, Okazaki T. Role of PD-1 in regulating T-cell immunity. *Curr Top Microbiol Immunol* 2011; **350**: 17-37.
68. Parry RV, Chemnitz JM, Frauwirth KA, Lanfranco AR, Braunstein I, Kobayashi SV, *et al.* CTLA-4 and PD-1 receptors inhibit T-cell activation by distinct mechanisms. *Mol Cell Biol* 2005 Nov; **25**(21): 9543-9553.
69. Sfanos KS, Bruno TC, Meeker AK, De Marzo AM, Isaacs WB, Drake CG. Human prostate-infiltrating CD8+ T lymphocytes are oligoclonal and PD-1+. *Prostate* 2009 Nov 1; **69**(15): 1694-1703.
70. Ahmadzadeh M, Johnson LA, Heemskerk B, Wunderlich JR, Dudley ME, White DE, *et al.* Tumor antigen-specific CD8 T cells infiltrating the tumor express high levels of PD-1 and are functionally impaired. *Blood* 2009 Aug 20; **114**(8): 1537-1544.

71. Tewalt EF, Cohen JN, Rouhani SJ, Guidi CJ, Qiao H, Fahl SP, *et al.* Lymphatic endothelial cells induce tolerance via PD-L1 and lack of costimulation leading to high-level PD-1 expression on CD8 T cells. *Blood* 2012 Dec 6; **120**(24): 4772-4782.
72. Dong H, Strome SE, Salomao DR, Tamura H, Hirano F, Flies DB, *et al.* Tumor-associated B7-H1 promotes T-cell apoptosis: a potential mechanism of immune evasion. *Nat Med* 2002 Aug; **8**(8): 793-800.
73. Thompson RH, Gillett MD, Cheville JC, Lohse CM, Dong H, Webster WS, *et al.* Costimulatory B7-H1 in renal cell carcinoma patients: Indicator of tumor aggressiveness and potential therapeutic target. *Proc Natl Acad Sci U S A* 2004 Dec 7; **101**(49): 17174-17179.
74. Dorfman DM, Brown JA, Shahsafaei A, Freeman GJ. Programmed death-1 (PD-1) is a marker of germinal center-associated T cells and angioimmunoblastic T-cell lymphoma. *Am J Surg Pathol* 2006 Jul; **30**(7): 802-810.
75. Liu J, Hamrouni A, Wolowiec D, Coiteux V, Kuliczkowski K, Hetuin D, *et al.* Plasma cells from multiple myeloma patients express B7-H1 (PD-L1) and increase expression after stimulation with IFN- γ and TLR ligands via a MyD88-, TRAF6-, and MEK-dependent pathway. *Blood* 2007 Jul 1; **110**(1): 296-304.
76. Iwai Y, Ishida M, Tanaka Y, Okazaki T, Honjo T, Minato N. Involvement of PD-L1 on tumor cells in the escape from host immune system and tumor immunotherapy by PD-L1 blockade. *Proc Natl Acad Sci U S A* 2002 Sep 17; **99**(19): 12293-12297.
77. Jia M, Feng W, Kang S, Zhang Y, Shen J, He J, *et al.* Evaluation of the efficacy and safety of anti-PD-1 and anti-PD-L1 antibody in the treatment of non-small cell lung cancer (NSCLC): a meta-analysis. *J Thorac Dis* 2015 Mar; **7**(3): 455-461.
78. Ansell SM, Lesokhin AM, Borrello I, Halwani A, Scott EC, Gutierrez M, *et al.* PD-1 blockade with nivolumab in relapsed or refractory Hodgkin's lymphoma. *The New England journal of medicine* 2015 Jan 22; **372**(4): 311-319.
79. Topalian SL, Hodi FS, Brahmer JR, Gettinger SN, Smith DC, McDermott DF, *et al.* Safety, activity, and immune correlates of anti-PD-1 antibody in cancer. *The New England journal of medicine* 2012 Jun 28; **366**(26): 2443-2454.
80. Ribas A. Tumor immunotherapy directed at PD-1. *The New England journal of medicine* 2012 Jun 28; **366**(26): 2517-2519.
81. Sundar R, Cho BC, Brahmer JR, Soo RA. Nivolumab in NSCLC: latest evidence and clinical potential. *Ther Adv Med Oncol* 2015 Mar; **7**(2): 85-96.

82. Brahmer JR, Drake CG, Wollner I, Powderly JD, Picus J, Sharfman WH, *et al.* Phase I study of single-agent anti-programmed death-1 (MDX-1106) in refractory solid tumors: safety, clinical activity, pharmacodynamics, and immunologic correlates. *Journal of clinical oncology : official journal of the American Society of Clinical Oncology* 2010 Jul 1; **28**(19): 3167-3175.
83. Motzer RJ, Rini BI, McDermott DF, Redman BG, Kuzel TM, Harrison MR, *et al.* Nivolumab for Metastatic Renal Cell Carcinoma: Results of a Randomized Phase II Trial. *Journal of clinical oncology : official journal of the American Society of Clinical Oncology* 2015 May 1; **33**(13): 1430-1437.
84. Topalian SL, Sznol M, McDermott DF, Kluger HM, Carvajal RD, Sharfman WH, *et al.* Survival, durable tumor remission, and long-term safety in patients with advanced melanoma receiving nivolumab. *Journal of clinical oncology : official journal of the American Society of Clinical Oncology* 2014 Apr 1; **32**(10): 1020-1030.
85. John LB, Devaud C, Duong CP, Yong CS, Beavis PA, Haynes NM, *et al.* Anti-PD-1 antibody therapy potentially enhances the eradication of established tumors by gene-modified T cells. *Clin Cancer Res* 2013 Oct 15; **19**(20): 5636-5646.
86. Liu X, Ranganathan R, Jiang S, Fang C, Sun J, Kim S, *et al.* A Chimeric Switch-Receptor Targeting PD1 Augments the Efficacy of Second-Generation CAR T Cells in Advanced Solid Tumors. *Cancer Res* 2016 Mar 15; **76**(6): 1578-1590.
87. Kobold S, Grassmann S, Chaloupka M, Lampert C, Wenk S, Kraus F, *et al.* Impact of a New Fusion Receptor on PD-1-Mediated Immunosuppression in Adoptive T Cell Therapy. *J Natl Cancer Inst* 2015 Aug; **107**(8).
88. Ran FA, Hsu PD, Wright J, Agarwala V, Scott DA, Zhang F. Genome engineering using the CRISPR-Cas9 system. *Nat Protoc* 2013 Nov; **8**(11): 2281-2308.
89. Horvath P, Barrangou R. CRISPR/Cas, the immune system of bacteria and archaea. *Science* 2010 Jan 8; **327**(5962): 167-170.
90. Bhaya D, Davison M, Barrangou R. CRISPR-Cas systems in bacteria and archaea: versatile small RNAs for adaptive defense and regulation. *Annu Rev Genet* 2011; **45**: 273-297.
91. Mali P, Yang L, Esvelt KM, Aach J, Guell M, DiCarlo JE, *et al.* RNA-guided human genome engineering via Cas9. *Science* 2013 Feb 15; **339**(6121): 823-826.
92. Jinek M, Chylinski K, Fonfara I, Hauer M, Doudna JA, Charpentier E. A programmable dual-RNA-guided DNA endonuclease in adaptive bacterial immunity. *Science* 2012 Aug 17; **337**(6096): 816-821.

93. Cong L, Ran FA, Cox D, Lin S, Barretto R, Habib N, *et al.* Multiplex genome engineering using CRISPR/Cas systems. *Science* 2013 Feb 15; **339**(6121): 819-823.
94. Doudna JA, Charpentier E. Genome editing. The new frontier of genome engineering with CRISPR-Cas9. *Science* 2014 Nov 28; **346**(6213): 1258096.
95. Hsu PD, Lander ES, Zhang F. Development and applications of CRISPR-Cas9 for genome engineering. *Cell* 2014 Jun 5; **157**(6): 1262-1278.
96. Mandal PK, Ferreira LM, Collins R, Meissner TB, Boutwell CL, Friesen M, *et al.* Efficient ablation of genes in human hematopoietic stem and effector cells using CRISPR/Cas9. *Cell Stem Cell* 2014 Nov 6; **15**(5): 643-652.
97. Liang X, Potter J, Kumar S, Zou Y, Quintanilla R, Sridharan M, *et al.* Rapid and highly efficient mammalian cell engineering via Cas9 protein transfection. *J Biotechnol* 2015 Aug 20; **208**: 44-53.
98. Kim S, Kim D, Cho SW, Kim J, Kim JS. Highly efficient RNA-guided genome editing in human cells via delivery of purified Cas9 ribonucleoproteins. *Genome Res* 2014 Jun; **24**(6): 1012-1019.
99. Schumann K, Lin S, Boyer E, Simeonov DR, Subramaniam M, Gate RE, *et al.* Generation of knock-in primary human T cells using Cas9 ribonucleoproteins. *Proc Natl Acad Sci U S A* 2015 Aug 18; **112**(33): 10437-10442.
100. Hultquist JF, Schumann K, Woo JM, Manganaro L, McGregor MJ, Doudna J, *et al.* A Cas9 Ribonucleoprotein Platform for Functional Genetic Studies of HIV-Host Interactions in Primary Human T Cells. *Cell Rep* 2016 Oct 25; **17**(5): 1438-1452.
101. Ren J, Liu X, Fang C, Jiang S, June CH, Zhao Y. Multiplex genome editing to generate universal CAR T cells resistant to PD1 inhibition. *Clin Cancer Res* 2016 Nov 4.
102. Chong EA, Melenhorst JJ, Lacey SF, Ambrose DE, Gonzalez V, Levine B, *et al.* PD-1 Blockade Modulates Chimeric Antigen Receptor (CAR) Modified T Cells and Induces Tumor Regression: Refueling the CAR. *Blood* 2016 Dec 28.
103. Riddell SR, Greenberg PD. The use of anti-CD3 and anti-CD28 monoclonal antibodies to clone and expand human antigen-specific T cells. *J Immunol Methods* 1990 Apr 17; **128**(2): 189-201.
104. Brown CE, Wright CL, Naranjo A, Vishwanath RP, Chang WC, Olivares S, *et al.* Biophotonic cytotoxicity assay for high-throughput screening of cytolytic killing. *J Immunol Methods* 2005 Feb; **297**(1-2): 39-52.

105. Sommermeyer D, Hudecek M, Kosasih PL, Gogishvili T, Maloney DG, Turtle CJ, *et al.* Chimeric antigen receptor-modified T cells derived from defined CD8+ and CD4+ subsets confer superior antitumor reactivity in vivo. *Leukemia* 2015 10/06/online.
106. Hudecek M, Sommermeyer D, Kosasih PL, Silva-Benedict A, Liu L, Rader C, *et al.* The nonsignaling extracellular spacer domain of chimeric antigen receptors is decisive for in vivo antitumor activity. *Cancer immunology research* 2015 Feb; **3**(2): 125-135.
107. Sanjana NE, Shalem O, Zhang F. Improved vectors and genome-wide libraries for CRISPR screening. *Nat Methods* 2014 Aug; **11**(8): 783-784.
108. Morgan M, Anders S, Lawrence M, Aboyoun P, Pages H, Gentleman R. ShortRead: a bioconductor package for input, quality assessment and exploration of high-throughput sequence data. *Bioinformatics* 2009 Oct 1; **25**(19): 2607-2608.
109. Langmead B, Trapnell C, Pop M, Salzberg SL. Ultrafast and memory-efficient alignment of short DNA sequences to the human genome. *Genome Biol* 2009; **10**(3): R25.
110. Quinlan AR, Hall IM. BEDTools: a flexible suite of utilities for comparing genomic features. *Bioinformatics* 2010 Mar 15; **26**(6): 841-842.
111. Sadelain M, Papapetrou EP, Bushman FD. Safe harbours for the integration of new DNA in the human genome. *Nat Rev Cancer* 2012 Jan; **12**(1): 51-58.
112. Schones DE, Cui K, Cuddapah S, Roh TY, Barski A, Wang Z, *et al.* Dynamic regulation of nucleosome positioning in the human genome. *Cell* 2008 Mar 7; **132**(5): 887-898.
113. Barski A, Cuddapah S, Cui K, Roh TY, Schones DE, Wang Z, *et al.* High-resolution profiling of histone methylations in the human genome. *Cell* 2007 May 18; **129**(4): 823-837.
114. Zhang Y, Liu T, Meyer CA, Eeckhoute J, Johnson DS, Bernstein BE, *et al.* Model-based analysis of ChIP-Seq (MACS). *Genome Biol* 2008; **9**(9): R137.
115. Bejerano G, Pheasant M, Makunin I, Stephen S, Kent WJ, Mattick JS, *et al.* Ultraconserved elements in the human genome. *Science* 2004 May 28; **304**(5675): 1321-1325.
116. Frigault MJ, Lee J, Basil MC, Carpenito C, Motohashi S, Scholler J, *et al.* Identification of chimeric antigen receptors that mediate constitutive or inducible proliferation of T cells. *Cancer immunology research* 2015 Apr; **3**(4): 356-367.

117. Wang GP, Levine BL, Binder GK, Berry CC, Malani N, McGarrity G, *et al.* Analysis of lentiviral vector integration in HIV+ study subjects receiving autologous infusions of gene modified CD4+ T cells. *Mol Ther* 2009 May; **17**(5): 844-850.
118. Papapetrou EP, Lee G, Malani N, Setty M, Riviere I, Tirunagari LM, *et al.* Genomic safe harbors permit high beta-globin transgene expression in thalassemia induced pluripotent stem cells. *Nat Biotechnol* 2011 Jan; **29**(1): 73-78.
119. Charrier S, Ferrand M, Zerbato M, Precigout G, Viornery A, Bucher-Laurent S, *et al.* Quantification of lentiviral vector copy numbers in individual hematopoietic colony-forming cells shows vector dose-dependent effects on the frequency and level of transduction. *Gene Ther* 2011 May; **18**(5): 479-487.
120. Severson JJ, Serracino HS, Mateescu V, Raeburn CD, McIntyre RC, Jr., Sams SB, *et al.* PD-1+Tim-3+ CD8+ T Lymphocytes Display Varied Degrees of Functional Exhaustion in Patients with Regionally Metastatic Differentiated Thyroid Cancer. *Cancer immunology research* 2015 Jun; **3**(6): 620-630.
121. Huang X, Guo H, Kang J, Choi S, Zhou TC, Tammana S, *et al.* Sleeping Beauty transposon-mediated engineering of human primary T cells for therapy of CD19+ lymphoid malignancies. *Mol Ther* 2008 Mar; **16**(3): 580-589.
122. Jin Z, Maiti S, Huls H, Singh H, Olivares S, Mates L, *et al.* The hyperactive Sleeping Beauty transposase SB100X improves the genetic modification of T cells to express a chimeric antigen receptor. *Gene Ther* 2011 Sep; **18**(9): 849-856.
123. Lukacs GL, Haggie P, Seksek O, Lechardeur D, Freedman N, Verkman AS. Size-dependent DNA mobility in cytoplasm and nucleus. *J Biol Chem* 2000 Jan 21; **275**(3): 1625-1629.
124. Yant SR, Wu X, Huang Y, Garrison B, Burgess SM, Kay MA. High-resolution genome-wide mapping of transposon integration in mammals. *Mol Cell Biol* 2005 Mar; **25**(6): 2085-2094.
125. de Jong J, Akhtar W, Badhai J, Rust AG, Rad R, Hilkens J, *et al.* Chromatin landscapes of retroviral and transposon integration profiles. *PLoS Genet* 2014 Apr; **10**(4): e1004250.
126. Papapetrou EP, Schambach A. Gene Insertion Into Genomic Safe Harbors for Human Gene Therapy. *Mol Ther* 2016 Apr 12; **24**(4): 678-684.
127. Grabundzija I, Irgang M, Mates L, Belay E, Matrai J, Gogol-Doring A, *et al.* Comparative analysis of transposable element vector systems in human cells. *Mol Ther* 2010 Jun; **18**(6): 1200-1209.

128. Huang X, Guo H, Tammana S, Jung YC, Mellgren E, Bassi P, *et al.* Gene transfer efficiency and genome-wide integration profiling of Sleeping Beauty, Tol2, and piggyBac transposons in human primary T cells. *Mol Ther* 2010 Oct; **18**(10): 1803-1813.
129. Maldarelli F, Wu X, Su L, Simonetti FR, Shao W, Hill S, *et al.* HIV latency. Specific HIV integration sites are linked to clonal expansion and persistence of infected cells. *Science* 2014 Jul 11; **345**(6193): 179-183.
130. Ivics Z, Katzer A, Stuwe EE, Fiedler D, Knespel S, Izsvak Z. Targeted Sleeping Beauty transposition in human cells. *Mol Ther* 2007 Jun; **15**(6): 1137-1144.
131. Voigt K, Gogol-Doring A, Miskey C, Chen W, Cathomen T, Izsvak Z, *et al.* Retargeting sleeping beauty transposon insertions by engineered zinc finger DNA-binding domains. *Mol Ther* 2012 Oct; **20**(10): 1852-1862.
132. June CH, Riddell SR, Schumacher TN. Adoptive cellular therapy: a race to the finish line. *Science translational medicine* 2015 Mar 25; **7**(280): 280ps287.
133. Ramos CA, Savoldo B, Dotti G. CD19-CAR trials. *Cancer J* 2014 Mar-Apr; **20**(2): 112-118.
134. Hudecek M, Lupo-Stanghellini MT, Kosasih PL, Sommermeyer D, Jensen MC, Rader C, *et al.* Receptor affinity and extracellular domain modifications affect tumor recognition by ROR1-specific chimeric antigen receptor T cells. *Clin Cancer Res* 2013 Jun 15; **19**(12): 3153-3164.
135. Riddell SR, Sommermeyer D, Berger C, Liu LS, Balakrishnan A, Salter A, *et al.* Adoptive therapy with chimeric antigen receptor-modified T cells of defined subset composition. *Cancer J* 2014 Mar-Apr; **20**(2): 141-144.
136. Gill S, Maus MV, Porter DL. Chimeric antigen receptor T cell therapy: 25years in the making. *Blood Rev* 2016 May; **30**(3): 157-167.
137. Fousek K, Ahmed N. The Evolution of T-cell Therapies for Solid Malignancies. *Clin Cancer Res* 2015 Aug 1; **21**(15): 3384-3392.
138. Oluwole OO, Davila ML. At The Bedside: Clinical review of chimeric antigen receptor (CAR) T cell therapy for B cell malignancies. *J Leukoc Biol* 2016 Dec; **100**(6): 1265-1272.
139. Pen JJ, Keersmaecker BD, Heirman C, Corthals J, Liechtenstein T, Escors D, *et al.* Interference with PD-L1/PD-1 co-stimulation during antigen presentation enhances the multifunctionality of antigen-specific T cells. *Gene Ther* 2014 Mar; **21**(3): 262-271.
140. Postow MA. Managing immune checkpoint-blocking antibody side effects. *Am Soc Clin Oncol Educ Book* 2015: 76-83.

141. Hemmi H, Takeuchi O, Kawai T, Kaisho T, Sato S, Sanjo H, *et al.* A Toll-like receptor recognizes bacterial DNA. *Nature* 2000 Dec 7; **408**(6813): 740-745.
142. Gabriel R, Lombardo A, Arens A, Miller JC, Genovese P, Kaepffel C, *et al.* An unbiased genome-wide analysis of zinc-finger nuclease specificity. *Nat Biotechnol* 2011 Sep; **29**(9): 816-823.
143. Hsu PD, Scott DA, Weinstein JA, Ran FA, Konermann S, Agarwala V, *et al.* DNA targeting specificity of RNA-guided Cas9 nucleases. *Nat Biotechnol* 2013 Sep; **31**(9): 827-832.

Curriculum vitae

